EFFICIENT TECHNIQUES FOR DETECTION AND MITIGATION OF POWER QUALITY EVENTS

BY

FOUAD RASHED FOUAD ZARO

A Dissertation Presented to the

DEANSHIP OF GRADUATE STUDIES

KING FAHD UNIVERSITY OF PETROLEUM & MINERALS

DHAHRAN, SAUDI ARABIA

In Partial Fulfillment of the

Requirements for the Degree of

DOCTOR OF PHILOSOPHY

In

ELECTRICAL ENGINEERING

June 2013

KING FAHD UNIVERSITY OF PETROLEUM & MINERALS

DHAHRAN 31261, SAUDI ARABIA

DEANSHIP OF GRADUATE STUDIES

This dissertation is written by **FOUAD RASHED FOUAD ZARO,** under the direction of his dissertation advisor and approved by his dissertation committee, has been presented to and accepted by the Dean of Graduate Studies, in partial fulfillment of the requirements for the degree of **DOCTOR OF PHILOSOPHY IN ELECTRICAL ENGINEERING.**

Dissertation Committee:

Prof. MOHAMMED ABIDO (Chairman)

Prof. IBRAHIM EL-AMIN (Co-Chairman)

Prof. MOHAMMED EL-GEBEILY (Member)

Prof. ZAKARIYA AL_HAMOUZ (Member)

Dr. MAHMOUD KASSAS (Member)

Dr. ALI AL-SHAIKHI
(Department Chairman)

Prof. SALAM ZUMMO
(Dean of Graduate Studies)

Date: 12/3/13

بسم الله الرحمن الرحيم

{ قُلْ إِنَّ صَلاَتِي وَنُسُكِي وَمَحْيَايَ وَمَمَاتِي لِلّهِ رَبِّ الْعَالَمِينَ }

[الأنعام 162]

Dedicated
To

My Beloved Parents…

My Wife…

My Children…

My Holy Homeland Palestine…

FOUAD

ACKNOWLEDGMENT

In the name of Allah, the most gracious, the most merciful all praise is to Almighty Allah for having guided me all over my life. Acknowledgement is due to King Fahd University of Petroleum and Minerals for the great support to this work. My deep appreciation is reserved for dissertation advisor ***Prof. Mohammed Abido*** for his guidance, valuable time and attention he devoted throughout the course of this work. My numerous intrusions into his office were always met with a considerate response and care. Thanks are also due to my co-advisor ***Prof. Ibrahim El-Amin*** and committee members ***Prof. Mohammed Elgebeily, Prof. Zakariya Alhamouz*** and ***Dr. Mahmoud Kassas*** for their interest, attention and suggestions. I wish also to thank all other parties who has contributed to support me in this work, namely department chairman ***Dr. Ali Alshaikhi*** and dean of graduate studies ***Prof. Salam Zummo*** and other faculty members for their support. My great appreciations are also due to all members of my family and to friends who give me the self-confidence to face the challenge.

Table of Contents

LIST OF TABLES

LIST OF FIGURES

FIGURE **PAGE**

FIGURE **PAGE**

FIGURE **PAGE**

THESIS ABSTRACT

Name: Fouad Rashed Zaro.
Title: Efficient Techniques for Detection and Mitigation of Power Quality Events
Major Field: Electrical Engineering.
Date of Degree: June 2013.

Modern electric power systems with new distributed renewable power sources such as wind power and solar power have seen the participation of a large amount of new power electronic devices. The recently developed technology related to the concept "smart grid" in power systems also contributes to make the system more complex. The increasing use of power electronics devices contributes further to the arising power quality (PQ) problem that is becoming more and more serious, and has been a great threat to the safety of electric power systems and the national economy as a whole.

In this dissertation, a comprehensive literature review has been accomplished for real time monitoring, detection, tracking, classification, and mitigation for PQ problems as well as optimal harmonic estimation. New efficient methods for PQ events monitoring, detection, and tracking have been proposed and developed. These methods are mainly based on wavelet multiresolution analysis and rms voltage calculation. Furthermore, a new efficient technique for online accurate harmonic estimation based on separable least squares has been proposed and simulated. Control strategies for mitigation devices for power quality problems are proposed and simulated.

The proposed monitoring, detection, tracking, and classification techniques for PQ events has been implemented in laboratory scale prototype using LabVIEW software, developed data acquisition cards, real time signal processors, and a simplified model for the distribution network with its associated bulk loads. The necessary experimental work to validate the proposed techniques has implemented. Additionally, the results of all proposed methods have been compared with the results of the conventional methods. The results demonstrate the superiority, accuracy, robustness, suitability and capability of the proposed methods for real time applications.

Doctor of Philosophy
King Fahd University of Petroleum & Minerals
Dhahran, Saudi Arabia.
June 2013

ملخص الرسالة

الاسم : **فؤاد راشد فؤاد الزرو**

عنوان الرسالة : **تقنيات فعالة للكشف والتخفيف من أحداث جودة الطاقة**

التخصص : **الهندسة الكهربائية**

تاريخ التخرج : **حزيران 2013 م**

إن أنظمة توزيع الطاقة الكهربائية الحديثة تشمل على أجهزة الطاقة البديلة والتي تتكون بشكل اساسي من أجهزة الكترونية مما زاد من تعقيد أنظمة التوزيع, ووجود الاجهزة الالكترونية في نظام التوزيع أثر بشكل سلبي على جودة الطاقة الكهربائية الى حد تهديد استقرار النظام الكهربائي والاقتصاد الوطني.

هذه الاطروحة تهدف الى تنفيذ و تطبيق نظام مراقبة جودة الطاقة في الوقت الحقيقي وبناء استراتيجيات ذكية للتخفيف من مشاكل جودة الطاقة التي يتم كشفها وذلك باستخدام احدث الاجهزة والتقنيات المستخدمة في معالجة الاشارات الكهربائية.

وفي هذه الأطروحة تم عمل مسح أدبي شامل عن أنظمة مراقبة جودة الطاقة الكهربائية والاجهزة والتقنيات والبرامج المستخدمة في ذلك. بالإضافة الى ذلك تم تطوير نظام مراقبة الجودة للطاقة الكهربائية واستراتيجية التحكم لأجهزة تخفيف مشاكل جودة الطاقة الكهربائية لتحقيق موثوقية وجودة عالية لمصدر الطاقة الكهربائية. وفي هذه الرسالة تم أيضاً تصميم استراتيجيات التحكم لأجهزة تخفيف مشاكل جودة الطاقة الكهربائية. الطرق المقترحة لمراقبة ومتابعة جودة الطاقة الكهربائية تم تطبيقها في معمل جودة الطاقة الكهربائية, وتم تشغيل النظام المقترح في الوقت الحقيقي واختبار فاعليته و أخذ النتائج للسيناريوهات المعدة لتحقيق أهداف الأطروحة.

درجة الدكتوراه في العلوم الهندسية
جامعة الملك فهد للبترول والمعادن
الظهران – المملكة العربية السعودية
حزيران 2013 م

NOMENCLATURE

AC	Alternating Current
CSI	Current Source Inverter.
CWT	Continuous Wavelet Transform.
DC	Direct Current
DFT	Discrete Fourier Transform.
DSP	Digital Signal Processing
DSTATCOM	Distribution Static Var Compensator
DWT	Discrete Wavelet transform
FACTS	Flexible AC Transmission System.
FFT	Fast Fourier Transform.
FPGA	Field Programmable Gate Array.
GA	Genetic Algorithm
LabVIEW	Laboratory Virtual Instrument Engineering Workbench.
LS	Least Square
MRA	Multi-Resolution Analysis
NI	National Instruments.
PCC	Point of Common Coupling
PLL	Phase Locked Loop.
PQ	Power Quality
PSO	Particle Swarm Optimization
PWM	Pulse Width Modulation.
RCGA	Real Coded Genetic Algorithm.
rms	Root Mean Squares
SAPF	Shunt Active Power Filter
SLS	Separable Least Square
SNR	Signal to Noise Ratio.
STFT	Short Time Fourier Transform.
SVC	Static Var Compensator.
VI	Virtual Instruments.
VSO	Voltage Source Converter.
WPT	Wavelet Packet Transform
WT	Wavelet Transform

CHAPTER ONE

INTRODUCTION

1.1 BACKGROUND

Power quality (PQ) is nowadays an important issue that involves electrical energy producers and consumers, and electrical equipment manufacturers. The widespread use of electronic equipment, such as computers, information technology equipment, power electronics devices such as drivers, controllers, and energy-efficient lighting, led to a complete change of electric loads nature. The increasing use of power electronics devices contributes further to the arising PQ problem that is becoming more and more a serious problem, and has been a great threat to the safety of electric power systems and the national economy as a whole [1].

There are numerous types of PQ problems which might have varying and diverse causes such as impulses, oscillations, sags, swells, interruptions, under-voltages, over-voltages, DC offset, harmonics, inter-harmonics, notches, noise, flicker, and frequency variation [2].

In order to understand the PQ problems better, developing a comprehensive monitoring system which integrates the effective measurement, control,

communication and supervision of PQ is important. Monitoring can serve as a vital diagnostic tool and help to identify the cause of PQ disturbances and even makes it possible to identify problem conditions before they cause interruptions or disturbances.

The international organizations working on PQ issues include the Institute of Electrical and Electronic Engineers (IEEE), International Electro-technical Commission (IEC). Standards IEEE-519 and IEC-61000 impose that electrical equipment and facilities should not produce harmonic contents greater than specified values, and also specify distortion limits to the supply voltage [3], [4]. They also recommended guidelines for PQ monitoring that were discussed in Standard IEEE 1159 and IEC-61000-4-30 classifying various electromagnetic phenomena in power systems voltage [4], [5].

Along with technology advance, all over the world there are many companies where PQ problems must be minimized or eliminated in order to increase productivity. The most affected areas by PQ problems are the continuous process industry and the information technology services. When a disturbance occurs, huge financial losses may happen, with the consequent loss of productivity and competitiveness.

Given this brief background, this dissertation proposes new and efficient techniques using the wavelet multiresolution analysis and rms calculation method to develop and test a prototype for a real time power quality monitoring system via LabVIEW software, advanced digital signal processors, and data acquisition modules. Furthermore, a control strategy of the Distribution Synchronous Static Var

Compensator (DSTATCOM) and shunt active power filter (SAPF) were designed and simulated.

1.2 DISSERTATION MOTIVATION

The motivation of this dissertation work is inspired by some of the non-resolved issues in the related work on the problems of characterization, feature extraction, and classification. There is always some detection delay due to the effect of the window size and the sliding window method used to calculate the detection index using rms method. Solving this problem is one of the motivations of this dissertation work. From the literature, it has been observed that there are available signal processing techniques which can be used for feature extraction and classification of power system disturbances. However, most of them are not suitable for on-line processing. Also, there is a drive to apply the latest technology for data acquisition and advanced signal processing tools (Wavelet transforms) using high level programing language (LabVIEW) to build complete monitoring system .

To conclude, all the problems mentioned show that research in this area is very challenging but promising. A system which is able to automatically monitor and efficiently analyze and classify disturbances is desired to cope with the era more complex power systems.

1.3 DISSERTATION OBJECTIVES

This dissertation aims at proposing, developing, and implementing new real time techniques to monitor, track, and identify PQ problems. Additionally, it aims at designing and simulating control strategies for PQ problems mitigation. Problems under investigations will include: voltage sag, voltage swell, voltage momentary interruption, and harmonics since these problems are the most severe PQ problems in the electrical distribution network and their presence greatly affect the reliability and efficiency of the network.

The specific objectives of the dissertation are:

1) Developing and implementing real time monitoring, tracking, and classification system for PQ problems in electric power distribution networks.
2) Designing and simulating control strategies for PQ problems mitigation systems.
3) Testing experimentally the proposed techniques for monitoring and classification of PQ problems.

1.4 METHODOLOGY OF THE DISSERTATION

The work of this dissertation involves theoretical investigation, laboratory implementation, and experimental investigation. The execution of this dissertation consists of five phases as follow:

1) Comprehensive literature review of: PQ events, monitoring, detection, tracking, classifying, and mitigation of PQ events. Literature review was also carried out for wavelet transforms application in power systems; rms calculation methods; intelligent techniques for optimal harmonics estimation as well as standards associated with PQ and harmonics in power systems.

2) Building a monitoring and tracking module: developing detection and classification techniques for PQ problems using wavelet multiresolution analysis and rms-based method, and then coding the proposed techniques via LabVIEW software. Further, implementing and testing the proposed techniques in real-time.

3) Design a control strategy for the mitigation device: developing and simulating control strategies for DSTATCOM and SAPF.

4) Building the complete prototype in the laboratory: interfacing the monitoring workstation, the signal processor and modules with the simplified model of the distribution network.

5) Experimental investigation of the prototype under different operating scenarios: experimental investigation of the prototype in dealing with various disturbances in the electric distribution network.

1.5 FINDINGS AND CONTRIBUTIONS

The main contribution of this dissertation is proposing new efficient techniques for real time detection and classification of voltage events in electrical distribution networks. Furthermore, rebuild a detection and classification system of PQ problems using the proposed methods in a laboratory.

The specific dissertation contributions are:

- Two new methods based on wavelet multiresolution analysis and rms calculation have been developed for real time detection and classification of voltage events.
- A prototype detection and classification system for PQ problems has been built in the laboratory using the developed methods, as well as using the conventional methods.
- A separable least square (SLS) algorithm has been developed for on-line optimal harmonics estimation in electrical power. The simulation results are compared with the results of other intelligent techniques to evaluate the efficiency of proposed SLS.
- Control strategies for DSTATCOM and SAPF devices have been designed and simulated.

1.6 DISSERTATION ORGANIZATION

This dissertation contains seven chapters as follows: besides the introduction of this dissertation. The second chapter presents a comprehensive literature review of the PQ problems, PQ monitoring, detection and classification systems, the DSTATCOM application in voltage regulation and SAPF for harmonics compensation. Chapter 3 presents intelligent computing techniques for optimal harmonics estimation in electrical power systems. The proposed work for the PQ problem detection, estimation and classification using rms-based methods and wavelet multi-resolution analysis are presented in Chapter 4 and Chapter 5, respectively. Chapter 6 presents

the proposed work for the mitigation of PQ problems and the control strategies of the DSTATCOM and SAPF. Finally, conclusions and suggestions for future work are pointed out in Chapter 7.

CHAPTER TWO

LITERATURE REVIEW

This chapter presents a comprehensive literature review of power quality events monitoring, tracking, classification, and characterization as well as control strategies of mitigation devices for power quality events. In addition, this chapter contains literature review of optimal harmonics estimation using several intelligent techniques.

2.1. OVERVIEW

The term “Power Quality” is, in general, a broad concept and is associated with electrical distribution and utilization systems that experience any voltage, current, or frequency deviation from normal operation. For ideal electrical systems, the supplied power should have perfect current and voltage sinusoidal waveforms, and should be safe and reliable. However, the reality is that the electric utilities control the voltage levels and quality but are unable to control the current, since the load profile dictates the shape of the current waveform. Thus, the utility should maintain the bus voltage quality at all times [6]-[11]. Figure 2.1shows this schematically.

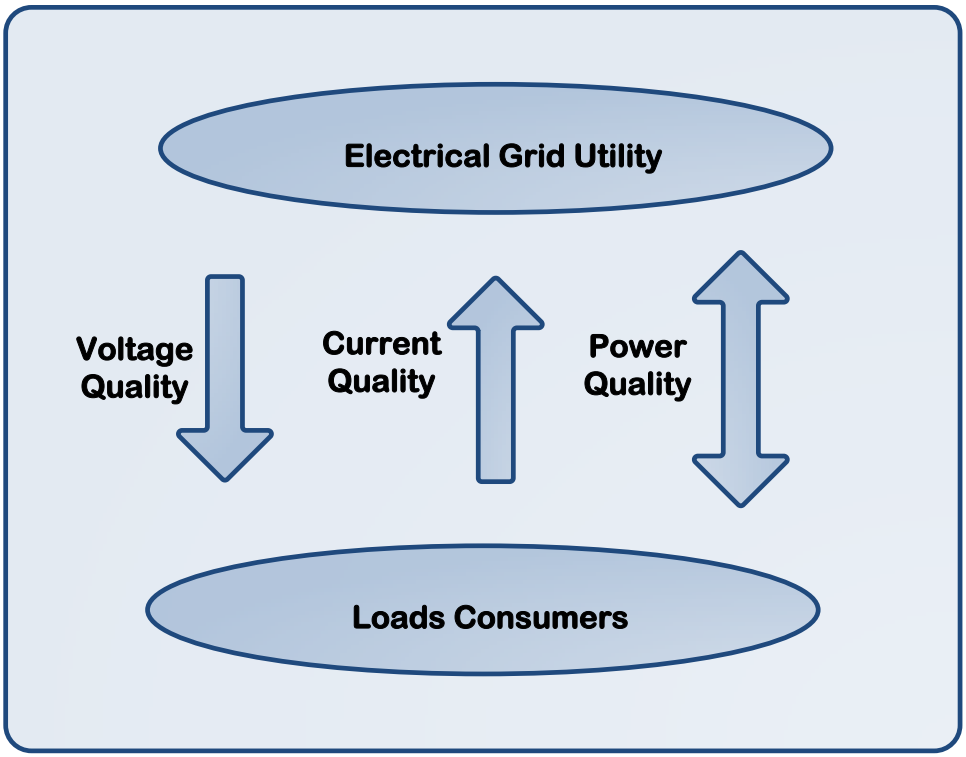

Figure 2.1: The power quality diagram.

Modern electric power systems with new distributed renewable power sources such as wind power and solar power have seen the participation of a large amount of new power electronic devices. The recently developed technology related to the concept "smart grid" in power systems also contributes to make the system more complex. The increasing use of power electronics devices contributes further to the growing power quality problem [1]-[2], [12]-[18].

2.2. POWER QUALITY EVENTS MONITORING, TRACKING AND CHARACTERIZATION

Accurate monitoring and tracking of PQ events improve the characterization and localization of PQ phenomena and enhance mitigation solutions. Pre-processing is needed for any automated PQ analysis.

2.2.1 Signal De-noising

The signal under investigation is often distorted by noises, especially the ones with high frequency that are mounted on the signal. The performance of detection techniques of PQ events would be greatly low, due to the difficulty of distinguishing the disturbances and noises. The elimination of the high frequency noise overlaps with the signal will lead to accurate localization and detection of PQ events. The wavelet transform can be utilized effectively for de-noising the signal to enhance the capability of the PQ monitoring system in a noisy environment [19]-[26].

2.2.2 Detection and Tracking of Power Quality Events

Detection technique of the existing PQ instruments is based on point-by-point comparison of two adjacent power cycles. The detection of an event is achieved when certain threshold is reached. This method is sensitive to the selected threshold value and insensitive to harmonics. To overcome these drawbacks, several techniques have been proposed in the literature for the detection of PQ problems. The Teager energy

operator (TEO), based on instantaneous energy extraction, has good capability for extracting the short time energy of the signal. A detecting method depends on fractal number computation integrated with moving average technique. However, both methods are sensitive to noise [27], [28].

The best technique for frequency-domain analysis is the Fourier transform (FT). However, it is impossible to tell when a particular event took place. The FT is not a suitable technique for non-stationary signals. To resolve this problem (Shortcoming), short-time Fourier transform (STFT) is capable of providing the time and the frequency information of the signal simultaneously. However, it has uniform time and frequency resolutions. Many signals require a more flexible approach. The wavelet transform (WT) has flexible time and frequency resolutions that allow detecting PQ disturbance accurately [29]-[33].

Figure 2.2 shows the Comparison of time and frequency resolutions for STFT and DWT. The selection of the most appropriate wavelet function depends on the type of disturbance to be detected and analyzed. In general, shorter wavelets are best suited for detecting fast transients, while slow transients are better detected using longer wavelets.

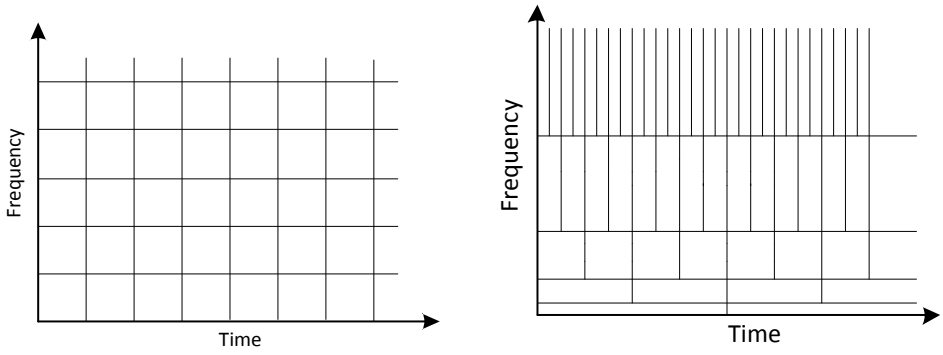

(a) Short-time Fourier transforms. (b) Discrete wavelet transforms.

Figure 2.2: Comparison of time and frequency resolutions.

However, WT capabilities are greatly degraded in real practice in a noisy environment. On the other hand, the S-Transform has the ability to detect PQ events correctly in the presence of noise. However, the S-Transform does quite satisfy the real-time requirement [34].

The wavelet packet transform (WPT) can be used to obtain uniform frequency splitting of the input signal as in the Fourier transform. In WPT, the details as well as the approximations coefficients can be further split to produce new coefficients [35]. WPT satisfies well the harmonics estimation and detection.

The detection stage is necessary in order to trigger the tracking and classification algorithms. There are several techniques for real time tracking of PQ problems based on Kalman filter [36], adaptive linear neuron [37], and Hilbert transform [38].

2.2.3 Classification of Power Quality Events

The classification of the PQ events is important in identifying the event type. Recently, many algorithms have been designed for the classification of PQ events. Typically, they are based on the FT or WT for feature extraction [39]-[41]. This allows obtaining unique signal characteristics that are classified according to their magnitude and duration. Artificial neural networks [42]-[44], support vector machine [45]-[46], Fuzzy logic [47], Fuzzy expert systems [48], or nearest neighbor [49] have all been used for classifying PQ events.

The challenge in the PQ events classification is the non-uniform time constancy between the test signal and the pre-stored feature which may lead to degradation of the classification robustness. In view of the different durations, frequencies, and magnitudes for each PQ event type [50]-[51].

2.3. APPLICATION OF WAVELET TRANSFORMS IN ELECTRICAL POWER SYSTEMS

The wavelet transform is a mathematical tool that cut up data into different frequency components, and then study each component with a resolution matched to its scale. It uses wavelets (small waves) which are functions with limited energy and zero average. Wavelet analysis plays the same role as the sine and cosine functions in the Fourier analysis. They have advantages over traditional Fourier methods in analyzing non stationary signals. WTs are distinguished from other transformations in that they

not only dissect signals into their component frequencies; they also vary the scale at which the component frequencies are analyzed [52]-[64].

The wavelet coefficients represent the information contained in the different decomposition levels of a distorted power signal. The most common distinguishing features for the detection, localization and classification of voltage events in power quality are the magnitude, the average value, the standard deviation, the distribution of energy pattern or the entropy of these coefficients at the different resolution levels [65]–[81].

Electrical power systems parameters, independently of the nature of the signal (stationary or not), need to be constantly measured and analyzed for reasons of control, protection, and supervision. Many of these tasks need specialized tools to extract information in time, in frequency, or both. Therefore, the WT has become an interesting, important and useful computational tool for evaluating the signal characteristics simultaneously in the time and frequency domains. The WT can be categorized as discrete wavelet transforms (DWT) or continuous wavelet transforms (CWT). CWTs operate over every possible scale and translation, whereas DWTs use a specific subset of scale and translation values or representation grid [82]-[86].

The CWT has been proposed to detect and analyze PQ disturbances like voltage sag and transients [87]. On the other hand, The CWT is not suitable for online analysis applications. The CWT adds excess redundancy and is computationally intensive. Furthermore, CWT does not provide the phase information of the analyzed signal, for that reasons, it’s not suitable for reconstructing the original signal.

Recent advances in WT provide a powerful tool for PQ disturbances detection, localization, and classification. The dyadic-orthonormal wavelet transform has been utilized to detect and localize various types of PQ disturbances including harmonics [88]-[93].

The wavelet multiresolution analysis (MRA) is an attractive technique for analyzing power quality waveform, particularly for studying disturbance or transient waveform where it is necessary to examine different frequency components separately. This can be attributed to its ability in segregating a signal into multiple frequency bands with optimized resolutions. MRA is capable of revealing aspects of data that other analysis tools would miss, like trends, discontinuities, breakdown points, and self-similarity. MRA has proven to be efficient in feature extraction from PQ disturbance data [94]-[105].

The delta standard deviation MRA has been proposed to classify PQ problems [106]. In addition, the inductive inference approach and self-organizing learning array system based on WT have been proposed to classify PQ disturbances [107]-[108]. On the other hand, the wavelet networks are proposed to be a classifier for PQ disturbance [109].

The MRA is the most powerful tool for detection, localization, and classification of PQ disturbances as mentioned above. However, MRA is sensitive to high frequency noises are superimposed on the signal. Also MRA needs complete information for all

the decomposition levels to calculate the rms value of the power signal. This will take a long time relatively to accomplish the rms calculations.

2.4. CHARACTERIZATION OF SHORT-DURATION VOLTAGE EVENTS

Short-duration voltage variations are interruption, sag (dip) and swell. Such events are always caused by fault conditions, energization of large loads that require high starting currents, or intermittent loose connections in power wiring. Voltage interruption occurs when the supply voltage decreases to less than 10% of nominal rms voltage for a time period not exceeding 1.0 min. Voltage interruptions are usually associated with power system faults, equipment failures, and control malfunctions. Voltage sag is a decrease in rms voltage to the range between 10% and 90% of nominal rms voltage for durations from 0.5 cycles to 1.0 min. Voltage sags can be a result of system faults, switching heavy loads, starting large motors or large load changes. A voltage swell is the converse to the sag where there is an increase in rms voltage above 110% to 180% of nominal voltage for durations of 0.5 cycle to 1.0 min. Voltage swells are usually associated with system faults, Switching on capacitor banks and incorrect settings off-tap changers in power substations [1]-[5],[110]-[111].

According to IEEE Std-1159, the short-duration voltage variations are variations of the rms value of the voltage over short time intervals. Therefore, based on this concept, the characterization of short-duration voltage variations, such as the duration and amplitude, should be quantified using the rms voltage not the instantaneous

voltage. There are several protocols for the rms values calculation of a voltage waveform.

In general, some PQ analyzers do not provide satisfactory results during testing, for several reasons [112]:

- Calculation method of the rms voltages, which directly influences the calculation of the magnitude and duration of short-duration voltage variations.
- The selected methodology for calculating voltage unbalance.
- The calculation method used to determine average values, that is, mean square or arithmetic mean.

But the rms-based methods suffer from the dependency on the window length and the time interval for updating the values. Depending on the selection of these two parameters, the magnitude and the duration of a voltage event can be very different [113]-[116].

2.5. OPTIMAL HARMONIC ESTIMATION

Harmonic distortion is one of the important problems that can significantly deteriorate the PQ in electrical power networks. Harmonic distortion can be caused either by the presence of power electronics equipment or by connection of nonlinear loads in a power system [117]. The harmonics in a power system result in increasing of transmission losses, reducing of equipment efficiency as well as malfunctioning in electronic circuits and communication systems. To obtain a suitable control strategy

for harmonic mitigation, the amplitudes and phases of the harmonics are to be estimated accurately. This will be used to mitigate the harmonics by injecting the corresponding portion into a power system [118]-[119].

Many algorithms are available to estimate the harmonic parameters. These include least square (LS) regression widely used and effective technique to estimate the harmonics in the system whose characteristics are not well known [120]. In addition, fast Fourier transforms (FFT) and discrete Fourier transforms (DFT) [121] are used for harmonics detection. Other algorithms include, Kalman filter (KF) for estimating different states and parameters of the harmonics in an electrical signal. However, KF cannot track sudden or dynamic changes of signal and its harmonics [122]-[123].To overcome this shortcoming, adaptive KF has been proposed for dynamic estimation of harmonic signals that is able to track dynamic and sudden changes of harmonics amplitudes [124]-[125].

The wavelet packet transform (WPT) can be used for the measurement of harmonics in power supply. The WPT allows decomposing a power system signal into uniform frequency bands. With proper selection of the sampling frequency and the wavelet resolution levels, the frequency of harmonics can be picked to be in the center of each band in order to avoid the spectral leakage related with the imperfect frequency response of the filter bank utilized [126]-[128].

Developments of artificial Intelligent (AI) techniques have encouraged the researchers to use these methods for harmonics estimation to obtain accurate solution if the system structure is well defined. The genetic algorithm (GA) provides excellent

results. However a main drawback is long convergence time. To overcome this shortcoming, hybrid algorithms have been proposed such as genetic algorithm with least square (GA-LS), and particle swarm optimization with least square (PSO-LS) [129]-[131]. The harmonics estimation based on an adaptive bacterial swarming algorithm has been proposed in [132], which is adaptive to dynamic environment in which the fundamental frequency deviates with time. Additionally, approach combining both recursive least square and bacterial foraging optimization has been introduced for optimal harmonic estimation in power systems [133].

2.6. MITIGATION DEVICES FOR POWER QUALITY PROBLEMS

2.6.1. Distribution Synchronous Static Compensator

The distribution synchronous static compensator (DSTATCOM) is becoming the trend of the reactive power compensation and the power quality control in distributing networks at the present time [135]-[145].

With the technology development of self-commutating controllable solid state switches such as gate turn-off thyristor (GTO) and insulated gate bipolar transistor (IGBT) and so on, it has declared voltage source inverter (VSI), known as DC to AC converter, is the backbone of the DSTATCOM. The DSTATCOM has several major attributes as compared to the conventional Static Var Compensator (SVC) using thyristor technology. It has fast response time, less space requirement, can produce

reactive power at low voltage, flexibility and excellent dynamic characteristics under different operating conditions [146]-[155].

The control strategy is the heart of the DSTATCOM controller for dynamic control of reactive power in electrical distribution system. The control methodology for DSTATCOM operated with pulse width modulation (PWM) mode employs control of phase angle (ϕ) and modulation index (m) to change the inverter AC voltages keeping V_{dc} constant [156]-[160].

For voltage regulation, two control-loop circuits are employed in DSTATCOM power circuit:

1. Inner current control loop produces the desired phase angle difference of the converter voltage relative to the system voltage.

2. Outer voltage control loop generates the reference reactive current for the current controller of the inner control loop.

The proportional and integral (PI) control algorithms have been implemented in this control methodology [161]-[166].

The voltage events detection and tracking technique is the core of mitigating control strategy of the DSTATCOM. Many techniques have been introduced in the literature to extract and track voltage events such as the FFT that can return magnitude and phase of the fundamental and harmonics component of the grid voltage. However, FFT takes at least one cycle of the fundamental when an event has commenced before information regarding the magnitude and phase angle can be assumed accurately. FFT

has low efficiency in tracking the signal dynamics and it relies on a uniform window, of the frequency components distribution [167].

The Phase Locked Loop (PLL) technique has been often utilized to mitigate voltage events. This technique can be combined with any other technique to detect the magnitude of the voltage event [168]-[172]. The PLL technique does not yield accurate results if the voltage events are associated with a phase angle jump such as in unbalance voltage events [173].

The *dq*-transformation has been also utilized to extract the voltage events, but its results are not satisfactory for unbalanced voltage events, a ripple of double the grid frequency will occur in the *dq*-reference frame [174]-[175]. To overcome this problem the *dq*-components are obtained by the symmetrical components using the Least Squares (LS) algorithm instead of the direct *dq*-transformation [176]. The instantaneous power theory (*pq*-theory) has been also used to extract voltage sags [177], but it does not give accurate results for non-pure voltage and current sinusoidal waveforms [178]. The KF has been used in building the control strategies of the DSTATCOM, and it gives accurate results for signal tracking [179]-[181].

2.6.2. Active Power Filter

The normal passive filter (PF) is the first option to mitigate current harmonics. PF is LC series circuits. However, these PFs may have some important drawbacks as follows [214]-[218].

1. Filtering characteristics are strongly affected by the source impedance.

2. The parallel resonance between the source and the PF may cause amplification of currents on the source side at specific frequencies.

3. Excessive harmonic currents flow into the PF owing to the voltage distortions caused by the possible series resonance with the source.

4. The ageing, deterioration and temperature effects may increase the designed tolerances and bring about detuning, although these effects can be considered in the design stage.

5. For changing system conditions the PFs are not suitable. Since the characteristics of PF such as the tuned frequency and the size of the filter can't be changed so easily.

6. LC PFs represent capacitive loads for the utility grid. In general, the total fundamental frequency capacitive harmonic current delivered in the mains by PFs of 5^{th}, 7^{th}, 11^{th} and 13^{th} order, attached to a classical diode rectifier, represents 30–35% of the active rated current absorbed by the rectifier. This high percentage can be considered a drawback if there is no means to compensate the reactive power in the utility grid.

Active compensators used in three-phase systems, including active power filter (APF), distribution static synchronous compensator (DSTATCOM) and thyristor controlled reactor (TCR). These devices have multiple compensation utilities and good transient performances [219]-[222]. Additionally, the single-phase APF is widely presented in the literature in recent years [223], [224].

The use of an active power filter (APF) to mitigate harmonic problems has drawn much attention since the 1970s [225]. The shunt APFs (SAPFs) are in parallel with the loads. The SAPF can be used under non-sinusoidal supply voltages, where the voltages at the PCC of the filter are harmonics-polluted and are caused by harmonic loads in the SAPF application environment [225]-[231]. The SAPF systems are the optimum solution for harmonics mitigation [232]. In general, the ratings of SAPFs are based on the rms filter terminal voltage and the rms compensating current [231]-[234].

SAPF is a power electronic converter that is switched to inject equal but opposite distorted current in the power supply line, connected to a nonlinear load. The APF injects the required compensation current to the system, and the amplitudes of characteristic harmonics are minimized in the supply current [232], [235]. Its switching, regulated by PWM, generates the harmonics and reactive power required to maintain the mains current sinusoidal and in phase with the mains voltage, irrespective of the load current. A number of methods exist for determining the reference switching current for the APF [232].

The SAPF compensates the harmonic currents due to the nonlinear load. The heart of SAPF is a bridge converter having a capacitor on the dc side [232]-[236]. Various topologies of SAPF are reported and discussed [237]-[239]. Various control methods to ensure expected performance are also discussed [240]. Several works offer switched capacitor SAPF topology [241-244].

2.7. POWER QUALITY MONITORING AND CONTROL BASED ON LABVIEW AND EMBEDED SYSTEM

LabVIEW software is a graphical programming language. It is a powerful analysis and presentation tools. It has been used in the literature to design live monitoring and control of PQ and the detection of PQ disturbances. A comprehensive monitoring and data capturing system are required to better understand and characterize the PQ disturbances. However, the LabVIEW software and reconfigurable embedded system can perform the required task. LabVIEW reduces development time and costs of design. With LabVIEW we can design higher quality products [182]-[183].

Real-time monitoring and analysis system based on LabVIEW software and NI hardware have been developed for frequency monitoring, voltage and current waveforms readings, and harmonics analysis [184]-[185]. A real-time data acquisition and instrumentation based on LabVIEW of renewable energy systems have been designed for providing real-time information about the system, such as direction and speed of wind, and readings of AC/DC voltage, current, and power [186]. The requirements of software and hardware for automatic measurements of electrical voltage and current based on virtual instruments have been described in [187].

PQ detection and analysis has been developed using LabVIEW platform for detecting and analysis the harmonics in voltage and current waveforms, as well as for detecting the voltage fluctuation, flicker, and unbalanced three-phase degrees [188]-[189].

Remote PQ monitoring and analysis systems based on LabVIEW platform have been developed for remote data acquisition, detection of voltage sag and swell, transient detection, voltage unbalance, and sag characteristics detection [190]-[191].

2.8. DISCUSSION

This literature survey has revealed the following limitations in power quality detection and mitigation:

- Most intelligent techniques proposed for harmonics estimation are not suitable for real-time applications, because they have long convergence time.
- The conventional wavelet multiresolution analysis (MRA) satisfies well PQ events detection. However, the MRA requires complete information for all the decomposition levels to calculate the rms value of the power signal. This causes long processing time and limits its capability for real-time detection of PQ disturbance.
- The standard methods for voltage events characterization are rms-based. They have limitations in detecting the start time, the end time, and the duration of the event.

This dissertation addresses these limitations through the development of a detection, analysis, and classification system for power quality disturbances based on:

- A new intelligent technique using separable least squares, which has been utilized for online optimal harmonics estimation [134].

- New rms-based methods. These methods need less memory and less processing time to accomplish the characterization of voltage events. They are perfect of suitable for real-time detection and monitoring applications.

- A new method that utilizes only two decomposition levels for MRA to accomplish the rms calculations. This method saves the processing time, accurately characterize the event, and is suitable for real-time PQ monitoring.

In this dissertation also, The National Instruments CompactRIO hardware, LabVIEW software, and power distribution network components have been utilized to implement the prototype system in the Laboratory environment. The developed system provides:

- Voltage and current waveforms monitoring and analysis.
- Voltage and current readings.
- Harmonics analysis for voltage and current signals.
- Power monitoring and readings.
- Voltage events characterization based on efficient methods.
- Data events logging.
- Control of the operation of the devices on the networks,
- Remote access to the system through a web server.

CHAPTER THREE

HARMONIC ESTIMATION USING INTELLIGENT TICHNIQUES

This chapter discusses several intelligent techniques for optimal estimation of harmonics. Furthermore, it introduces a new intelligent technique for optimal harmonics estimation using the separable least squares algorithm.

3.1 OVERVIEW

Harmonics results in increased transmission losses, reduced efficiency as well as causing malfunction in electronic circuits and communication systems. To obtain suitable control strategies for harmonics mitigation, the amplitudes and phases of the harmonics present in the system are to be estimated accurately, which will be possibly used to mitigate the harmonics by injecting the corresponding portion into a power system. Recent developments of artificial Intelligent (AI) techniques have encouraged the researchers to use these methods for harmonics estimation to obtain accurate solution if the system structures are well defined.

3.2 HARMONICS FORMULATION

- The assumed signal structure is

$$x(t) = \sum_{n=1}^{N} A_n \, sin(\omega_n t + \emptyset_n) + v(t) \tag{3.1}$$

Where

- $n = 1,2,..,N$ represents the harmonic order;
- A_n : the amplitude of the n^{th} harmonic
- ω_n : the angular frequency of the n^{th} harmonic, and $\omega_n = 2\,\pi f_n$.
- f_n : the frequency of the n^{th} harmonic.
- $\emptyset_n$: the phase angle of the n^{th} harmonic
- $v(t)$: the additive noise.

- **The estimation signal structure is**

$$\hat{x}(t) = \sum_{n=1}^{N} \hat{A_n} \, sin(\hat{\omega_n} t + \hat{\emptyset_n}) \tag{3.2}$$

Where $\hat{A_n}, \hat{\omega_n}$, and $\hat{\emptyset_n}$ are the estimation of A_n, $\omega_n$and $\emptyset_n$ respectively.

- **The objective function is**

$$J = \sum_{k=1}^{K} (x(k) - \hat{x}(k))^2 \tag{3.3}$$

Where *K* is the number of samples. The error minimization between actual and estimated signal is taken up as the objective function.

The harmonics phases in the model are nonlinear and are limited in$[0 \ \ 2\pi]$. The recursive optimization algorithm is used to estimate the values of $\emptyset_n$ as well as ω_n. Once the phases and the frequencies are estimated in each iteration, the amplitude $A_n^{\wedge}$ is obtained by the least squares method.

Sampling the signal $x^{\wedge}(t)$ with *K* samples, the discrete linear model is given as

$$x(k) = H(k) \,.A + v(k), \qquad k = 1,2, \dots, K \tag{3.4}$$

$$H(k) = [\sin(w_1 t_k + \emptyset_k) \quad \dots \quad \sin(w_N t_k + \emptyset_N)] \tag{3.5}$$

Where

- *x(k)* is the k[th] sample of the measured values with additive noise *v(k).*
- $A=[A_1 \, A_2 \, \dots \, A_N]^T$ is the vector of the amplitudes needing to be evaluated.
- *H* is the system structure matrix.

The target is to find out the best $A^{\wedge}$, $\emptyset^{\wedge}$ and $\omega^{\wedge}$ which minimizes the difference between $x(k)$ and $x^{\wedge}(k) = H^{\wedge}(k).A^{\wedge}$.

$H^{\wedge}(k)$ can be calculated after the values of $\omega_n^{\wedge}$ and $\emptyset_n^{\wedge}$ are estimated using real coded genetic algorithm or particle swarm optimization technique. Assuming that $H^{\wedge}$ is a full-rank matrix, the estimation of $A^{\wedge}$ is be obtained via the LS method as

$$A^{\wedge} = [H^{\wedge T}.H^{\wedge}]^{-1} H^{\wedge T} x \tag{3.6}$$

$$x^{\wedge} = H^{\wedge}.A^{\wedge} \quad (3.7)$$

This guarantees that the estimation of the signal is the best in the conditioned on $\omega_n^{\wedge}$ and $\emptyset_n^{\wedge}$.

3.3 INTELLIGENT TECHNIQUES FOR HARMONICS ESTIMATION

3.3.1 Hybrid Real Coded Genetic Algorithm-Least Square

The execution steps of the hybrid real coded genetic algorithm-least square (RCGA-LS) technique can be described as follows:

1. Load the data set of the distorted signal.
2. Initialize number of parameters.
3. Calculate *H* using (3.5) for each encoded chromosome.
4. Estimate $A^{\wedge}$ using (3.6).
5. Evaluate the performance criterion and decode it to chromosome space.
6. Apply genetic operators, crossover, mutation, and reproduction based on the fitness values.
7. Repeat steps three to six until the performance index is minimized or convergence is reached.

Figure 3.1 shows flow chart of the execution steps of the hybrid genetic algorithm-least square technique [200].

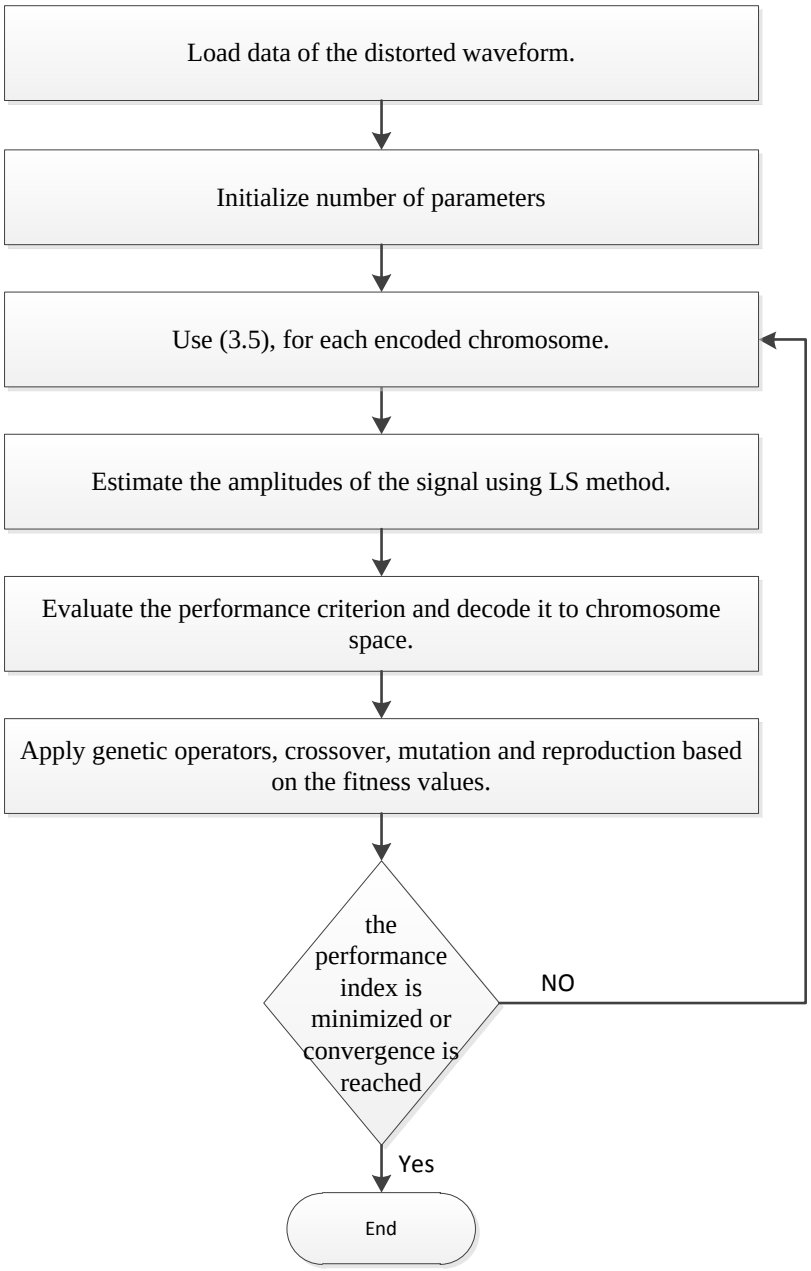

Figure 3.1: The flowchart of the RCGA-LS.

3.3.2 Hybrid Particle Swarm Optimization-Least Square

Particle Swarm Optimization (PSO) is initialized with a group of random solutions and then searches for the optimal solution by updating generations. Each particle is

updated by following two best values in every iteration. The first one is the local best (*pbest*), the second one is the global best (*gbest*). After finding the two best values, the particle updates its velocity and positions with following equations

$$v[\,] = v[\,] + c_1 * rand(\,) * (pbest[\,] - present[\,]) + c_2 * rand(\,) * (gbest[\,] - resent[\,]) \tag{3.8}$$

$$present[\,] = present[\,] + v[\,] \tag{3.9}$$

Where, $v[\,]$ is the particle velocity; $present[\,]$ is the current particle solution; $pbest[\,]$ and $gbest[\,]$ are defined as stated before; $rand(\,)$ is a random number between $\{0, 1\}$. c_1 and c_2 are learning factors and usually $c_1 = c_2 = 2$.

The application procedures of the particle swarm optimization with least square (PSO-LS) technique are described in Figure 3.2, [201].

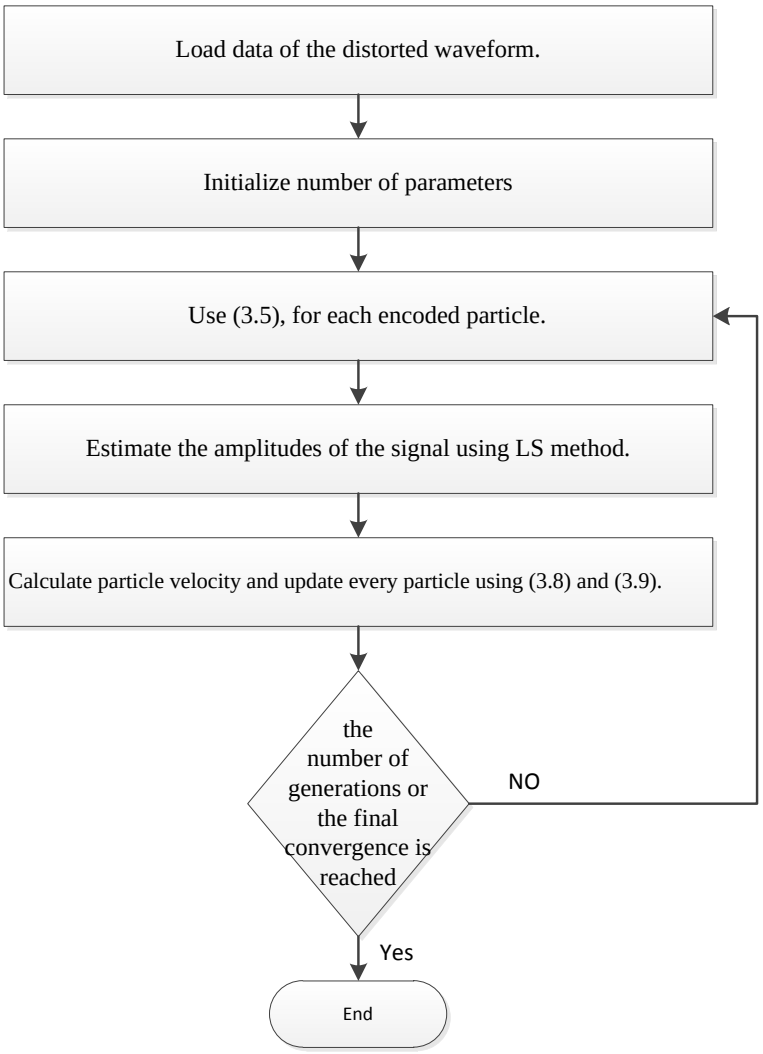

Figure 3.2: The flowchart of the PSO-LS.

3.3.3 Harmonic Estimation Using Adaptive Linear Neural Network

The adaptive linear network (Adaline) is utilized for harmonics estimation. By Fourier analysis the periodic signal can be expanded as the summation of the sine and cosine frequency components [202].

The periodic signal can be modeled as follow [203]:

$$f(t) = \sum_{n=1}^{N} (X_n \cos(n\omega t) + Y_n \sin(n\omega t)) \tag{3.10}$$

Where, X_n and Y_n are the amplitudes of the cosine and sine frequency components of the n[th] order harmonic.

$$f(t) = W^T . x(t) \tag{3.11}$$

$$W^T = [X_1 Y_1 \, X_2 Y_2 \, \ldots \, X_N Y_N \,] \tag{3.12}$$

$$x(t) = \begin{bmatrix} \cos(\omega_1 t) \\ \sin(\omega_1 t) \\ \cos(\omega_2 t) \\ \sin(\omega_2 t) \\ \vdots \\ \cos(\omega_N t) \\ \sin(\omega_N t) \end{bmatrix} \tag{3.13}$$

The sampling time of the signal is Δt, so that the time value of the k[th] sample is $k\Delta t$ with k = 0, 1, 2, ... W^T is the weights vector of the Neural network. After the initial estimation, Adaline updates the weights so that the convergence becomes better.

The network topology and the algorithm of updating weight are shown in Figure 3.3.

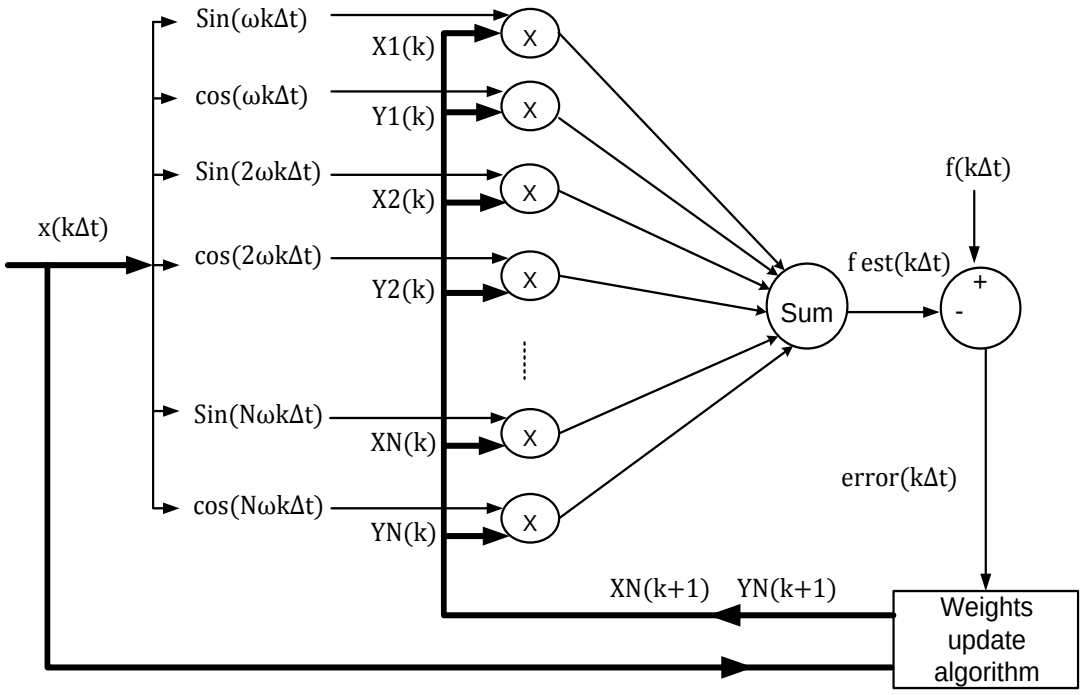

Figure 3.3: Adaptive linear neural network topology.

Where

- $f(k\Delta t)$: represents the actual signal at time $k\Delta t$.
- $x(k\Delta t)$: represents the base signal model at time $k\Delta t$.
- $f_{est}(k\Delta t)$: represents the estimated signal at time $k\Delta t$.
- $error(k\Delta t)$ is the difference between $f(k\Delta t)$ and $x(k\Delta t)$.

Number of inputs for the Adaline is the double of the number of harmonics to be estimated. Since each harmonic order requires two inputs, one for sine component and other for cosine component.

3.4 THE PROPOSED INTELLIGENT TECHNIQUE FOR HARMONICS ESTIMATION

The separable least squares (SLS) algorithm has been utilized for optimal harmonic estimation. SLS utilized specifically to estimate the amplitudes and phases of the harmonics to minimize the error between the actual signal and the estimated signal.

The minimization of the sum of the squares of the residuals is the target when the least square method is utilized instead of solving the equations exactly [204]-[206].

Let *t* be the independent variable and let *y(t)* represents an unknown function of *t* that is to be estimated or approximated.

$$y_i = y(t_i);\ i = 1, \dots, m \tag{3.14}$$

Where *m* represents the number of observations. The objective is to model *y(t)* by a linear combination of *n* basis functions as follows:

$$y(t) \approx \beta_1\ \emptyset_1(t) + \cdots + \beta_n\ \emptyset_n(t) \tag{3.15}$$

In matrix-vector notation, the model is

$$y = X\beta \tag{3.16}$$

$$x_{i,j} = \emptyset_j(t_i) \tag{3.17}$$

Where *X* represents the design matrix, it usually has more rows than columns.

The basic functions $\emptyset_j(t)$ can be nonlinear functions of *t*, but the unknown parameters, β_j , appear in the model linearly.

$$X\beta = y \tag{3.18}$$

The system of linear equations as in (3.18) is over determined if there are more equations than unknowns. The basic functions might also involve some nonlinear parameters; $\alpha_1, \dots, \alpha_p$ the problem is separable if it involves both linear and nonlinear parameters [204]:

$$y(t) \approx \beta_1\ \emptyset_1(t, \alpha) + \cdots + \beta_n\ \emptyset_n(t, \alpha) \tag{3.19}$$

$$x_{i,j} = \emptyset_j(t_i, \alpha) \tag{3.20}$$

The residuals are the differences between the observations and the model:

$$r_i = y_i - \sum_{1}^{n} \beta_j \emptyset_j(t_i, \alpha), \quad i = 1, \dots, m \tag{3.21}$$

Or, in matrix-vector notation,

$$r = y - X(\alpha)\beta \tag{3.22}$$

$$\beta = X^{-1}y \tag{3.23}$$

The simulation results are presented to demonstrate the suitability of the utilized technique for online harmonics estimation.

3.5 SIMULATION RESULTS

The simulation module is shown in Figure 3.4 for a simple power system consisting of a two bus three phase system with a full wave six-pulse bridge rectifier at the load bus [207]. Test signal, denoted as $x_o(t)$, is a distorted voltage signal taken from the load bus in the test system and it is shown in Figure 3.5. The frequencies and phases of the harmonics of the test signal are listed in Table 3.1.

The test signal is sampled 100 samples per cycle from a 60-Hz voltage signal. A Gaussian noise is employed in simulation studies with several signal-to-noise ratios (SNR). Furthermore, at the end of this section, the results of all considered algorithms have been tabulated in terms of processing time and percentage of error.

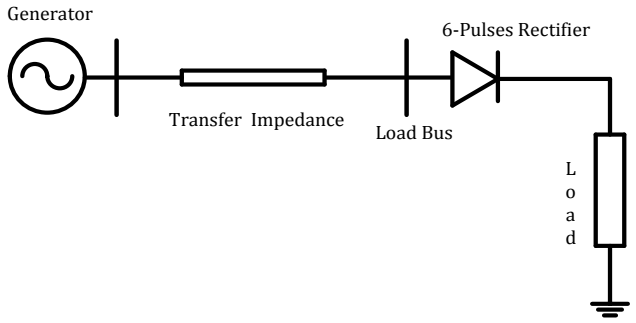

Figure 3.4: Simple power system, two-bus architecture with six-pulse full-wave bridge rectifier supplying the load.

TABLE 3.1
HARMONIC CONTENT OF THE TEST SIGNAL.

Harmonic Order	Amplitude (p.u.)	Phase (rad)
Fundamental (60 Hz)	0.950	-0.03
5^{th} (300 Hz)	0.090	1.43
7^{th} (420 Hz)	0.043	0.14
11^{th} (660 Hz)	0.030	-2.57
13^{th} (780 Hz)	0.033	2.84

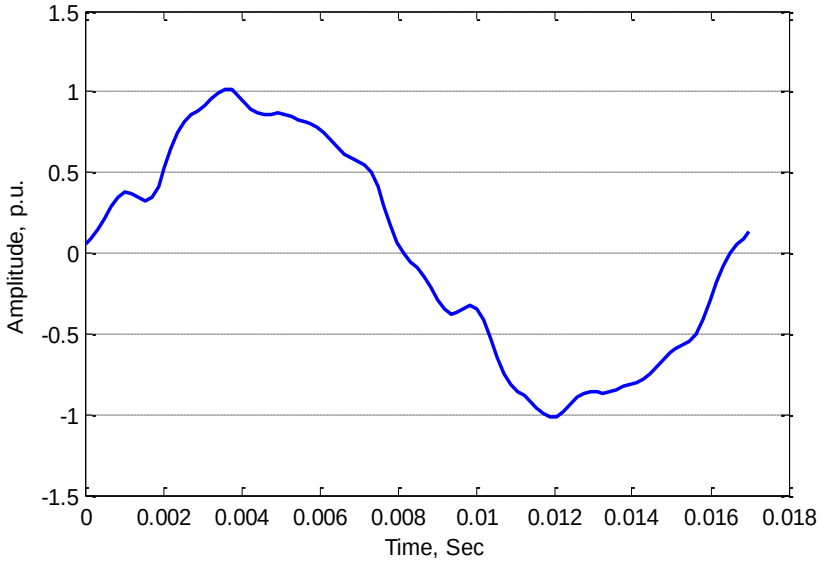

Figure 3.5: Sample distorted signal.

3.5.1 The Hybrid RCGA-LS Technique

In hybrid RCGA-LS, a variable size is selected as 5 genes. To estimate 5 variables the chromosome size is taken as 50. The RCGA-LS is run for a maximum of 200 generations. However, it is observed that the algorithm converged to the final solution in less than 200 generations with mutation probability 10% and crossover probability 80%.

The waveform is reconstructed using the obtained results and then compared with the actual waveform. The results of these graphical comparisons are depicted in Figure 3.6. The estimated and actual signals are almost identical even with a high noise. The performance index of RCGA-LS for the objective function is shown in Figure 3.7. The performance index indicates that the convergence occurs after approximately 50 iterations.

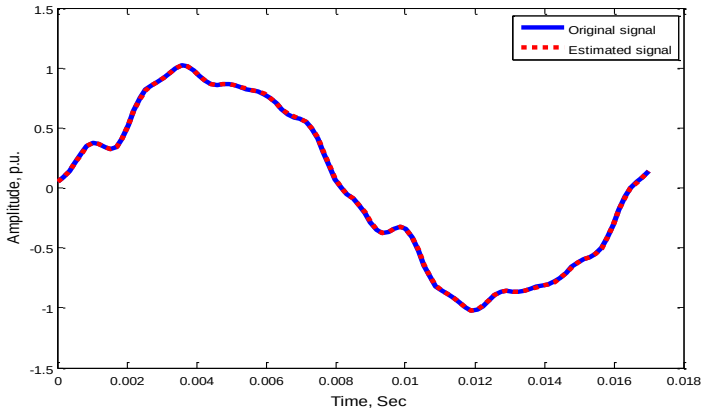

(a)

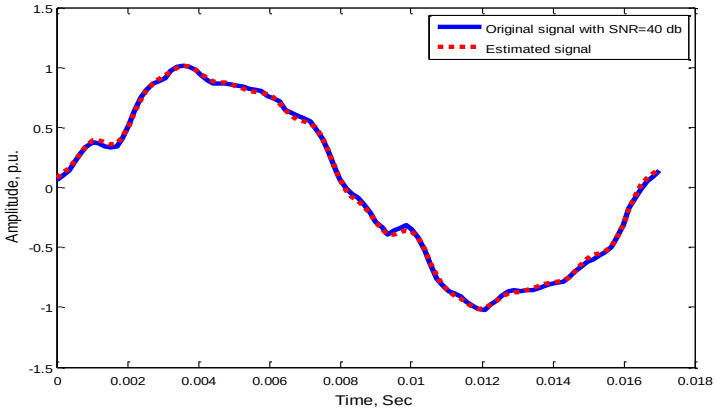

(b)

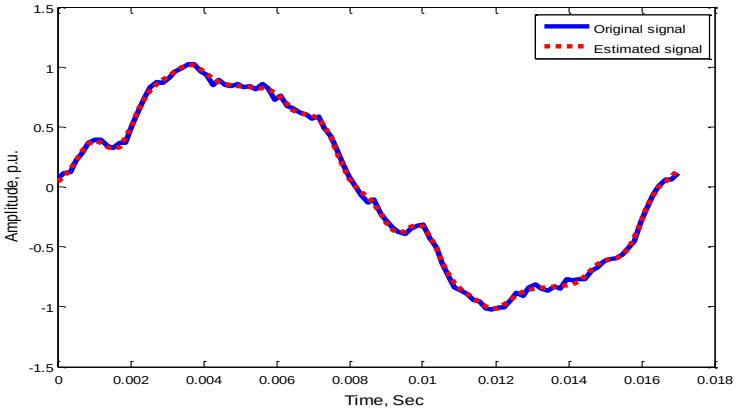

(c)

Figure 3.6: The actual and estimated waveforms for all harmonics using RCGA-LS.
(a) No noise. (b) SNR=40 dB. (c) SNR=30 dB.

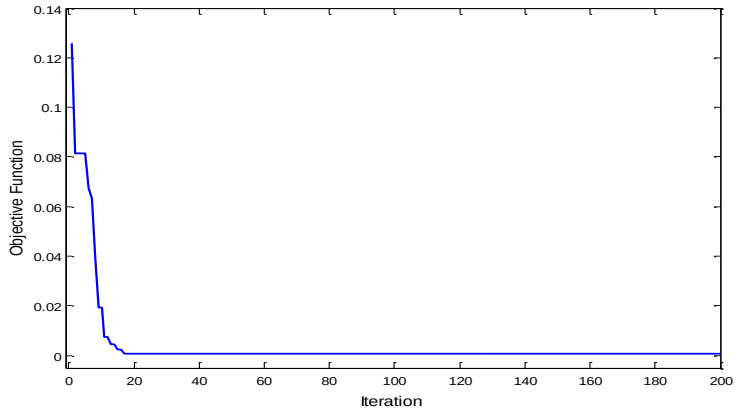

(a)

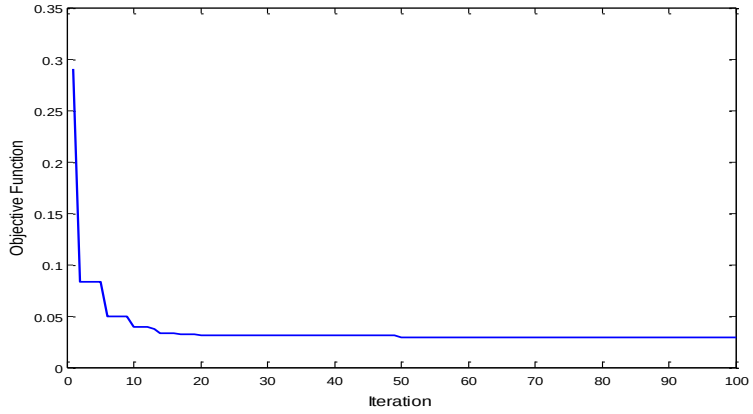

(b)

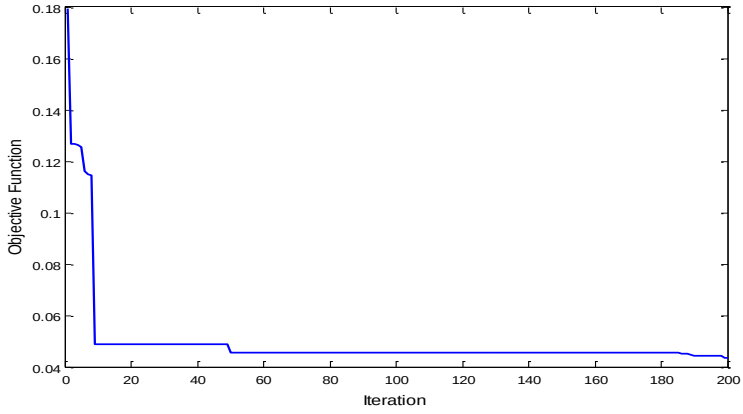

(c)

Figure 3.7: Performance index of objective function for RCGA-LS technique.

(a) No noise. (b) SNR=40 dB. (c) SNR=30 dB.

3.5.2 The Hybrid PSO-LS Technique

The parameters of this technique are chosen as follows: population size is 50, number of iterations is 200, and inertia weight is 0.98. The waveform reconstructed from the estimated harmonics is compared with the actual waveform and the results are shown in Figure 3.8. As can be seen from Figure 3.8, the reconstructed waveform is almost corresponding to the original signal shape for all considered conditions. Figure 3.9 shows the fitness curves of the hybrid PSO-LS technique for the objective function, the convergence occurs after 30 iterations approximately. The convergence of hybrid PSO-LS technique is faster than the convergence of hybrid RCGA-LS technique.

3.5.3 The Adaline Technique

The results of harmonics estimation via the adaptive neural network are used to reconstruct the waveforms. The graphical comparisons between the original test signal and the estimated signal are depicted in Figure 3.10. The estimation of waveform with the adaptive neural network gives accurate results even in the presence of noise.

3.5.4 The Proposed Algorithm

The results of the proposed SLS algorithm for optimal harmonics estimation are compared with original test signal graphically as shown in Figure 311. The results

show that, the proposed algorithm can maintain the identical shape of the original signal under all considered conditions.

3.5.5 Discussion of the Results

The results of the four tested techniques are compared together in terms of the computation time and the accuracy. The results show that, the fastest technique in the harmonics estimation is the proposed one as listed in Table 3.2.

The proposed technique provides results with excellent accuracy for estimating the harmonics even in noisy environment as listed in Tables 3.3 and 3.4. Figure 3.12 shows the graphical comparison between the actual harmonics magnitude and the estimated magnitude using the SLS technique.

The simulation results demonstrate the suitability and capability of the proposed technique for online harmonics estimation. The simulation work is carried out on a PC with processor Intel Core 2 Duo CPU 2.66 GHz, RAM 2 GB, and 32-bit operating system.

TABLE 3.2
COMPARISON OF THE COMPUTATION TIME OF COMPUTING TECHNIQUES.

Technique	Computing Time (s)
RCGA-LS	6.516
PSO-LS	2.781
Adaline	0.780
SLS	0.474

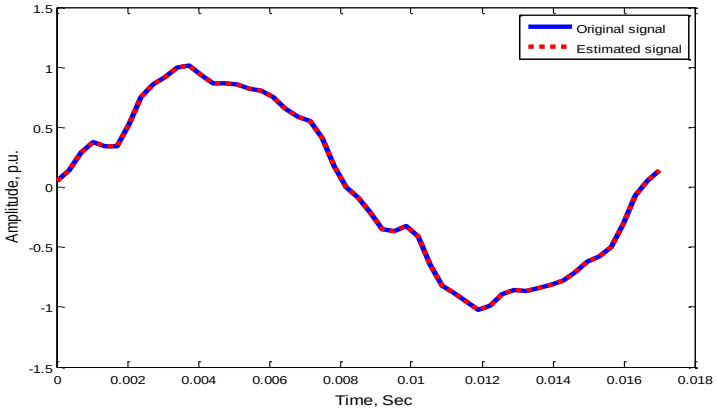

(a)

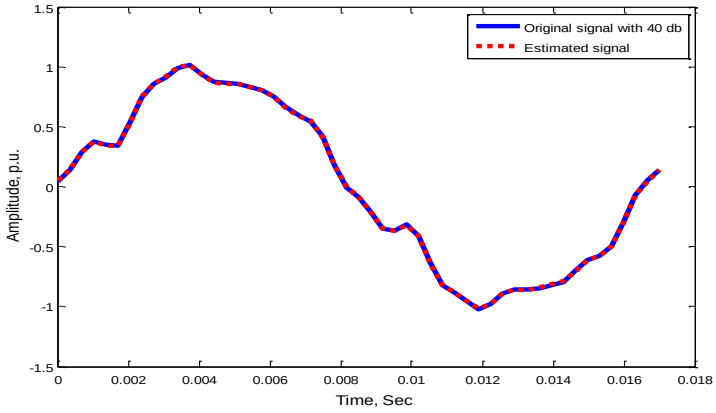

(b)

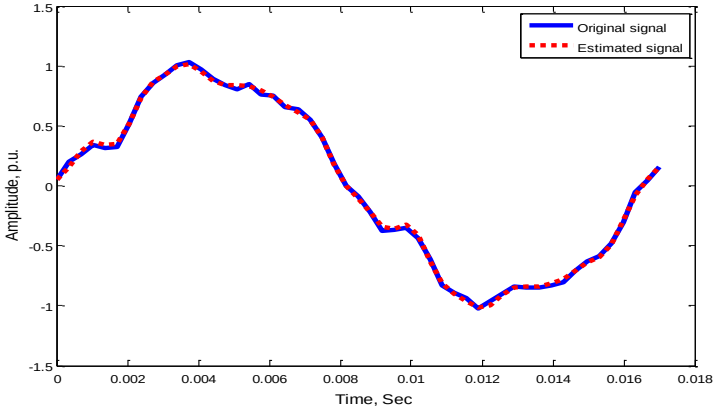

(c)

Figure 3.8: The actual and estimated waveforms using PSO-LS algorithm.
(a) No noise. (b) SNR=40 dB. (c) SNR=30 dB.

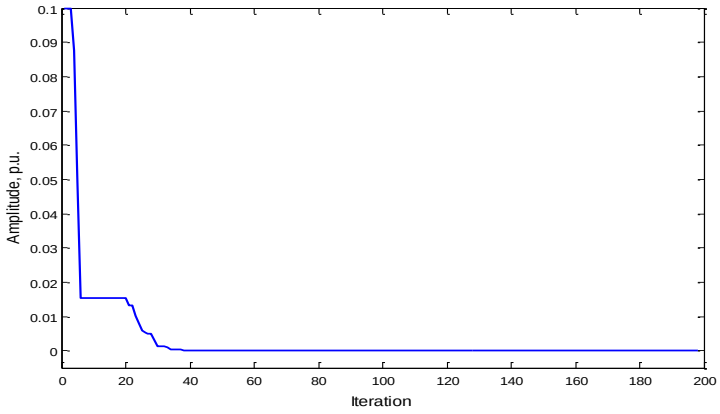

(a)

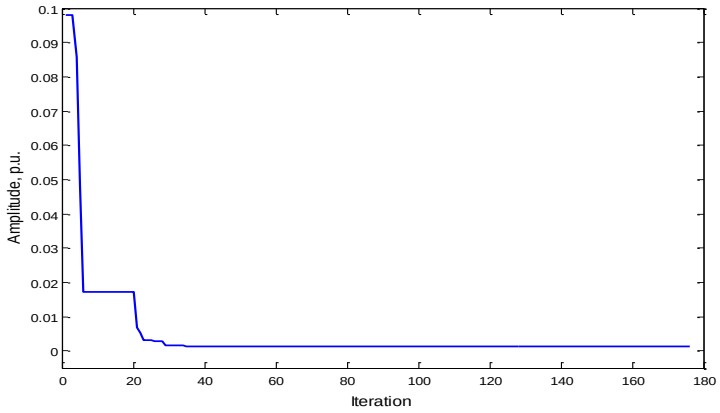

(b)

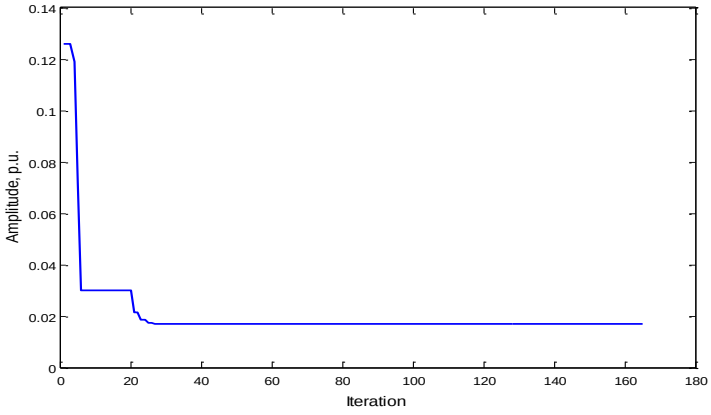

(c)

Figure 3.9: Performance index of objective function for hybrid PSO-LS. (a) No noise. (b) SNR=40 dB. (c) SNR=30 dB.

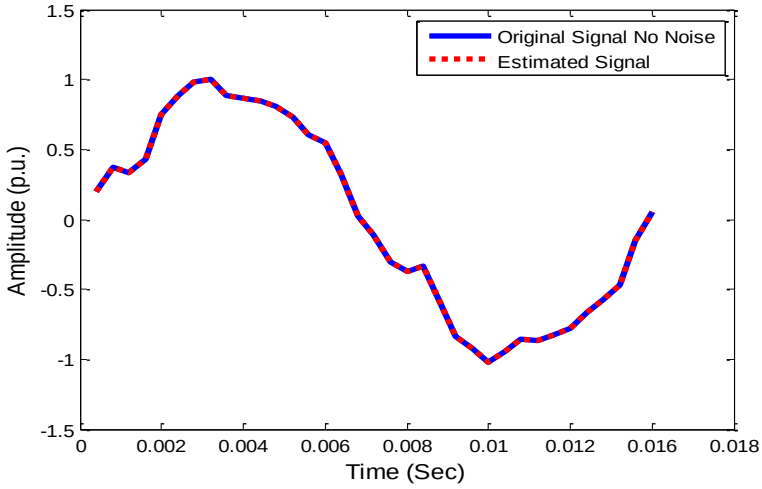

(a)

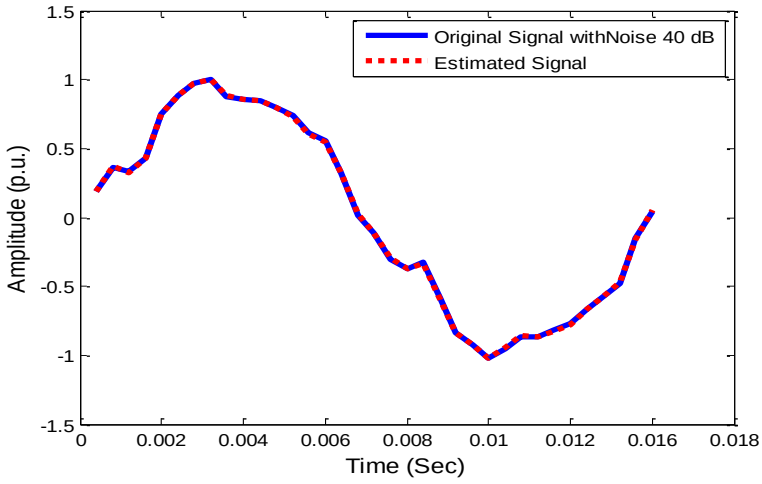

(b)

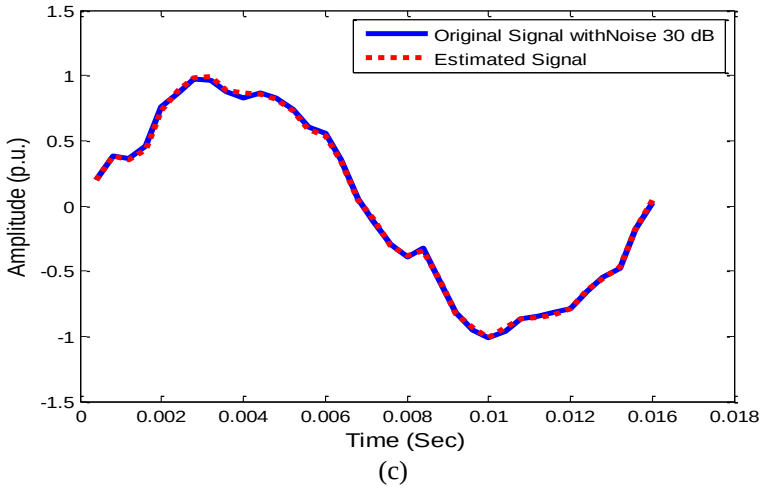

(c)

Figure 3.10: The actual and estimated waveforms using Adaline.

(a) No noise. (b) SNR=40 dB. (c) SNR=30 dB.

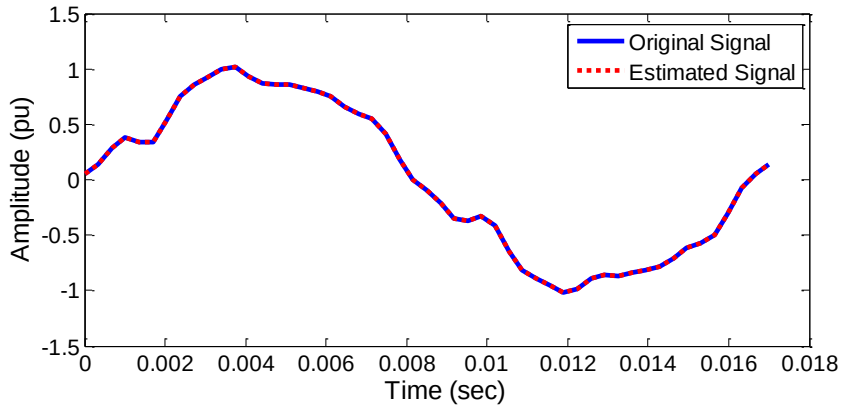

(a)

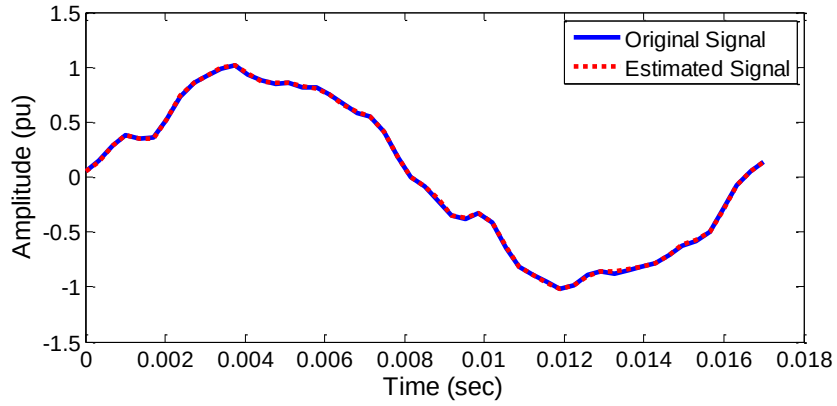

(b)

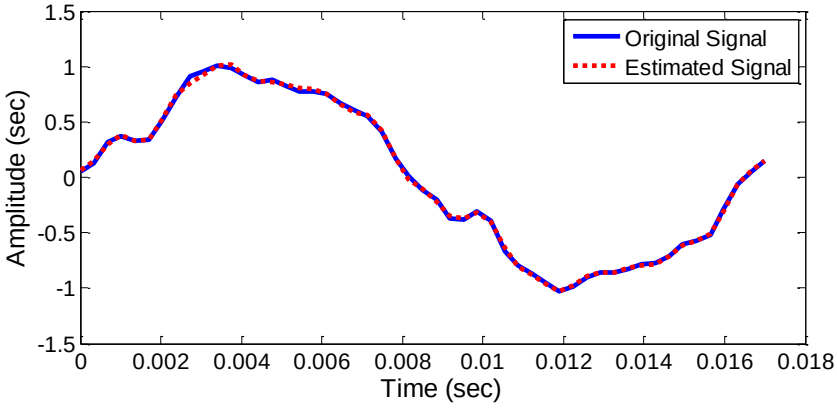

(c)

Figure 3.11: The actual and estimated waveforms using SLS algorithm.

(a) No noise. (b) SNR=40 dB. (c) SNR=30 dB.

TABLE 3.3
COMPARISON OF THE ERRORS IN THE RESULTS OF COMPUTING TECHNIQUES.

	RCGA-LS	PSO-LS	Adaline	SLS
No noise	0.001	0.000	0.000	0.000
With SNR = 40 dB	0.029	0.001	0.001	0.002
With SNR = 30 dB	0.043	0.017	0.009	0.011
With SNR = 20 dB	0.268	0.376	0.433	0.109

TABLE 3.4
ESTIMATED HARMONICS CONTENTS USING THE PROPOSED SLS TECHNIQUE

Harmonic Order	Actual		Estimated							
			Without noise		*With SNR=40dB*		*With SNR=30dB*		*With SNR=20dB*	
	A pu	Φ rad	A pu	Φ rad	A pu	Φ rad	A pu	Φ rad	A pu	Φ rad
Fundamental (60 Hz)	**0.95**	**-0.03**	**0.95**	**3.10**	**0.95**	**3.10**	**0.95**	**3.10**	**0.93**	**3.08**
5th (300 Hz)	**0.09**	**1.43**	**0.09**	**1.43**	**0.09**	**1.44**	**0.09**	**1.41**	**0.11**	**1.29**
7th (420 Hz)	**0.04**	**0.14**	**0.04**	**3.27**	**0.04**	**3.22**	**0.04**	**3.22**	**0.05**	**3.36**
11th (660 Hz)	**0.03**	**-2.57**	**0.03**	**3.71**	**0.03**	**3.73**	**0.03**	**3.70**	**0.03**	**3.37**
13th (780 Hz)	**0.03**	**2.84**	**0.03**	**2.83**	**0.03**	**2.85**	**0.04**	**2.94**	**0.04**	**2.65**

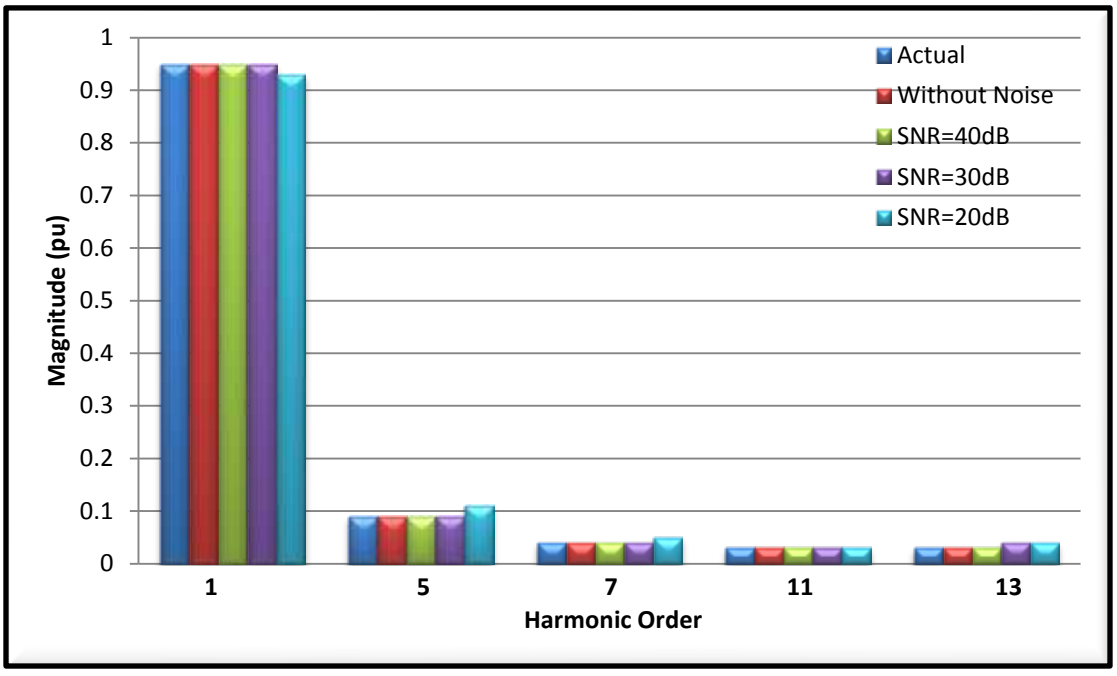

Figure 3.12: The actual and the estimated harmonics amplitude using SLS.

CHAPTER FOUR

RMS-BASED METHODS FOR POWER QUALITY MONITORING

In this chapter, several rms-based calculation methods are proposed and utilized to detect and track the voltage events. The accuracy and efficiency of different rms voltage calculation methods have been investigated. Several cases for voltage events are considered to examine the effectiveness of the proposed methods. The simulation and experimental results of the proposed methods are compared with those of the conventional methods.

4.1 CONVENTIONAL RMS CALCULATION METHODS

Generally, the rms value can be calculated if the waveform is sampled as follows.

$$V_{rms} = \sqrt{\frac{1}{N}\sum_{i=1}^{N} {v_i}^2} \tag{4.1}$$

Where N is the number of samples per cycle and v_i is the sampled voltages in time domain.

The following approaches can be used to calculate the rms value of a voltage waveform:

- rms value calculation using one cycle sampling windows of the voltage waveform with different sliding window methods.
- rms value calculation using half-cycle sampling windows of the voltage waveform with different sliding window methods.

Figure 4.1 shows the calculation methods of rms values using *N* samples per-cycle with different refresh rates. These rates are: every sample, every half cycle, and every one cycle.

RMS #	**Window size (N sample per cycle)**								
RMS #1	1	2	3	…	N/2	…	N-2	N-1	N
RMS #2	2	3	4	…	N/2 +1	…	N-1	N	N+1
RMS #3	3	4	5	…	N/2 +2	…	N	N+1	N+2
…	…	…	…	…	…	…	…	…	…
RMS #N	N	N+1	N+2				2N-2	2N-1	2N
…	…	…	…	…	…	…	…	…	…

(a)

RMS #	**Window size (N sample per cycle)**								
RMS #1	1	2	3	…	N/2	…	N-2	N-1	N
RMS #2	N/2	N/2 +1	N/2 +2	…	N	…	3N/2 -2	3N/2 - 1	3N/2
RMS #3	3N/2	3N/2 +1	3N/2 +2	…	2N	…	2N -2	2N -1	2N
…	…	…	…	…	…	…	…	…	…

(b)

RMS #	**Window size (N sample per cycle)**								
RMS #1	1	2	3	…	N/2	…	N-2	N-1	N
RMS #2	N	N+1	N+2	…	3N/2	…	2N -2	2N - 1	2N
…	…	…	…	…	…	…	…	…	…

(c)

Figure 4.1: Sliding window methods for calculating the rms values with sampling window *N* samples. (a) Sample to sample sliding, (b) Half- cycle sliding and (c) One cycle sliding.

Figure 4.2 shows the calculation methods of rms values using *N/2* samples each half cycle with different refresh rates like each sample or each half cycle.

The methods of sliding window and the sampling windows size have an important effect in calculating and updating the rms values. Most of the existing monitoring devices obtain the magnitude variation from the rms value of voltages [196]-[197].

RMS #	**Window size (N/2 sample per ½ cycle)**								
RMS #1	1	2	3	…	N/4	…	N/2 -2	N/2 -1	N/2
RMS #2	2	3	4	…	N/4 +1	…	N/2 -1	N/2	N/2+1
RMS #3	3	4	5	…	N/4 +2	…	N/2	N/2 +1	N/2 +2
…	…	…	…	…	…	…	…	…	…
RMS #N	N/2	N/2 +1	N/2 +2		3N/4		N-2	N-1	N
…	…	…	…	…	…	…	…	…	…

(a)

RMS #	**Window size (N/2 sample per ½ cycle)**								
RMS #1	1	2	3	…	N/4	…	N/2 -2	N/2 -1	N/2
RMS #2	N/2	N/2 +1	N/2 +2	…	3N/4	…	N -2	N - 1	N
…	…	…	…	…	…	…	…	…	…

(b)

Figure 4.2: Measuring rms values with Half-cycle sample window,
(a) Sample to sample sliding and (b) Half-cycle sliding window.

4.2 THE PROPOSED QUADRATURE METHOD

Similar to the conventional methods, the proposed quadrature method calculates the rms value based on the sampled time-domain voltage. However, it uses only two samples per half cycle with 90 degrees shift between them as shown in Figure 4.3. This is done by using the following equations [198], [199].

$$v(t) = V_p \, sin(wt) \tag{4.2}$$

$$S_1 = V_p \, sin(\theta) \tag{4.3}$$

$$S_2 = V_p \, sin(\theta + \pi/2) \tag{4.4}$$

$$S_2 = V_p \, cos(\theta) \tag{4.5}$$

$${S_1}^2 + {S_2}^2 = {V_p}^2\left(sin^2(\theta) + cos^2(\theta)\right) \tag{4.6}$$

$$\sqrt{{S_1}^2 + {S_2}^2} = \sqrt{{V_p}^2} \tag{4.7}$$

$$\sqrt{{S_1}^2 + {S_2}^2} = V_p \tag{4.8}$$

$$V_{rms} = \frac{V_p}{\sqrt{2}} = \frac{\sqrt{{S_1}^2 + {S_2}^2}}{\sqrt{2}} \tag{4.9}$$

v(t), V_p and V_{rms} are instantaneous, peak, and rms values of the voltage waveform. S_1 and S_2 are the 1st and 2nd samples, respectively.

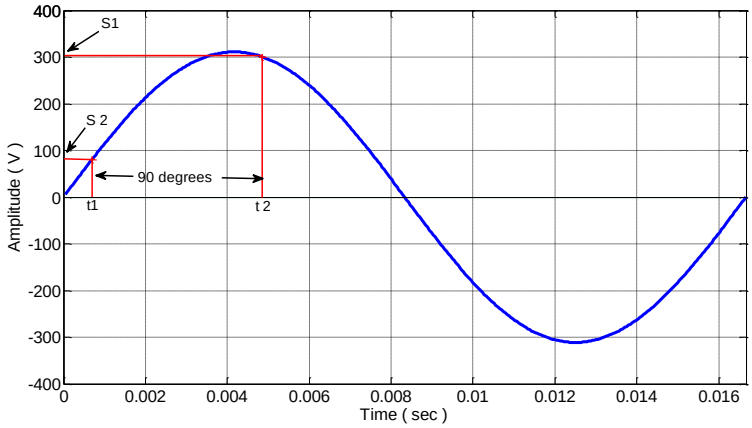

Figure 4.3: Two samples per half-cycle used by the proposed method.

The proposed approach has been implemented in Matlab and LabVIEW to demonstrate its effectiveness.

4.3 SIMULATION RESULTS AND DISCUSSIONS

To examine the effectiveness and robustness of the proposed quadrature method for estimating the magnitude and duration of the voltage events, three voltage events have been considered: sag, interruption and swell. The results of the proposed method are compared with the conventional rms calculation methods. In this study, a 6-cycles event is applied. The sampling rate considered is 166 samples per cycle:

4.3.1 Case1: Voltage Sag Event

As per IEEE definition [110], Voltage sag occurs when rms voltage decreases to value between 10% and 90% of nominal rms voltage for duration from 0.5 cycles to 1.0 min. A 50% reduction in the voltage magnitude is considered in this study. For

the testing purposes of the proposed quadrature method, sample to sample sliding window method has been used to calculate the rms values of the voltage waveform. Figure 4.4 shows the performance of the proposed method at zero time. In this case, the detected duration by the proposed method is 101.34 ms with deviation of 1.34 ms from the exact duration of 100 ms.

For comparison purposes, the conventional sliding window methods shown in Figure 4.1, have been employed to calculate the rms values of the voltage waveform for the same event. Figure 4.5 presents the results obtained by *N* samples per cycle with various sliding window sizes. It was observed that the best result was achieved for the case of sample to sample sliding window where the duration of the event is estimated as 108.24 ms. This gives rise to an error 8.24 ms which is too high as compared to that of the proposed quadrature method.

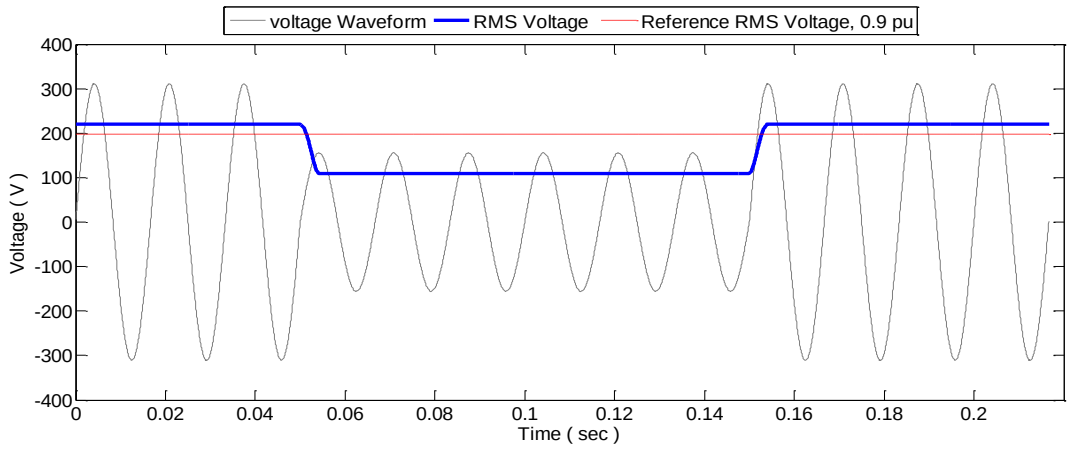

Figure 4.4: rms voltage using Quadrature method with sample to sample sliding method.

It is obvious that the proposed method is much more accurate than the conventional methods. The best accuracy of rms value calculation is achieved with sliding window of sample-to-sample for all sampling windows. Table 4.1 presents the performance of the methods presented with all possible starting times of the sag event.

The results given in Table 4.1 demonstrate clearly that the best results are achieved by the proposed method for any expected starting time of the voltage sag. The average error observed is 1.39 ms and standard deviation equals to 0.05 which demonstrate the robustness of the proposed quadrature method. The performance of different methods is compared in Figure 4.7. It can be seen that the proposed method has the best performance in terms of detection accuracy.

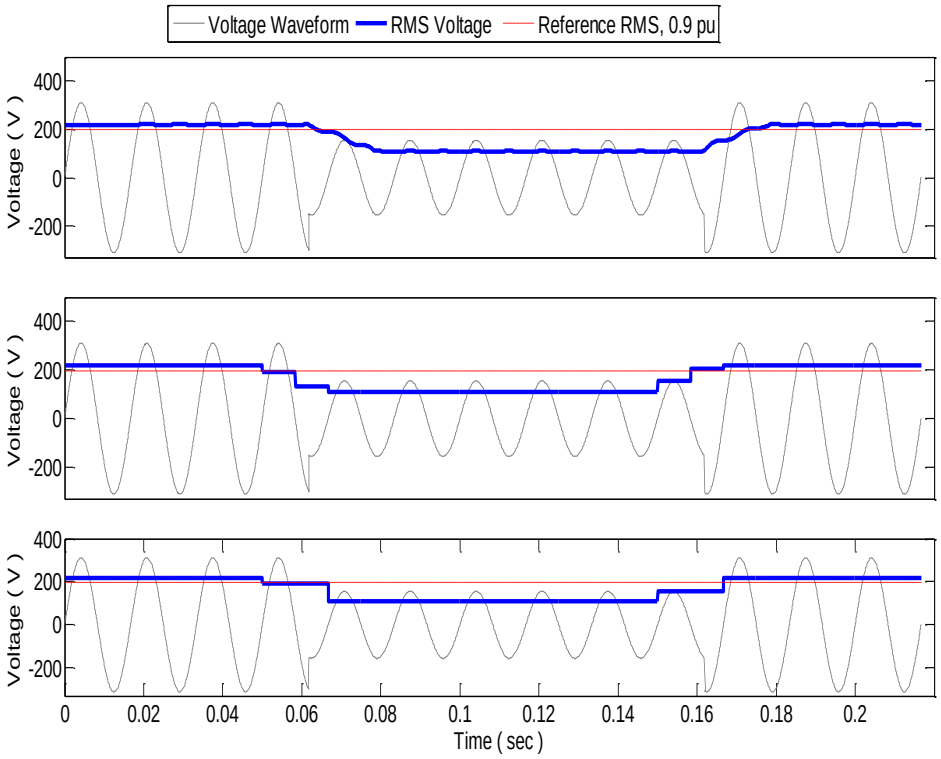

Figure 4.5: N sample per cycle method: (a) sliding window of each sample, (b) Half- cycle sliding window and (c) a cycle sliding window.

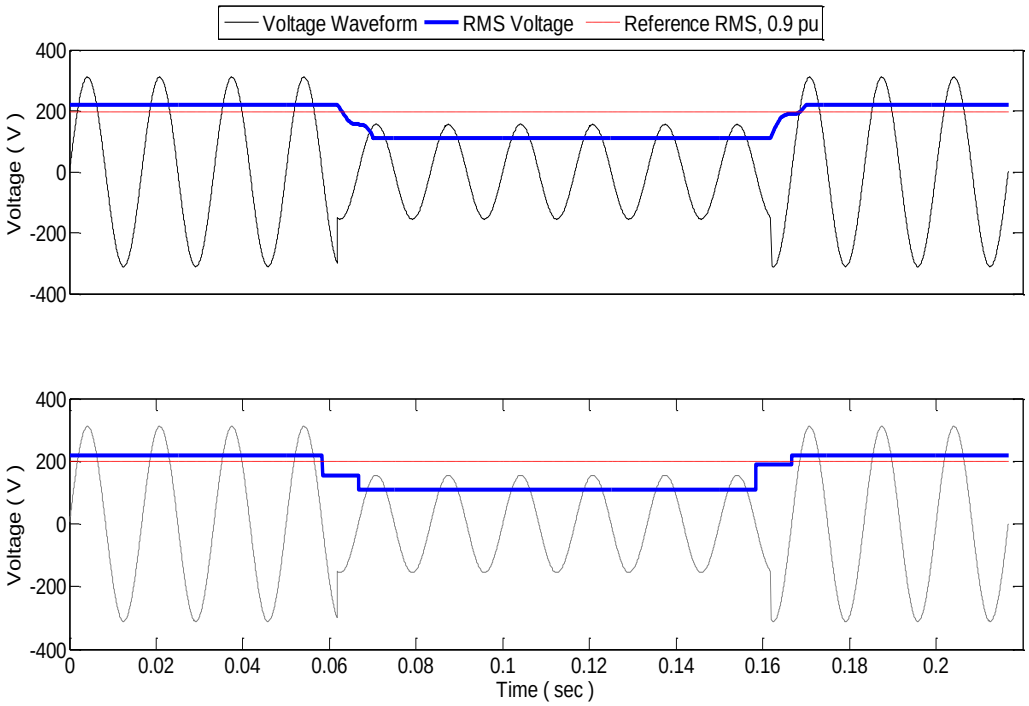

Figure 4.6: rms value calculation using *N/2* sample per half- cycle: (a) sliding window of each sample and (b) Half-cycle sliding window.

The results of the half cycle sliding window and the complete cycle sliding window methods are less accurate as the estimated duration of the event is 108.34 ms and 116.67 ms respectively. Figure 4.6 presents the results obtained by *N/2* sample per half-cycle method with various sliding windows. It was observed that the best result was achieved for the case of sample to sample sliding window where the duration of the event is estimated as 105.65 ms with an error of 5.65 ms.

TABLE 4.1
COMPARISON BETWEEN THE ACHIEVED RESULTS OF THE METHODS FOR VOLTAGE SAG.

Electrical degrees from cross zero point of instantaneous voltage waveform	*rms calculation methods*		
	Proposed Quadrature (ms)	N/2 samples per half-cycle (ms)	N samples per cycle (ms)
0	101.34	102.09	108.20
15	101.34	102.13	108.20
30	101.34	102.09	108.24
45	101.39	102.18	108.24
60	101.44	102.64	108.24
75	101.44	105.84	108.29
90	101.44	106.07	109.08
105	101.44	105.79	108.29
120	101.44	102.64	108.24
135	101.39	102.18	108.24
150	101.34	102.13	108.24
165	101.34	102.13	108.24
180	101.34	102.09	108.20
195	101.34	102.13	108.20
210	101.34	102.09	108.24
225	101.39	102.18	108.24
240	101.44	102.64	108.24
255	101.44	105.84	108.29
270	101.44	106.07	109.08
285	101.44	105.79	108.29
300	101.44	102.64	108.24
315	101.39	102.18	108.24
330	101.34	102.13	108.24
345	101.34	102.13	108.24
Best	**101.34**	**102.09**	**108.20**
Worst	**101.44**	**106.07**	**109.08**
Average	**101.39**	**103.16**	**108.31**
Standard Deviation	**0.05**	**1.63**	**0.24**

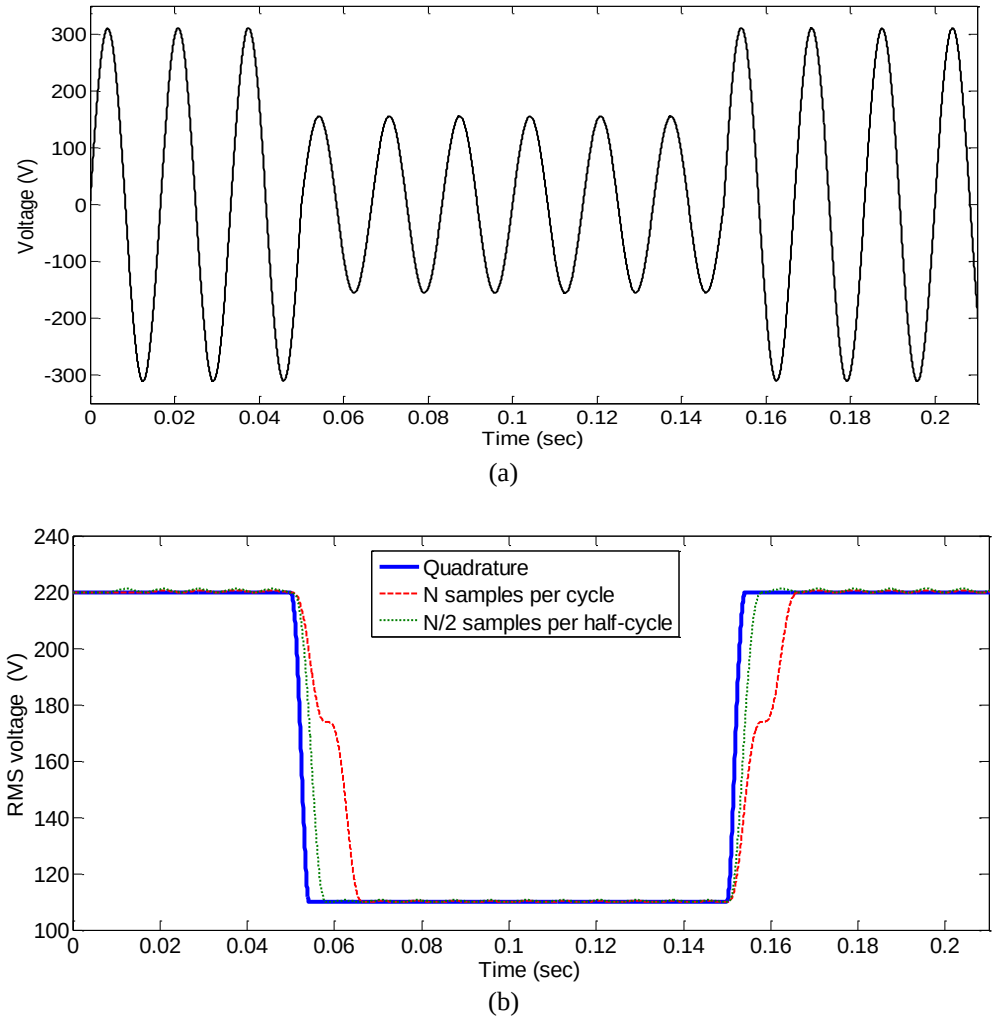

Figure 4.7: rms value calculation methods with sample sliding approach for voltage sag. (a) Instantaneous waveform, (b) rms voltage track

4.3.2 Case 2: Voltage Interruption Event

Voltage interruption occurs when the rms voltage decreases to less than 10% of nominal rms value, for time period not exceeding 1.0 min. In this work, the voltage interruption event considered has amplitude zero. Table 4.2 presents the results of all methods considered with sample sliding window for all possible starting times of the voltage interruption event. The best result was achieved by the proposed method for

any expected starting time of the voltage interruption. The average error observed for duration of the event is 1.85 ms with a standard deviation of 0.03 which confirms the superiority and robustness of the proposed method. It can be seen also that the average error in other methods is much higher than that of the proposed method. In addition, Figure 4.8 shows that the performance of the proposed method is much superior compared to conventional methods in terms of the high speed response in identifying the event.

TABLE 4.2
COMPARISON BETWEEN THE ACHIEVED RESULTS OF THE METHODS FOR VOLTAGE INTERRUPTION

Electrical degrees from cross zero point of instantaneous voltage waveform	*rms calculation methods*		
	Proposed Quadrature (ms)	N/2 samples per half- cycle (ms)	N samples per cycle (ms)
0	101.81	102.83	109.31
15	101.81	102.78	109.31
30	101.85	102.83	109.35
45	101.85	102.97	109.35
60	101.85	105.65	109.49
75	101.90	106.58	110.05
90	101.90	106.72	113.01
105	101.90	106.58	110.00
120	101.85	105.60	109.49
135	101.85	102.97	109.35
150	101.85	102.83	109.31
165	101.81	102.78	109.31
180	101.81	102.83	109.31
195	101.81	102.78	109.31
210	101.85	102.83	109.35
225	101.85	102.97	109.35
240	101.85	105.65	109.49
255	101.90	106.58	110.05
270	101.90	106.72	113.01
285	101.90	106.58	110.00
300	101.85	105.60	109.49
315	101.85	102.97	109.35
330	101.85	102.83	109.31
345	101.81	102.78	109.31
Best	**101.81**	**102.78**	**109.31**
Worst	**101.90**	**106.72**	**113.01**
Average	**101.85**	**104.26**	**109.76**
Standard Deviation	**0.03**	**1.73**	**1.03**

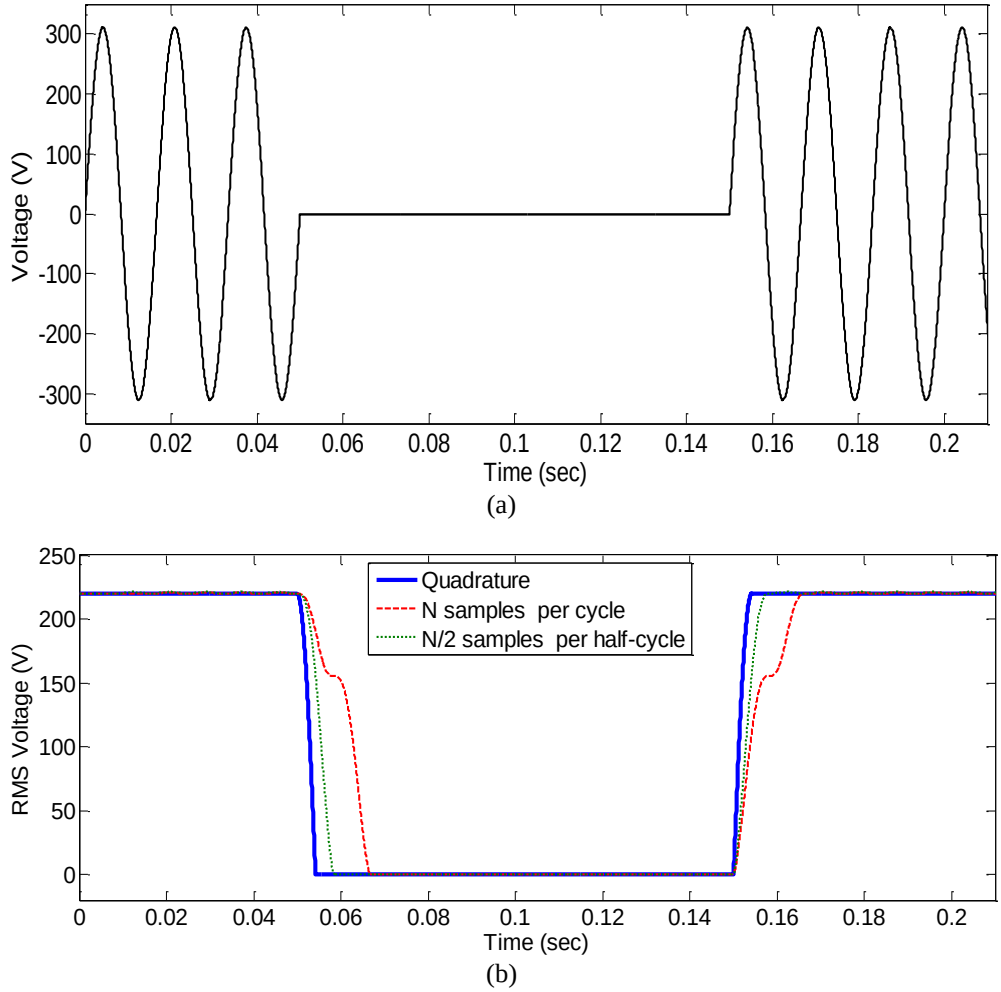

Figure 4.8: rms calculation methods with sample sliding approach for voltage interruption. (a) Instantaneous waveform, (b) rms voltage track

4.3.3 Case 3: Voltage Swell Event

Generally, the voltage swell occurs when the rms voltage increases above 110% and less than 180% of the nominal rms value for durations of 0.5 cycles to 1.0 min. A 150% increasing in the voltage magnitude is considered. Table 4.3 presents the results of the discussed methods with all expected starting time of the voltage swell event.

The best results are obtained with the proposed method for any expected starting time of the voltage swell.

The average error in estimation of the event duration is 0.19 ms with a standard deviation of 0.04. Comparing with conventional methods results, the proposed method is far accurate, superior, and robust. Figure 4.9 shows the performance of all methods. It can be seen that the proposed method is the fastest to identify the event.

TABLE 4.3
COMPARISON BETWEEN THE ACHIEVED RESULTS OF THE METHODS FOR VOLTAGE SWELL.

Electrical degrees from cross zero point of instantaneous voltage waveform	*rms calculation methods*		
	Proposed Quadrature (ms)	N/2 samples per half- cycle (ms)	N samples per cycle (ms)
0	100.14	100.42	103.38
15	100.14	100.42	103.38
30	100.14	100.46	103.29
45	100.19	100.46	100.97
60	100.23	100.51	100.74
75	100.23	100.60	100.70
90	100.23	102.97	100.60
105	100.23	100.60	100.70
120	100.23	100.51	100.79
135	100.19	100.46	101.02
150	100.14	100.46	103.29
165	100.14	100.46	103.43
180	100.14	100.42	103.38
195	100.14	100.42	103.38
210	100.14	100.46	103.29
225	100.19	100.46	100.97
240	100.23	100.51	100.74
255	100.23	100.60	100.70
270	100.23	102.97	100.60
285	100.23	100.6	100.70
300	100.23	100.51	100.79
315	100.19	100.46	101.02
330	100.14	100.46	103.29
345	100.14	100.46	103.43
Best	**100.14**	**100.42**	**100.60**
Worst	**100.23**	**102.97**	**103.43**
Average	**100.19**	**100.69**	**101.81**
Standard Deviation	**0.04**	**0.70**	**1.30**

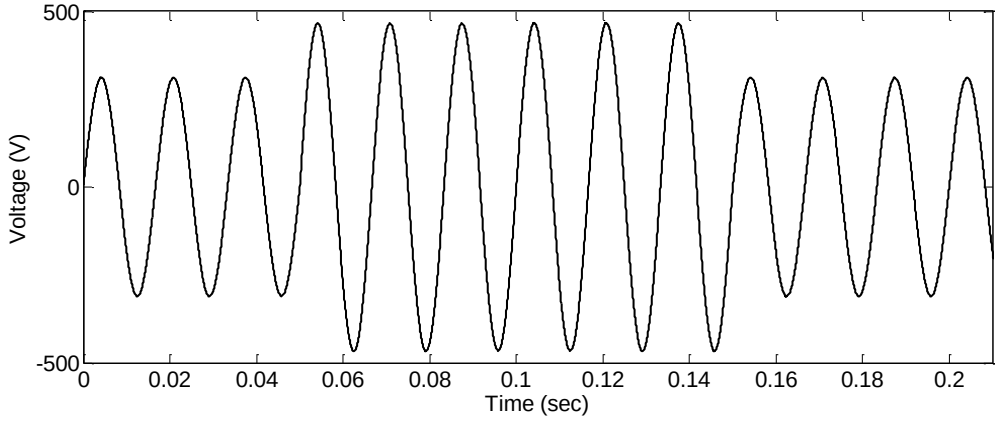

(a)

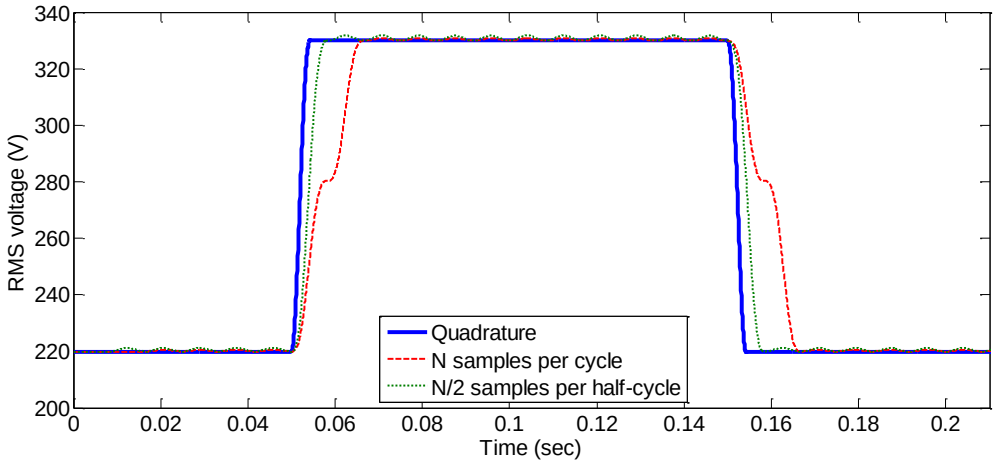

(b)

Figure 4.9: rms calculation methods with sample sliding approach for voltage swell. (a) Instantaneous waveform, (b) rms voltage track.

Table 4.1 shows that the worst performance of the proposed method occurs if the voltage sag event starts close to the positive or negative peaks of the voltage waveform. Figure 4.10(a) shows the performance of the proposed method if the event starts at the positive peak of the waveform. It was observed that there are some ripples in rms calculation at starting time and end time of the event. However, these ripples have limited impact on voltage characterization as the error in the estimated duration is only 1.44 ms. Figure 4.10(b) shows the performance of the proposed

method if the event signal contains harmonics such as 11^{th} and 13^{th} orders with amplitude around 3% of the fundamental component. As can be seen from Figure 4.10(b) there are ripples in the rms tracking voltage by the three considered method, these ripples constitute around 2% of the rms value of the signal.

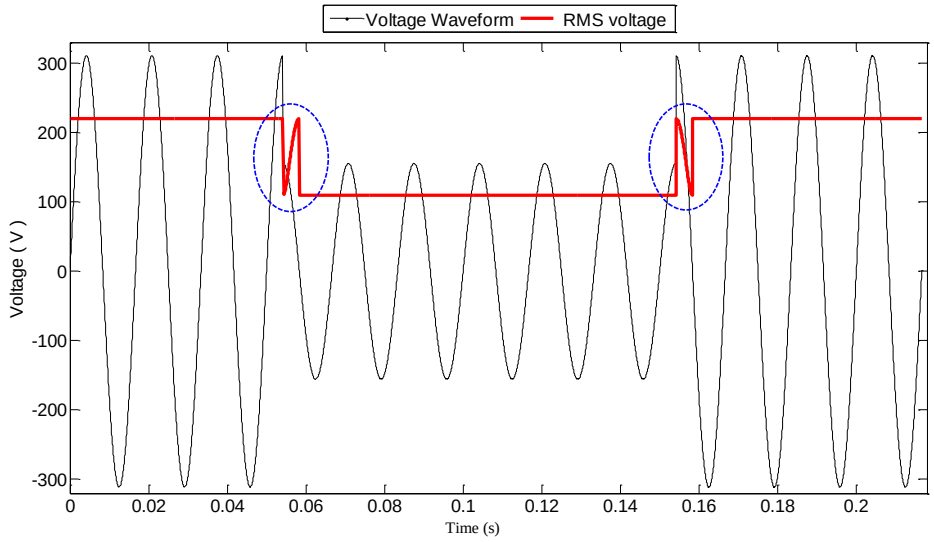

(a)

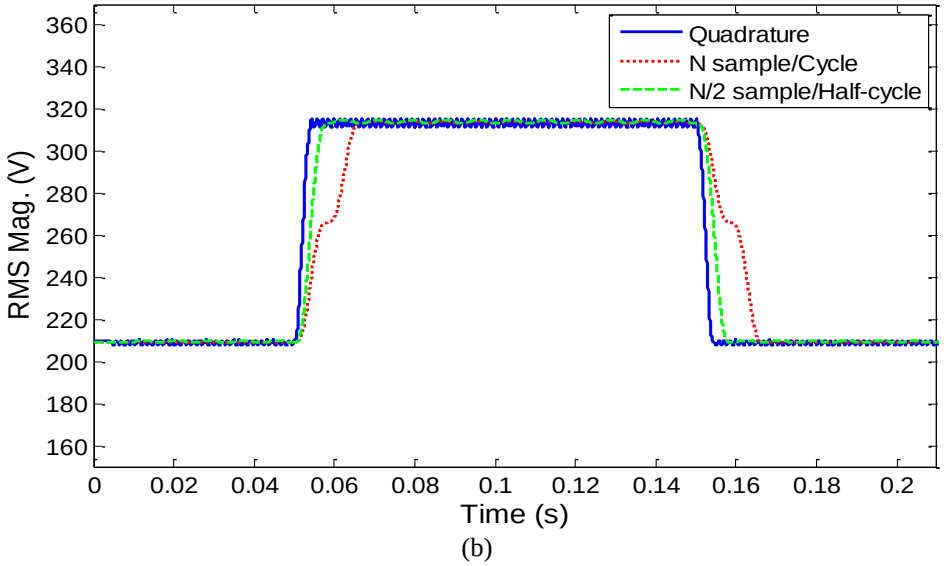

(b)

Figure 4.10: Minor limitation on the quadrature method. (a) Event starts at any point of the voltage waveform; (b) The event signal contains harmonics.

4.4 EXPERIMENTAL SETUP

The experimental setup diagram including all components is shown in Figure 4.11. Furthermore, the experimental setup as carried out in a power quality laboratory is shown in Figure 4.12.

The complete setup structure of the developed PQ monitoring and controlling system is shown in Figure 4.13. The setup consists of:

1. The workstation running LabVIEW software for data acquisition, monitoring, and analysis.
2. The National Instruments CompactRIO which is the heart of the system containing the real-time processor, FPGA chassis, and I/O modules.
3. The power interface containing the measurement transformers (CTs) and control switching circuit (relays).
4. The power distribution network components containing programmable AC power source, programmable electronic loads, static and dynamic loads, and a mitigation device.

Appendix A gives more details about each component of the developed system and the developed graphical user interface as well.

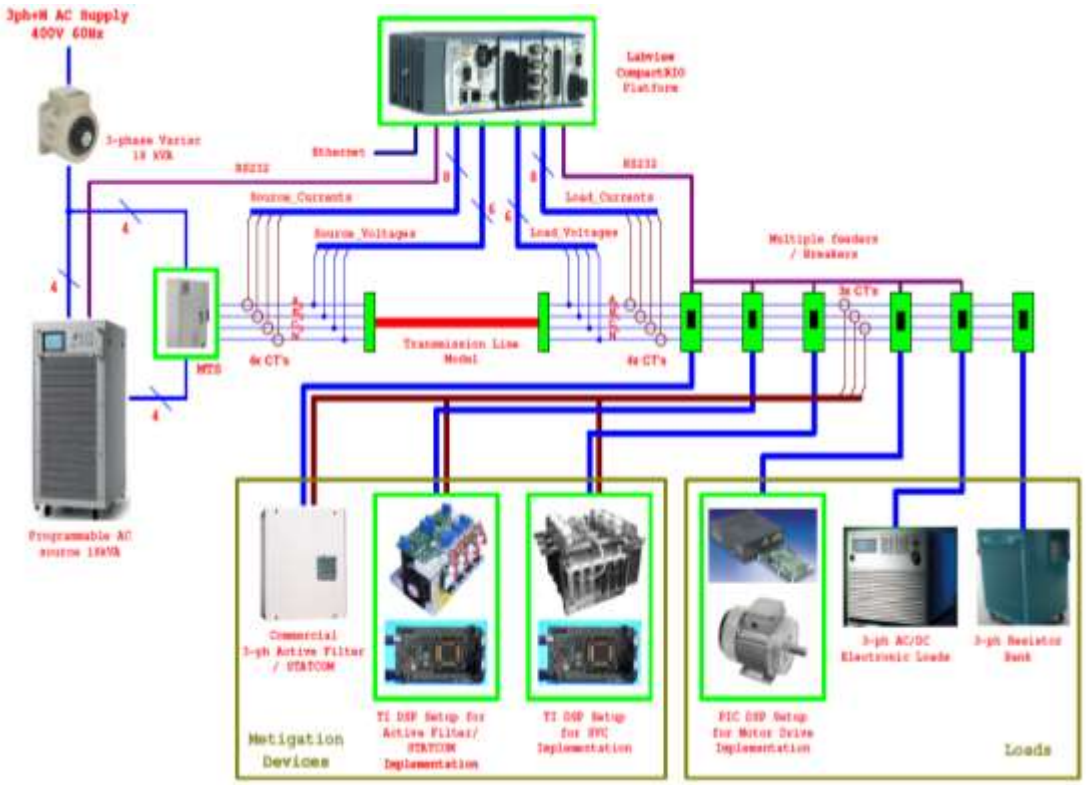

Figure 4.11: The experimental setup diagram.

Figure 4.12: The experimental setup in a power quality laboratory.

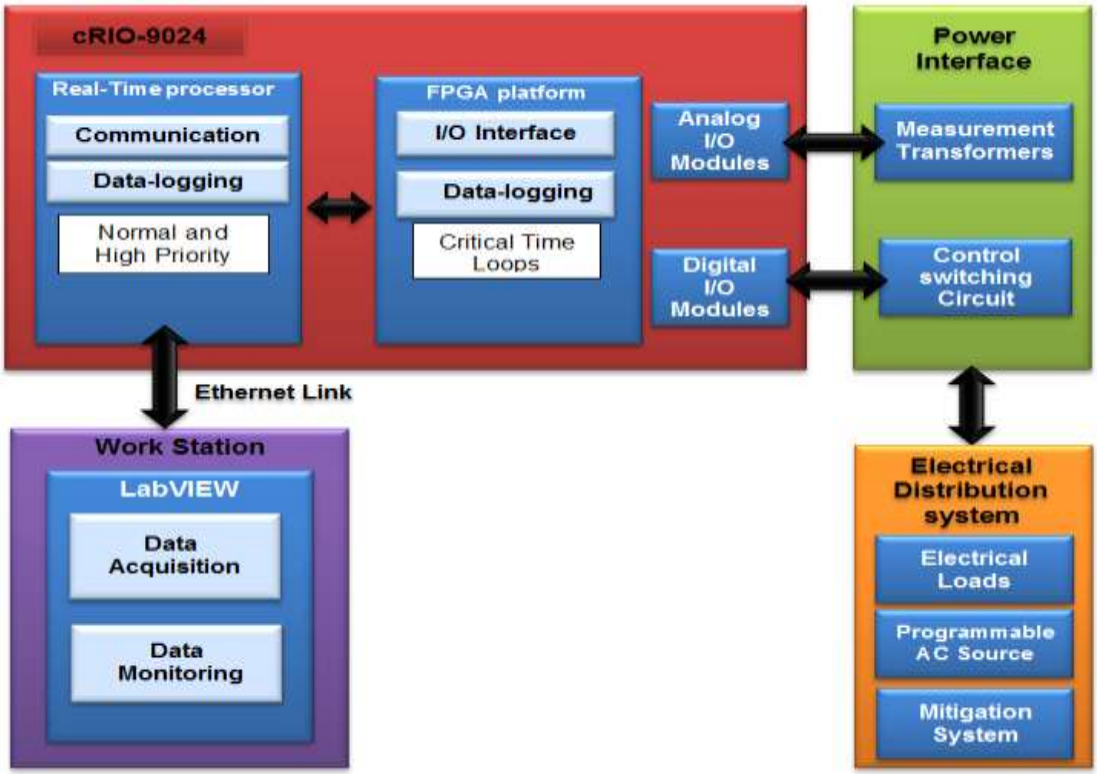

Figure 4.13: Overall structure of the proposed detection and mitigation system

4.5 EXPERIMENTAL RESULTS

Experimental implementation has been carried out to verify the effectiveness of the proposed rms-based method,. The test signal that utilized to evaluate the experimental real-time performance of the proposed technique was generated by the programmable AC power source. The test signals consist of 12 cycles with a rated voltage of 220V, 60Hz and sampling frequency of 10 kHz (166 sample/cycle). The event duration for each considered voltage events is 6 cycles (100 ms) starting at 50 ms and ending at 150 ms.

Experimentally, the results of the proposed quadrature method with a half-cycle sliding window have been compared with the results of the two most common methods that utilize the rms voltage to detect the voltage events. i.e.

1. IEEE method that utilizes the rms voltage measured over one cycle, commencing at a fundamental zero crossing, and refreshed each half cycle [110].
2. The method used until now in the majority of PQ-instruments utilizes rms voltage measured over one cycle and refresh each cycle [210].

Similar to the simulation, the voltage sag, interruption, and swell events are examined experimentally as follow:

4.5.1 Case 1- Voltage Sag Event

Figure 4.14 shows the experimental real time results of the voltage sag detection and characterization based on rms voltage values utilizing the three considered methods. Figure 4.14 (a) shows the instantaneous waveform of three phase voltage sag. The tracking rms voltage using the proposed method, IEEE method and the commercial method are shown in Figure 4.14 (b) to Figure 4.14 (d), respectively. While Figure 4.14 (e) shows the results of the three methods.

The voltage sag occurs at 50 ms and ends at 150 ms, the estimated start time and end time of the voltage sag using the proposed and commercial methods are almost the same which are 51ms and 157ms respectively, while the estimated start time using the IEEE method is 45ms and the end time is 154 ms.

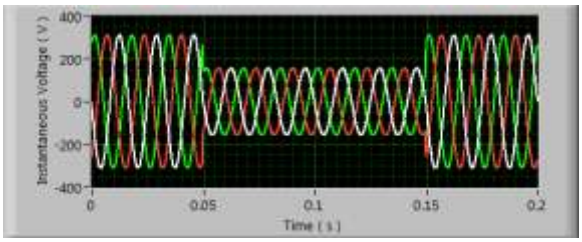

(a)

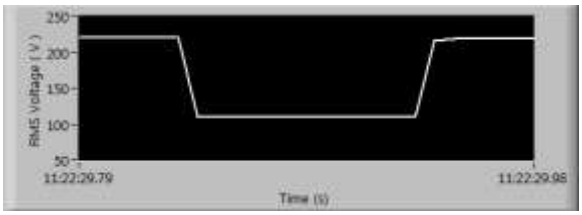

(b)

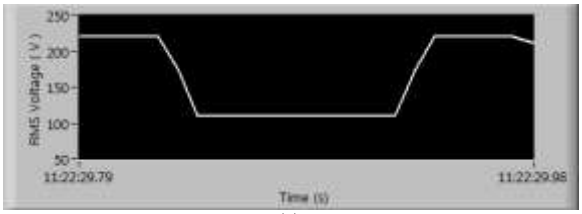

(c)

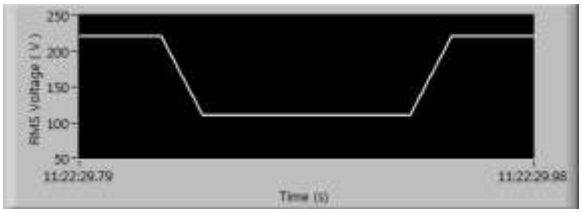

(d)

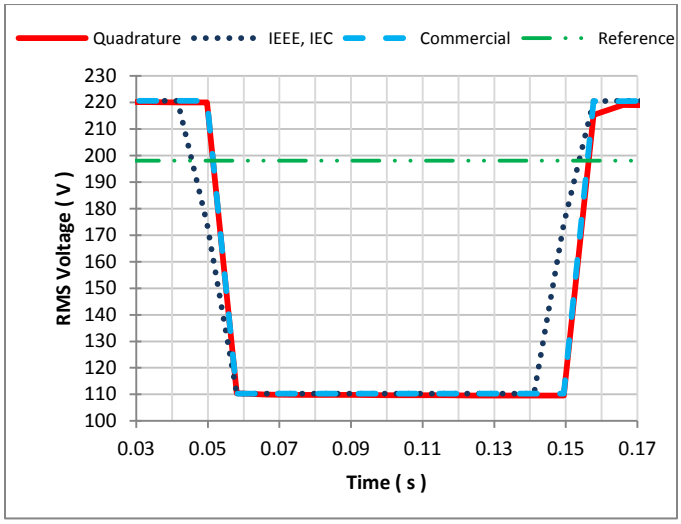

(e)

Figure 4.14: Voltage sag results, (a) instantaneous three phase waveform, (b) rms voltage track via quadrature method, (c) rms voltage track via IEEE method, (d) rms voltage track via commercial method, (e) rms voltage track via the three methods.

4.5.2 Case 2- Voltage Interruption Event

The instantaneous voltage interruption waveforms as well as the real-time tracking rms magnitudes of the event using the considered methods are shown in Figure 4.15. The results of the three methods for trending the voltage interruption and the reference voltage of detecting the voltage interruption that is 0.1pu (22V) are shown in Figure 4.15 (e). The estimated start time of the voltage interruption using the three methods is almost the same, it is 58 ms. The estimated end time using the IEEE method is 141ms whereas the estimated end time using the proposed and commercial methods is the same, it is 150 ms.

4.5.3 Case 3- Voltage Swell Event

Figure 4.16 shows the instantaneous voltage swell waveforms and the real-time results of the three considered methods for detecting and localizing the voltage swell. Figure 4.16 (e) shows the results of the considered methods for detecting the voltage swell and the reference voltage of detecting the event that is 1.1pu (286V). The estimated start time of the voltage swell using the IEEE method is 47 ms, using the proposed method is 52 ms, and using the commercial method is 54 ms. The estimated end time using the IEEE method is 153ms, whereas the estimated end time using the proposed and commercial methods is 155 ms and 166 ms respectively.

The proposed method with half-cycle sliding window gives encouraging results comparing with the results of the other two methods as can be observed from the real-time results of the all considered cases.

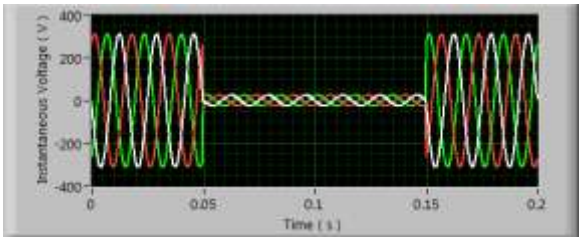

(a)

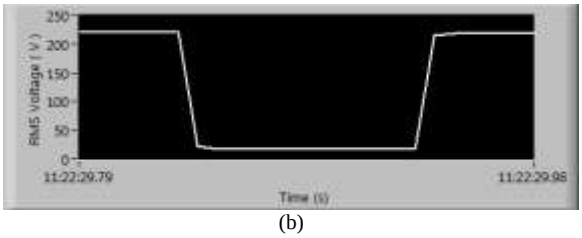

(b)

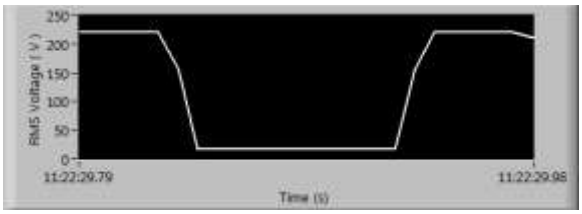

(c)

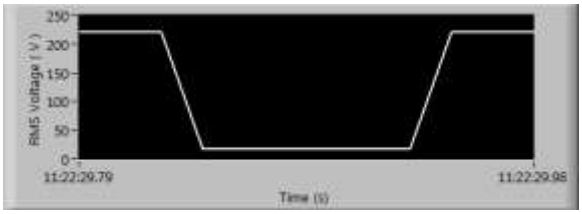

(d)

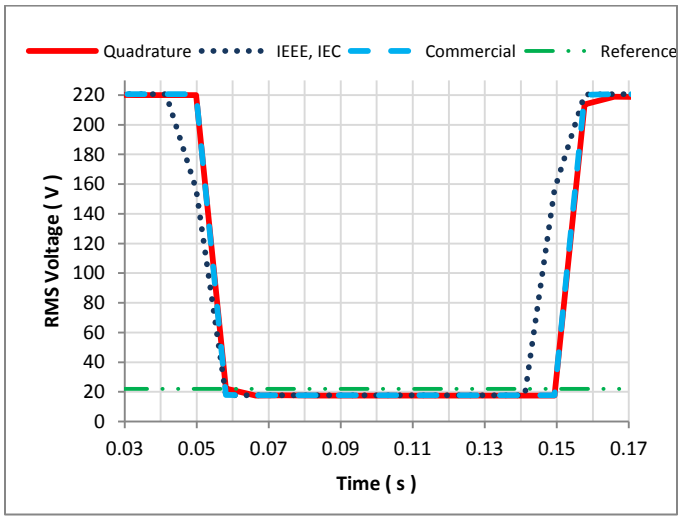

(e)

Figure 4.15: Voltage Interruption results, (a) instantaneous three phase waveform, (b) rms voltage track via quadrature method, (c) rms voltage track via IEEE method, (d) rms voltage track via commercial method, (e) rms voltage track via the three methods.

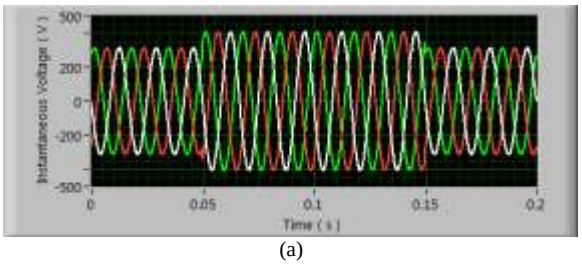

(a)

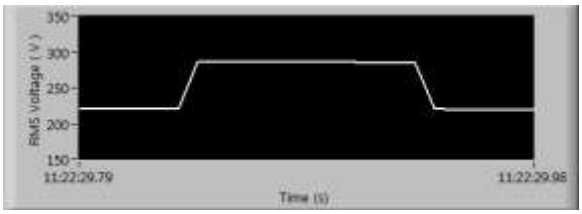

(b)

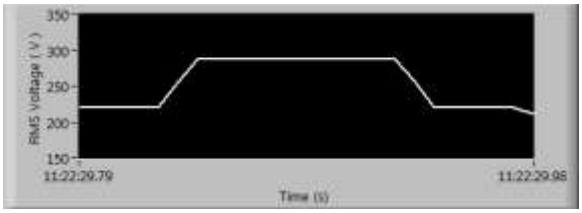

(c)

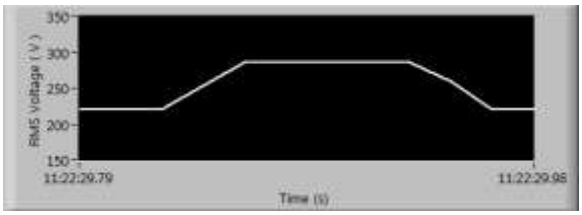

(d)

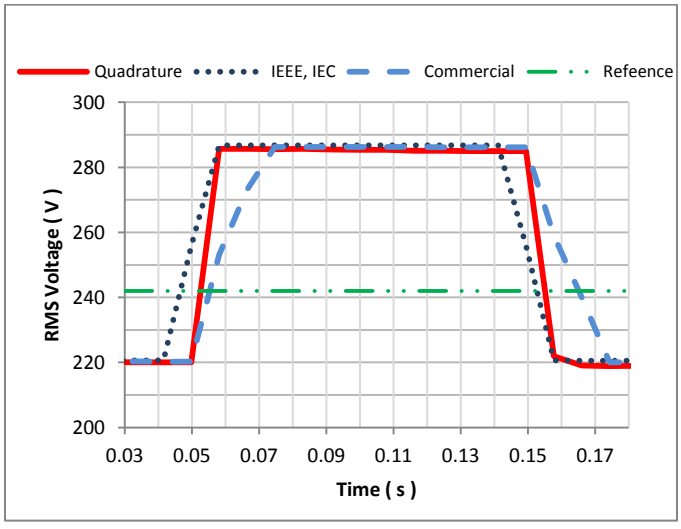

(e)

Figure 4.16: Voltage swell results, (a) instantaneous three phase waveform, (b) rms voltage track via quadrature method, (c) rms voltage track via IEEE method, (d) rms voltage track via commercial method, (e) rms voltage track via the three methods.

4.5.4 Case 4- Multiple Power Quality Events

The proposed method has been examined to characterize multiple voltage events that can occur simultaneously. In this case, double line to ground fault is applied on the distribution system model. The result is a temporary voltage rises on the unfaulted phase, whereas the voltages decrease on the faulted phases, which last for the duration of the fault that is 10-cycles as shown in Fig. 4.17(a). As it can be seen from Fig. 4.17 (b), the proposed method detected the start time and end time for each event with high accuracy as well as it estimated the duration. The results show the capability of the proposed method for real time detection of multiple voltage events simultaneously.

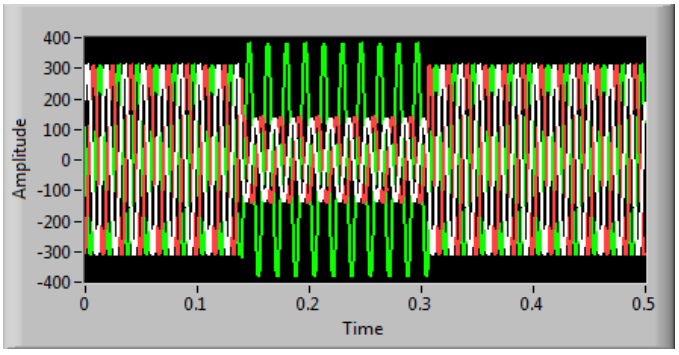

(a)

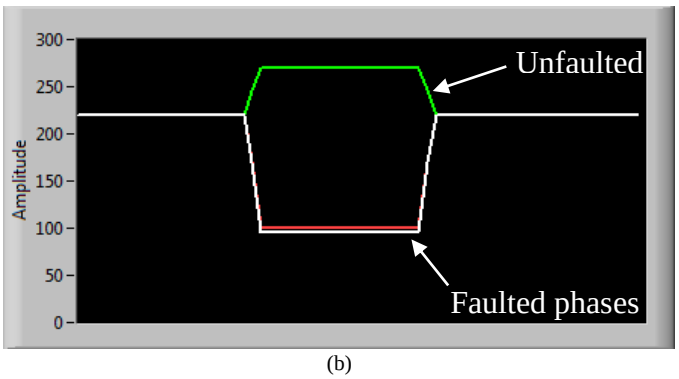

(b)

Fig. 4.17: Voltages during double line to ground fault,
(a) Instantaneous three phase waveform, (b) tracking rms voltage using the quadrature method.

Table 4.4 shows the comparison between the simulation and experimental results of the quadrature method. However, all rms-based detection method has shortcoming, for that reason the research starting using others techniques for voltage event detection such as wavelet multiresolution analysis.

TABLE 4.4
THE PERFORMANCE OF THE QUADRATURE METHOD

The Voltage Event	Actual Duration (ms)	Simulation Results (ms)	Experimental Result (ms)
Sag	**100**	**101.4**	**106**
Swell	**100**	**100.2**	**103**
Interruption	**100**	**101.9**	**92**

CHAPTER FIVE

POWER QUALITY DETECTION USING WAVELET ANALYSIS

This chapter introduces a new detection and classification method for voltage events based on wavelet multiresolution analysis. This chapter also compares the results of the proposed method with that of the conventional method in terms of processing time and percentage error. Furthermore, the experimental results of the proposed method are presented in this chapter.

5.1 INTRODUCTION

In this section, the basic equations of CWT, DWT, and MRA that are used to formulate the proposed method have been described.

5.1.1 Continuous Wavelet Transforms

CWT, that is applied to the signal *x(t),* can be defined as,

$$w(a,b) = \frac{1}{\sqrt{a}} \int_{-\infty}^{\infty} f(t)\, \psi^* \left(\frac{t-b}{a}\right) dt \qquad (5.1)$$

Where

- *a* is the dilation factor.
- *b* is the translation factor.
- *ψ(t)* is the mother wavelet.
- *1/√a* is an energy normalization term that makes wavelets of different scale have the unit of energy.

There are several different wavelet families: Haar, Daubechies, Biorthogonal, Coiflets, Symlets, Morlet, Mexican Hat, and Meyer. Wavelets are classified within a family most often by the number of vanishing moments [53]-[54].

5.1.2 Discrete Wavelet Transforms

The DWT is considerably easier to implement in practical applications when compared to the CWT [55]-[57], [192]. DWT is implemented by using discrete values of the scaling parameter $a = a_0^m$ and translation parameter $b = nb_0a_0^m$, then

$$\psi_{m,n}(t) = a_0^{-m/2}\, \psi(a_0^{-m}t - nb_0) \qquad (5.2)$$

Where *m* indicates frequency location and *n* indicates time location. The simplest choice of a_0 and b_0 are a_0 = 2 and b_0 = 1 to provide a dyadic-orthonormal wavelet transform and the basis for MRA. The number of decomposition levels depends on the number of samples taken by the sampling window, such as $2^s = N$, where *N* and *s*

are the number of samples taken in the sampling window, and the highest scaling level, respectively.

5.1.3 Multiresolution Analysis

In MRA, signal *x(t)* is decomposed in terms of approximations and details that are provided by a scaling function $\emptyset_{m,n}(t)$ and a wavelet $\psi_{m,n}(t)$, respectively

$$\phi_{m,n}(t) = 2^{-(m/2)}\, \phi(2^{-m}t - n) \tag{5.3}$$

$$\psi_{m,n}(t) = 2^{-(m/2)}\, \psi(2^{-m}t - n) \tag{5.4}$$

The scaling function is associated with a low-pass filters (with filter coefficients *h(n)*) and the wavelet function is associated with a high-pass filters (with filter coefficients *g(n)*) , so that

$$\phi(t) = \sqrt{2} \sum_n h(n)\, \phi(2t - n) \tag{5.5}$$

$$\psi(t) = \sqrt{2} \sum_n g(n)\, \phi(2t - n) \tag{5.6}$$

There are some important properties of these filters, including

$$\sum_n h(n)^{\,2} = 1 \quad \text{and} \quad \sum_n g(n)^{\,2} = 1 \tag{5.7}$$

$$\sum_n h(n) = \sqrt{2} \quad \text{and} \quad \sum_n g(n) = 0 \tag{5.8}$$

Filter *g(n)* is an alternating flip of filter *h(n)* and there exists an odd integer *N* such that

$$g(n) = \ (-1)^n \, h(N-n) \tag{5.9}$$

The low-pass filter produces the approximations A_j (low frequency) while the high-pass filter produces the details D_j (high frequency) of the decomposition. First, the original signal is passed through the two filters producing the detail coefficient (D_1) and approximation coefficients (A_1) for $j = 1$ (scale $a = 2^1$). After down-sampling by a factor of 2, the approximation coefficients A_1 are passed through the same filters again to obtain the coefficients for $j = 2$ (scale $a = 2^2$). After another down-sampling, the approximation coefficients A_2 are then filtered again to obtain the next level of coefficients as shown in Figure 5.1.

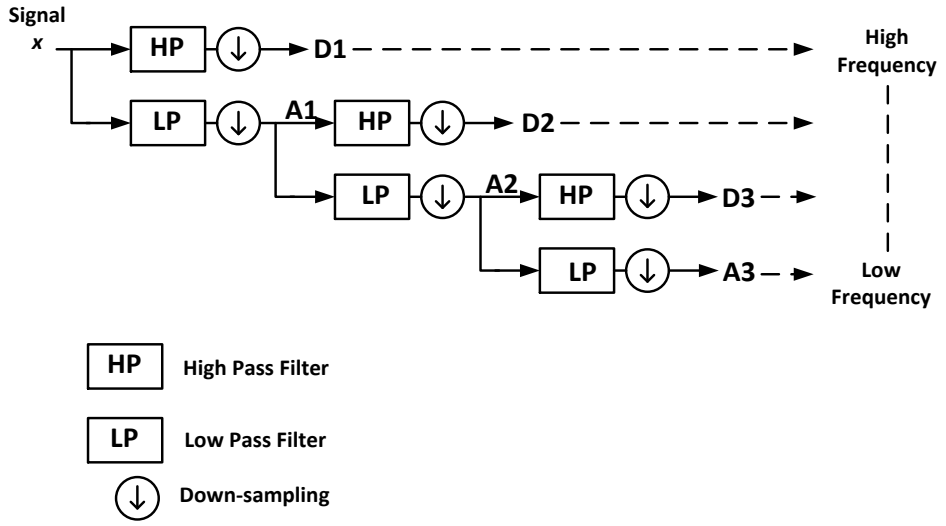

Figure 5.1: DWT Decomposition.

The relationship of the detail and approximation coefficients between two adjacent levels are given as

$$A_{j+1}(k) = \sum_{n} h(n-2k)\, A_j(n) \tag{5.10}$$

$$D_{j+1}(k) = \sum_{n} g(n-2k)\, A_j(n) \tag{5.11}$$

Where A_j and D_j represent the approximation and detail coefficients of the signal at level j respectively. k denotes the coefficient index at each decomposition level.

The MRA decomposition in frequency domain for a signal sampled with 10 kHz can be demonstrated in Figure 5.2. On the right-hand side of Figure 5.2, the typical power quality phenomena of interested are listed [193].

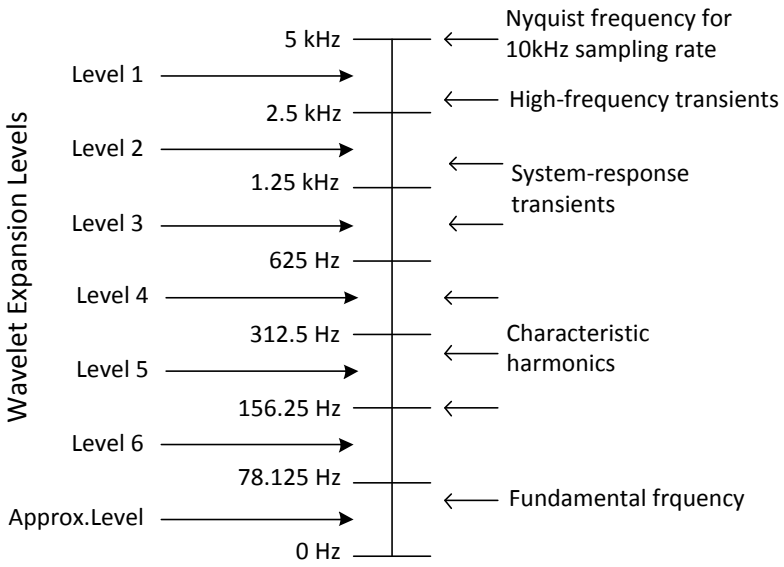

Figure 5.2: Frequency division of DWT filter for 10 kHz sampling rate.

During a transient disturbance, the distorted power signal will generate a discontinuous state at the start and end points of the disturbance duration. Through the first level decomposition of the MRA, will cause the wavelet coefficients D_1 at the start and end points of the disturbance to generate severe variation. Therefore, the start time (t_s) and end time (t_e) of the disturbance duration from the variations in absolute wavelet coefficients D_1 can be easily obtained, and then the disturbance duration (t_t) can be calculated as.

$$t_t = t_e - t_s \tag{5.12}$$

The distribution of energy across the multiple frequency bands forms patterns that have been found to be useful for classifying PQ disturbances. The energy or norm of the signal can be partitioned according to the following:

$$\int |f(t)|^2 \, dt = \sum_k \left|A_{j0}(k)\right|^2 + \sum_{j \le j_0} \sum_k \left|D_j(k)\right|^2 \tag{5.13}$$

These squared wavelet coefficients in the above multiresolution expansion (5.13) to be useful features for identifying PQ disturbances.

5.2 THE PROPOSED METHOD

Generally, a signal f can be decomposed into approximation and details components as follow:

$$f = \sum_k a_{j_0 k} \varphi_{j_0 k} + \sum_{j \le j_0} \sum_k d_{jk} \psi_{jk} \tag{5.14}$$

Where

$$\psi_{jk}(t) = 2^{-j/2}\psi\left(2^{-j}t - k\right) \tag{5.15}$$

$$\varphi_{j_0k}(t) = 2^{-j_0/2}\varphi\left(2^{-j_0}t - k\right) \tag{5.16}$$

ψ(t) and *φ(t)* represent the mother wavelet and the scaling function respectively.

$$d_{jk} = \int f(t)\psi_{jk}(t)dt \tag{5.17}$$

$$a_{j_0k} = \int f(t)\varphi_{j_0k}(t)dt \tag{5.18}$$

It is observed that coefficients corresponding to orthogonal signals are orthogonal sequences. Suppose f , $\tilde{f}$ are orthogonal signals. i.e.

$$\langle f\ , \tilde{f}\rangle = 0\ , \quad \left(\int f(t)\tilde{f}(t)\ dt = 0\right) \tag{5.19}$$

Where

$$f = \sum_{j,k} d_{jk}\psi_{jk} \quad , \qquad \tilde{f} = \sum_{j',k'} \tilde{d}_{j'k'}\psi_{j'k'} \tag{5.20}$$

This yield

$$0 = \langle f\ , \tilde{f}\rangle = \langle \sum_{j,k} d_{jk}\psi_{jk} \quad , \sum_{j',k'} \tilde{d}_{j'k'}\psi_{j'k'}\rangle \tag{5.21}$$

$$0 = \langle f\ , \tilde{f}\rangle = \sum_{j,k}\sum_{j',k'} d_{jk}\ \tilde{d}_{j'k'}\langle\psi_{jk}\ , \psi_{j'k'}\rangle \tag{5.22}$$

Since

$$\langle \psi_{jk} , \psi_{jk'} \rangle = \delta_{jkj'k'} \tag{5.23}$$

Therefore,

$$0 = \sum_{jk} d_{jk} \tilde{d}_{j'k'} \tag{5.24}$$

According to Eqn. (5.24) (d_{jk}) and ($\tilde{d}_{j'k'}$) are orthogonal sequences.

The following notations have been used:

f: Pure signal.

$(d_{jk})_{k \in \mathbb{Z}}$: Wavelet detail coefficients of the pure signal at the scale level *j*.

s: Disturbance signal which is zero outside I_d, that is $s(t) = 0$ for $t \notin I_d$. I_d will be called the support of s .

$(\tilde{d}_{jk})_{k \in \Delta_j}$: Wavelet coefficients of the disturbance signal at the coarsest approximation level j_0 over the disturbance interval I_d, where

$$\Delta_j = \{k: supp\ \psi_{jk} \subseteq I_d\} \tag{5.25}$$

Therefore the pure sinusoidal signal is orthogonal to high frequency disturbances. The same argument is true about the wavelet coefficients. Thus, taking inner product of a pure signal (*f*) with one that has high frequency disturbance (g+h) eliminates the effect of the high frequency disturbance (h). Therefore,

$$\langle f, g + h \rangle = \langle f, g \rangle + \langle f, h \rangle = \langle f, g \rangle. \tag{5.26}$$

The voltage sag, swell, and interruption are scaled versions of the original pure signal over the disturbance period (I_d). Therefore, they should correlate well over I_d with the pure signal at the coarsest approximation level.

To discriminate between the three types of considered disturbances the following procedure is proposed:

- *Compute*

$$\left\|(d_{j_0k})\right\|_{\Delta_{j_0}} = \left(\sum_{k\in\Delta_{j_0}} {d_{j_0k}}^2\right)^{\frac{1}{2}} \tag{5.27}$$

$$\left\|(\tilde{d}_{j_0k})\right\|_{\Delta_{j_0}} = \left(\sum_{k\in\Delta_{j_0}} {\tilde{d}_{j_0k}}^2\right)^{\frac{1}{2}} \tag{5.28}$$

$$r = \frac{\left\|(\tilde{d}_{j_0k})\right\|_{\Delta_{j_0}}}{\left\|(d_{j_0k})\right\|_{\Delta_{j_0}}} \tag{5.29}$$

If $(1-\varepsilon) \le r \le (1+\varepsilon)$ then there is no event, (ε is a preassigned threshold; assumed in this work $\varepsilon = 0.1$ according to the threshold values of voltage sag, swell, and interruption).

If $r > (1+\varepsilon)$ the disturbance corresponds to a swell.

If $\varepsilon \le r < (1-\varepsilon)$ the disturbance corresponds to a sag.

If $r < \varepsilon$, then Compute F_j as

$$F_j = \sum_{k \in \Delta_j} d_{jk}\, \tilde{d}_{jk} \ , \qquad j = 1, \dots, j_0 - 1 \tag{5.30}$$

- *Check the following condition,*

$$\sum_{j=1}^{j_0-1} F_j^2 \leq \varepsilon^2 \tag{5.31}$$

If satisfied then the disturbance corresponds to an interruption. Otherwise, it corresponds to some other high frequency disturbance.

Figure 5.3 shows the flow chart of the proposed approach.

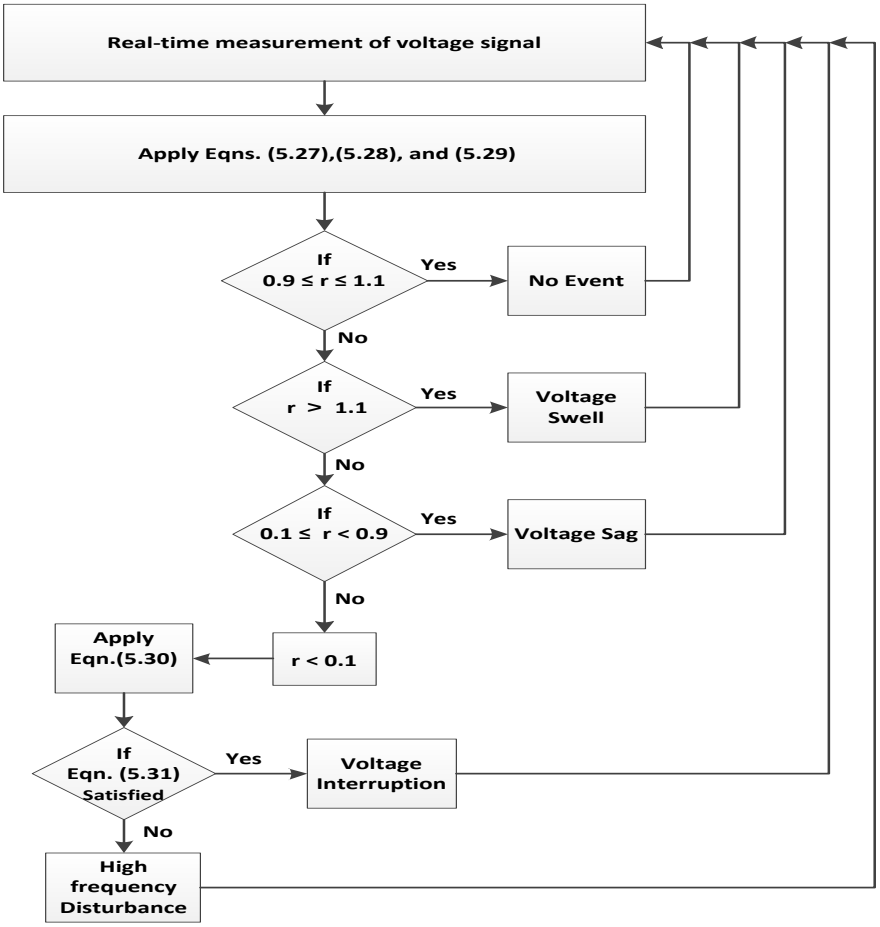

Figure 5.3: The flow chart of the proposed MRA method.

It is worth mentioning that the proposed approach employs Daubechies 6 (db6) as the mother wavelet to detect and classify all the transient disturbances in the distorted signal since it is the most appropriate mother wavelet used to detect the voltage events [194]-[195].

5.3 VALIDATION OF THE PROPOSED METHOD

Conventionally, rms value of voltage can be calculated as follow

$$V_{rms} = \sqrt{{V_{j_0}}^2 + \sum_{j \le j_0} {V_j}^2} \tag{5.32}$$

Where the V_{j0} is the rms voltage value of the coarsest approximation wavelet decomposition level j_0(lowest frequency subband) which includes the fundamental frequency and $\{V_j\}$ are the set of rms voltage values of each detail wavelet decomposition level j higher than or equal to j_0. The conventional method of rms voltage calculation based on DWT utilizes all the detail wavelet decomposition levels as well as the coarsest approximation wavelet decomposition level to calculate the rms voltage as given in (5.32).

Unlike the conventional method, the proposed approach utilizes single level to accomplish the calculation of rms voltage which is the coarsest approximation level that includes the fundamental frequency. According to the execution manner of the proposed and the conventional methods, the proposed method has less complexity than the conventional methods.

The conventional method of rms voltage calculation based on DWT has been applied on test voltage signal that consist of 12 cycles, with 60Hz, 220V and sampling frequency equals to 10 kHz (166 sample/cycle). The applied event is voltage sag with duration equals to 8 cycles (132.8 ms) that occurs at 33.2 ms and ends at 166 ms and its magnitude is 154Vrms. Figure 5.4 displays the first six decomposition levels of the test signal. According to (5.32), V_{j0} represents the rms voltage of the sixth approximation level (A_6) and $\{V_j\}$ represents $\{V_{D1}, V_{D2} \dots V_{D6}\}$, therefore (5.32) can be rewritten as

$$V_{rms} = \sqrt{{V_{A6}}^2 + \sum_{j=1}^{6} {V_{Dj}}^2} \tag{5.33}$$

It is observed from the simulation results that the accuracy of the estimated voltage magnitude for different voltage events using the conventional and the proposed methods are almost the same. The Table 5.1 represents comparison between the conventional and the proposed methods for voltage events characterization in terms of the accuracy percentage. On the other hand, the average execution time for ten runs of the conventional method for analyzing data of one window (12 cycles) is 51 ms, while the average execution time for ten runs of the proposed method for analyzing the same data size is 11 ms. Hence, the proposed method will save more than 78% from the processing time to accomplish the analysis of the voltage events. This makes the proposed method more suitable for online implementation.

TABLE 5.1

ACCURACY PERCENTAGE OF THE PROPOSED AND THE CONVENTIONAL METHODS FOR VOLTAGE EVENTS CHARACTERIZATION

Event Characterization	**Voltage Event**					
	Interruption		*Sag*		*Swell*	
	Conventional	Proposed	Conventional	Proposed	Conventional	Proposed
The Start Time	99.8	99.8	99.8	99.8	99.8	99.8
The Stop Time	99.7	99.7	99.7	99.7	99.6	99.6
The Magnitude	98.7	99.2	99.9	99.8	98.8	99.9

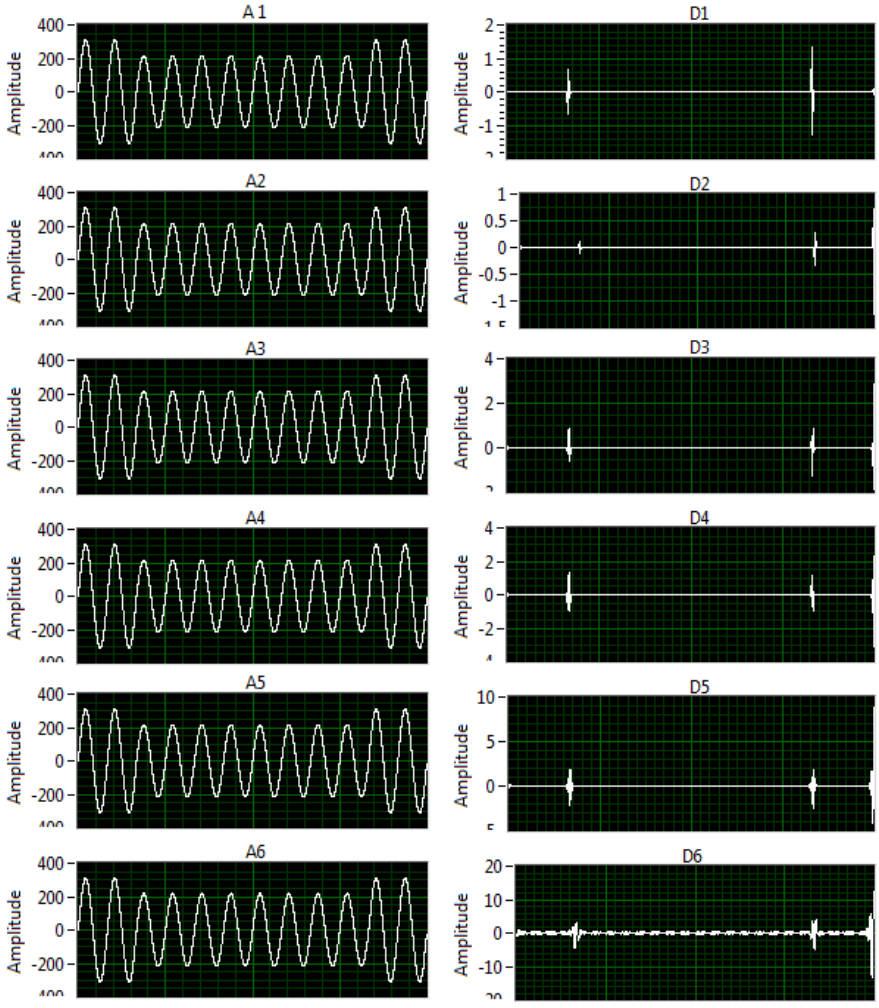

(a) (b)

Figure 5.4: The first six decomposition levels of the test signal.

(a) The approximation levels, (b) The detail levels.

5.4 EXPERIMENTAL RESULTS

The experimental setup for this method is the same setup in the previous chapter. The test signals consist of 12 cycles with rated voltage equals to 220V, 60Hz and sampling frequency equals to 10 kHz (166 sample/cycle). The event duration for each considered case is 8 cycles (132.8 ms) that occurs at 33.2 ms and ends at 166 ms. The experiments include the voltage interruption, sag and swell events. Each event has been carried out for three times with different values. The average results are discussed below.

5.4.1 Case 1- Voltage Interruption Event

Figure 5.5 shows the results of the voltage interruption, and the voltage value during the interruption is 11V (0.05pu). Figure 5.5 (a) shows the details of the voltage event that is detected, characterized, and classified by the proposed method. These details are: 1) the start time of the event that has been estimated at time equals to 33.24 ms with accuracy reach to more than 99.8%, 2) the stop time of the event that has been estimated at time equals to 166.49 ms with accuracy reach to 99.7%, 3) the event duration that is calculated with accuracy more than 99.6%, 4) the estimated magnitude of the voltage interruption event is 10.93V that has been estimated with accuracy reach to more than 99.3%, and 5) the voltage event type.

Figure 5.5 (b) shows measured waveform corresponding to the monitoring system behavior in response to voltage interruption. The first and the second peaks of the

coefficients of the first detail level (D_1) have been utilized to detect the details of the voltage events as shown in Figure 5.5 (c). The waveforms of the distorted and pure voltage signals within the event duration are shown in Figure 5.5 (d) and Figure 7.6 (e) respectively. Figure 5.5 (f) and Figure 5.5 (g) show the coarsest approximation level (A_6) of the distorted and pure voltage signals within the voltage event duration respectively.

5.4.2 Case 2- Voltage Sag Event

Figure 5.6 shows the results of the voltage sag with value equals to 110V (0.5pu). Figure 5.6 (a) shows the details of the voltage sag that has been estimated using the proposed method like the event start time is estimated at time equals to 33.24 ms, the stop time of the event that has been estimated at time equals to 166.49 ms, the event duration is 133.24ms, the estimated magnitude of the voltage sag event is 109.8V.All these details of voltage sag have been estimated using the proposed method with accuracy reach to more than 99.7%. Figure 5.6 (b) shows measured waveform corresponding to the monitoring system behavior in response to voltage sag. Figure 5.6 (c) to Figure 5.6 (g) show the waveforms that are used to characterize and classify the voltage sag.

5.4.3 Case 3- Voltage Swell Event

Figure 5.7 shows the results of the proposed method for detecting, characterizing, and classifying the voltage swell with value equals to 286V (1.3pu). Figure 5.7 (a) shows

the estimated details of the voltage swell such as the start time, the stop time and the duration are 33.24 ms, 166.53 ms, and 133.29 ms respectively. The estimated magnitude of the voltage swell is 285.9 V. All these details of voltage swell have been estimated with an accuracy of more than 99.6%. Figure 5.7 (b) shows measured waveform corresponding to the monitoring system behavior in response to voltage swell. While Figure 5.7 (c) to Figure 5.7 (g) show the waveforms that are used to characterize and classify the voltage swell.

The simulation and experimental results of the proposed MRS for detection the event duration are listed in the Table 5.2. The experimental results showed the same general patterns as simulation results .The results demonstrate the superiority, suitability and capability of the proposed method for real time applications.

TABLE 5.2
DETECTION OF VOLTAGE EVENT DURATION USING THE PROPOSED MRA

Voltage Event	Actual (ms)	Simulation (ms)	Experimental (ms)
Interruption	**132.80**	**133.11**	**133.24**
Sag	**132.80**	**133.14**	**133.24**
Swell	**132.80**	**133.18**	**133.29**

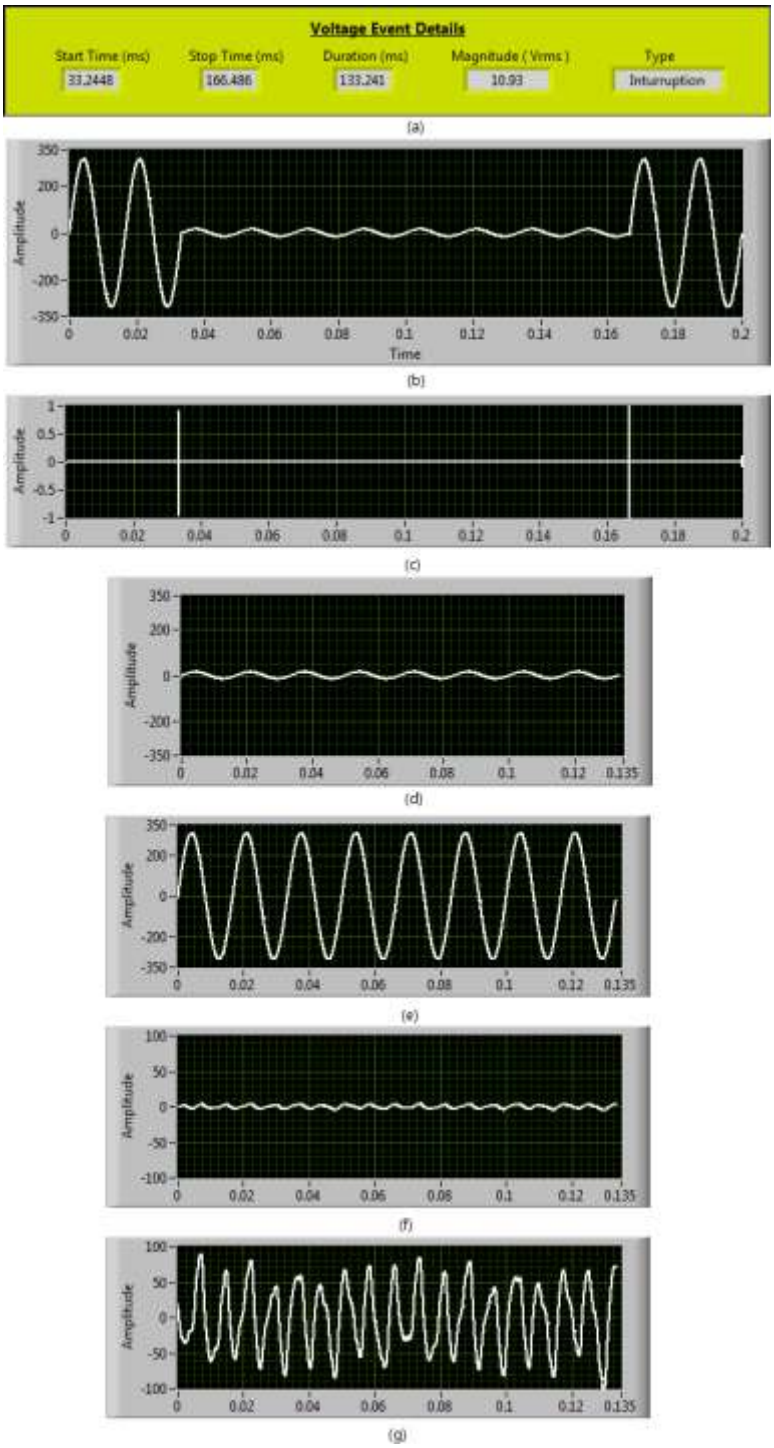

Figure 5.5: Experimental results for detecting and classifying voltage interruption:
(a) Voltage interruption details,
(b) Voltage interruption waveform,
(c) The first detail MRA level (D_1) for (b),
(d) Voltage interruption waveform within the disturbance period,
(e) Nominal voltage waveform within the disturbance period,
(f) The coarsest approximation MRA level (A_6) for (d),
(g) The coarsest approximation MRA level (A_6) for (e).

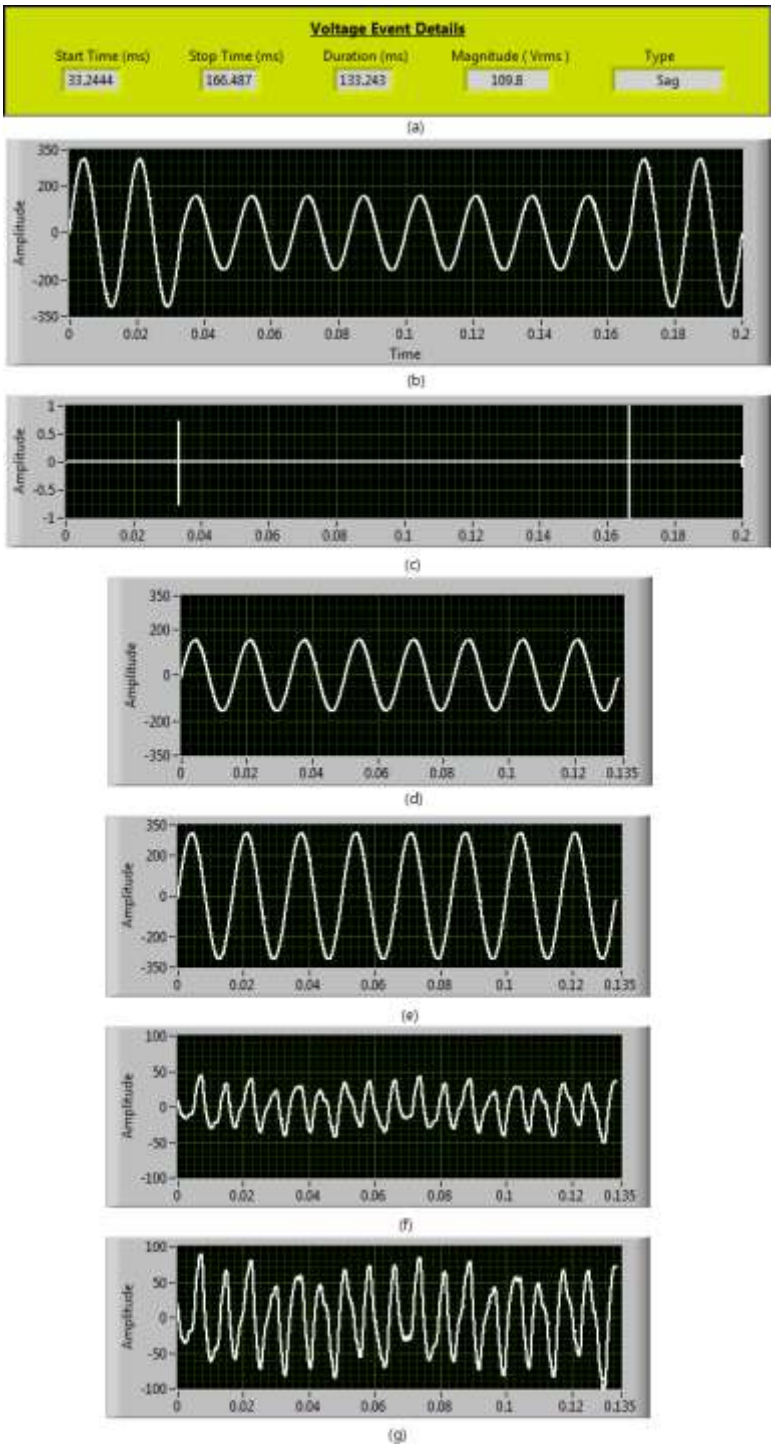

Figure 5.6: Experimental results for detecting and classifying voltage sag:
(a) Voltage sag details,
(b) Voltage sag waveform,
(c) The first detail MRA level (D_1) for (b),
(d) Voltage sag waveform within the disturbance period,
(e) Nominal voltage waveform within the disturbance period,
(f) The coarsest approximation MRA level (A_6) for (d),
(g) The coarsest approximation MRA level (A_6) for (e).

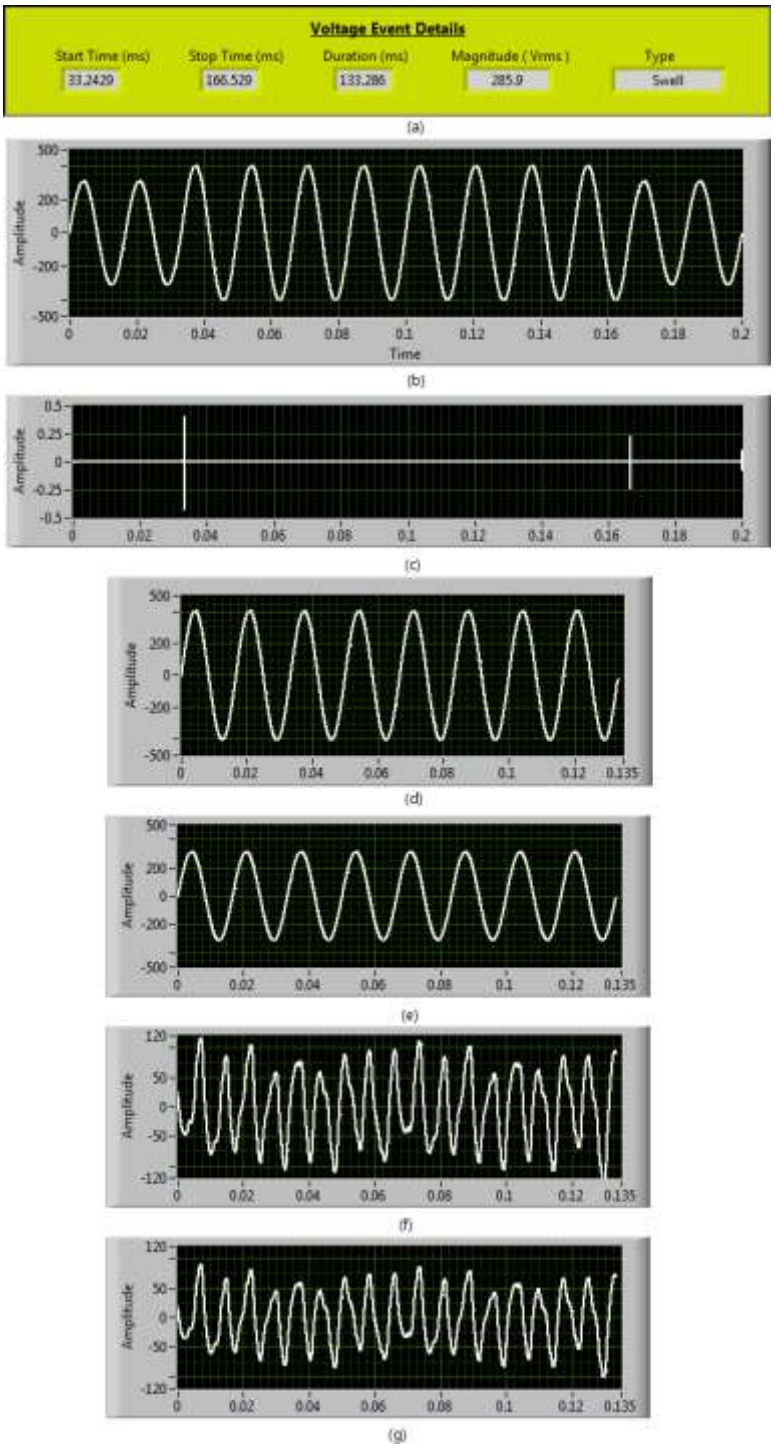

Figure 5.7: Experimental results for detecting and classifying voltage swell:
(a) Voltage swell details,
(b) Voltage swell waveform,
(c) The first detail MRA level (D_1) for (b),
(d) Voltage swell waveform within the disturbance period,
(e) Nominal voltage waveform within the disturbance period,
(f) The coarsest approximation MRA level (A_6) for (d),
(g) The coarsest approximation MRA level (A_6) for (e).

CHAPTER SIX

MITIGATION OF POWER QUALITY PROBLEMS

This chapter presents the proposed mitigation techniques for PQ events on power distribution networks. Voltage regulation at the point of common coupling (PCC) using distribution synchronous static compensator (DSTATCOM) and harmonics mitigation using shunt active power filter (SAPF) are proposed. The simulation models and results of DSTATCOM and SAPF are discussed.

6.1 DISTRIBUTION STATIC SYNCHRONOUS COMPENSATOR

6.1.1 Overview

The DSTATCOM is a shunt compensator that is suitable for distribution networks. It has been widely used since the 1990s to precisely regulate system voltage at the PCC by absorbing or generating reactive power.

From the viewpoint of device topology, DSTATCOM is identical with STATCOM. The difference between them is the location of installation. A DSTATCOM is installed on the distribution network whereas a STATCOM is installed on the transmission system [208].

6.1.2 Topology of DSTATCOM

The DSTATCOM consists mainly of:

1. **A voltage source converter (VSC)** connected to the distribution network through a transformer. VSC converts an input DC voltage into a three phase AC output voltage at fundamental frequency. The active power flow is controlled by the angle between the PCC voltage and VSC voltage. On the other hand, the reactive power flow is controlled by the difference between the magnitudes of these voltages.
2. **A DC link voltage** is provided by the capacitor (C_{dc}) which is charged with power taken from the network.
3. **A control system** that ensures the regulation of the bus voltage and the DC link voltage. The controller continuously monitors the voltages and currents at the PCC and determines the required amount from reactive power by the grid for mitigating the disturbance.
4. **Coupling transformer and line AC filter.**

   Figure 6.1 shows the general structure of the DSTATCOM connected to distribution system.

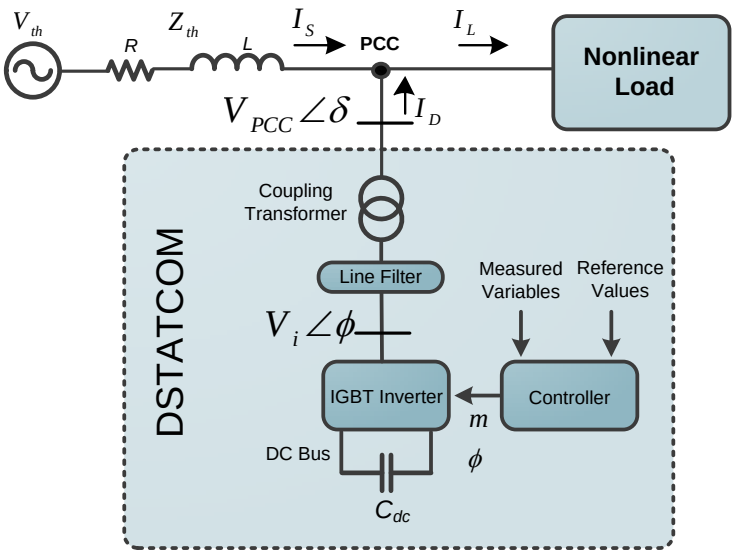

Figure 6.1: Schematic diagram of DSTATCOM.

6.1.3 Parameters Design and Characteristics of DSTATCOM

The DSTATCOM function in this work is to regulate the bus voltage during the swell and sag conditions by absorbing or generating reactive power at PCC. The center part of the DSTATCOM is a voltage-source pulse width modulator (PWM) converter.

The adopted schematic diagram of the DSTATCOM connected to PCC is illustrated in Figure 6.2. The design and selection of the DSTATCOM components such as dc bus voltage, dc-link capacitor, ac-link reactor and line filter are explained in details in the following subsections [247]-[251].

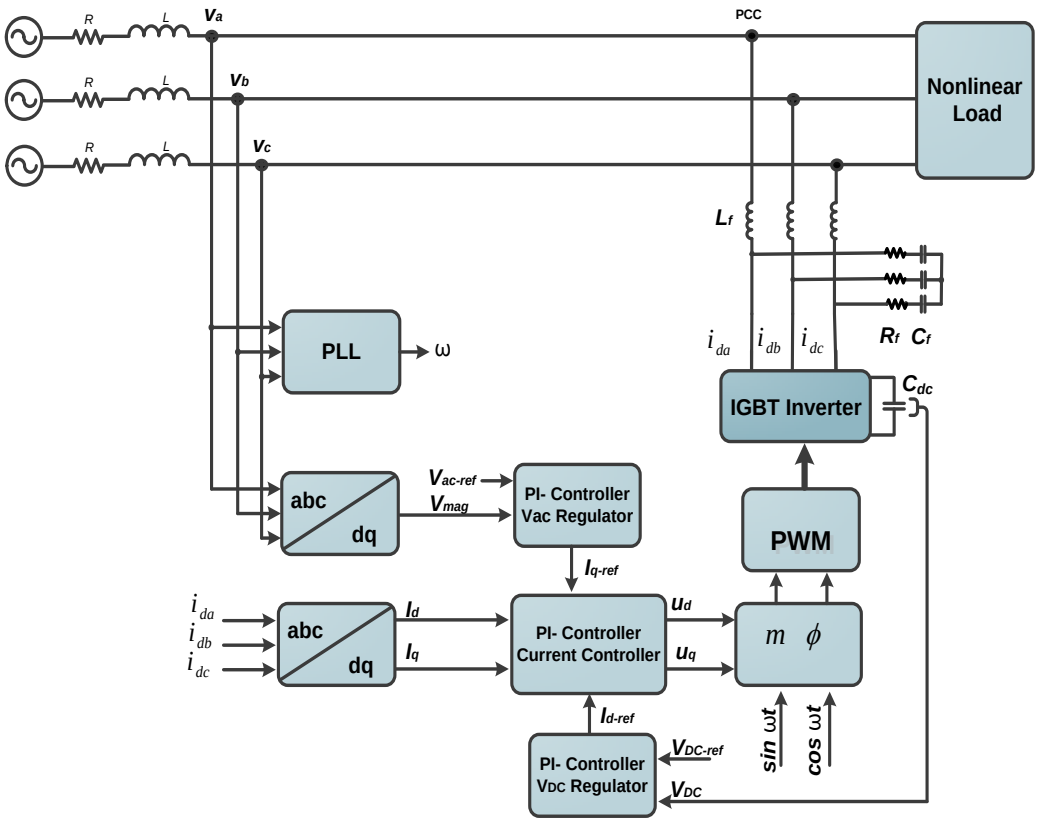

Figure 6.2: Adopted model of the DSTATCOM and Controller.

6.1.3.1 DC Bus Voltage

The VSC generates a controllable AC voltage (V_i). This voltage is given by

$$V_i = C\, V_{dc} \angle \emptyset$$
$$C = m\, k \tag{6.1}$$

Where

- m is the modulation ratio defined by pulse width modulation (PWM), and its range values is between 0 and 1.

- k is the ratio between the AC and DC voltage depending on the converter structure, and its value for the considered structure is $\sqrt{3/8}$.
- V_{dc} is the DC voltage.
- ∅ is the phase defined by PWM.

In this work the wanted output line voltage of the DSTATCOM to be 380V. Thus V_{dc} can be determine using the (6.1) as follow

$$V_{dc} = \frac{V_i}{k\ m} = \frac{380}{\sqrt{3/8} * 1} = 620.54$$

The selected value of V_{dc} is 650V.

The magnitude and the phase of V_i can be controlled through m and ϕ respectively.

The DC voltage (V_{dc}) is governed by:

$$\dot{V}_{dc} = \frac{I_{dc}}{C_{dc}} = \frac{C}{C_{dc}}\left(i_{dd}\cos\phi + i_{dq}\sin\phi\right) \qquad (6.2)$$

Where

- C_{dc} is the value of the DC capacitor.
- I_{dc} is the capacitor current.
- i_{dd} and i_{dq} are the d and q components of the DSTATCOM current, respectively.

6.1.3.2 DC Bus Capacitor

From the principle of energy conservation, the equation governing C_{dc} is

$$\frac{1}{2}\, C_{dc}\left({V_{dc}}^2 - {V_{dc1}}^2\right) = 3\; b\; a\; I\; V_{ph} t \tag{6.3}$$

$$C_{dc} = \frac{3\; b\; a\; I\; V_{ph} t}{0.5\left({V_{dc}}^2 - {V_{dc1}}^2\right)} \tag{6.4}$$

Where

- V_{dc1} is the minimum voltage level of DC bus.
- b is a factor varying between [0.05 0.15].
- a is the over loading factor.
- I is the phase current of the VSC.
- V_{ph} is the phase voltage of the VSC.
- t is the time for which DC bus voltage is to be covered.

Let considered the following:

V_{dc} = 650V, V_{dc1}=620V, b=0.1, a=1.2, I=20A, V_{ph}=220, t=100ms. Then

$$C_{dc} = \frac{3\;\; b\;\; a\;\; I\;\; V_{ph}\; t}{0.5\left({V_{dc}}^2 - {V_{dc1}}^2\right)} = \frac{3 * 0.1 * 1.2 * 20 * 220 * 0.1}{0.5(650^2 - 620^2)} = 8315\; \mu F$$

The selected value of C_{dc} is 10,000µF.

6.1.3.3 AC Link Reactor

The choice of the AC link reactor depends on the switching frequency (f_s) of the modulator and the ripple current (I_{ripp}). As per [250], the AC link reactor can be selected using the following formula

$$L_f = \frac{\sqrt{3}\ m\ V_{dc}}{12\ a\ f_s\ I_{ripp}} \tag{6.5}$$

For, f_s = 10 kHz, I_{ripp} = 0.2I,

$$L_f = \frac{\sqrt{3}\, m\, V_{dc}}{12\ a\ f_s I_{ripp}} = \frac{\sqrt{3} * 1 * 650}{12 * 1.2 * 10 * 10^3 * 0.2 * 20} = 1.95mH$$

The selected value of L_f is 2mH.

6.1.3.4 The Ripple Filter

The ripple filter helps to improve the damping of the switching ripple in the output voltage waveform of the DSTATCOM. The considered ripple filter is a capacitor (C_f) in series with resistance (R_f). The ripple filter used is a first order high pass filter tuned at half of the f_s. The ripple filter allows the flow of high frequency noises through its branch when the frequency higher than the fundamental frequency. The value of the components of the selected filter are C_f equals to 5µF and R_f equals to 5Ω [247].

6.1.4 Control Strategy of DSTATCOM

The proposed control strategy of the DSTATCOM for voltage regulation during the sag and swell conditions consists of four parts: phase locked-loop, ac voltage regulator, dc voltage regulator and current controller. These parts are designed and explained in the following subsections.

Referring to Figure 6.2, the ac side equations can be written as follows [251]-[253]:

$$L_f \frac{d\, i_{da}}{dt} + R_L\, i_{da} = v_a - v_{ia}$$

$$L_f \frac{d\, i_{db}}{dt} + R_L\, i_{db} = v_b - v_{ib} \tag{6.6}$$

$$L_f \frac{d\, i_{dc}}{dt} + R_L\, i_{dc} = v_c - v_{ic}$$

Where

- R_L is the equivalent series resistance of the inductor.
- v_{ia}, v_{ib} and v_{ic} represent the output phase voltage of the VSC.

Using the *dq*-transformations, The Eqn. (6.6) can be transformed to dq- frame as follows [251]-[253]:

$$L_f \frac{d\, i_d}{dt} - \omega\, L_f i_q + R_L\, i_d = v_{PCCd} - v_{id}$$

$$L_f \frac{d\, i_q}{dt} + \omega\, L_f\, i_d + R_L\, i_q = v_{PCCq} - v_{iq} \tag{6.7}$$

The command voltages in d-axis and q-axis are given by [252]

$$v_{id} = \omega\, L_f\, i_q + v_{PCCd} - \left(K_P + \frac{K_I}{S}\right)\ \left(i_{d-ref} - i_d\right)$$

$$v_{iq} = -\omega\, L_f\, i_d + v_{PCCq} - \left(K_P + \frac{K_I}{S}\right)\ \left(i_{q-ref} - i_q\right) \tag{6.8}$$

6.1.4.1 The Phase Locked-Loop

The phase locked-loop (PLL) is providing a reference phase signal synchronized with the ac system. This reference phase signal is used as a basic carrier wave for generating firing pulses of insulated gate bipolar transistors (IGBT) bridge in the inverter control circuit. The actual thyristor-firing pulses are determined using the provided phase signal by PLL adding the desired firings that are calculated in the main control circuit achieving regulation of some output system variables. PLL plays an important role in the system dynamic performance since the PLL dynamically change the reference signal therefore influences actual firings.

In this dissertation, PLL is used to detect the phase angle, frequency, and amplitude of the utility-voltage vector, to obtain an accurate synchronization to the gird. The inputs of PLL are the three phases voltages of the PCC (v_a, v_b, and v_c), the outputs of the PLL are the phase angle (ω), $\sin(\omega t)$, and $\cos(\omega t)$.

The grid voltages (v_a, v_b, and v_c) and filter currents (i_{da}, i_{db}, and i_{dc}) are discretized and transformed into DC quantities by using Park's transformation (*dq*-transformation) as given in (6.9) and (6.10). Both equations can be used for current and voltage transformation.

$$\begin{bmatrix} I_d \\ I_q \end{bmatrix} = \sqrt{\frac{2}{3}} \begin{bmatrix} \cos(\theta) & \cos(\theta - 2\pi/3) & \cos(\theta + 2\pi/3) \\ -\sin(\theta) & -\sin(\theta - 2\pi/3) & -\sin(\theta + 2\pi/3) \end{bmatrix} \begin{bmatrix} I_a \\ I_b \\ I_c \end{bmatrix} \tag{6.9}$$

$$\begin{bmatrix} I_a \\ I_b \\ I_c \end{bmatrix} = \sqrt{\frac{2}{3}} \begin{bmatrix} \cos(\theta) & -\sin(\theta) \\ \cos(\theta - 2\pi/3) & -\sin(\theta - 2\pi/3) \\ \cos(\theta + 2\pi/3) & -\sin(\theta + 2\pi/3) \end{bmatrix} \begin{bmatrix} I_d \\ I_q \end{bmatrix} \quad (6.10)$$

6.1.4.2 The AC Voltage Regulator

The converted voltage quantities (V_d and V_q) of the v_a, v_b, and v_c are used to calculate the voltage magnitude (V_{mag}) as given in (6.11). V_{mag} is one of the inputs of the PI-controller for regulating the ac voltage. The second input of this controller is the reference value of the ac voltage ($V_{ac\text{-}ref}$) which is usually 1pu. The output of this controller is the q-axis reference current ($I_{q\text{-}ref}$) as shown in Figure 6.3.

$$V_{mag} = \sqrt{{V_d}^2 + {V_q}^2} \quad (6.11)$$

$$I_{q-ref} = \left(K_{Pac} + \frac{K_{Iac}}{S}\right)\left(V_{ac-ref} - V_{mag}\right) \quad (6.12)$$

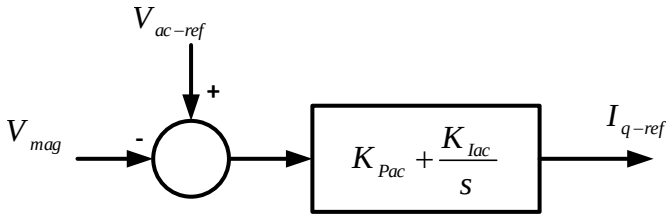

Figure 6.3: The diagram of PI-controller for ac voltage regulator.

6.1.4.3 The DC Voltage Regulator

The dc link voltage (V_{DC}) is the actual voltage cross the dc link. V_{DC} is one of the inputs of the PI controller for dc voltage regulator. The second input of this controller is the desired dc voltage amplitude ($V_{DC\text{-}ref}$). The output of the regulator is the *d*-axis reference current ($I_{d\text{-}ref}$) as shown in Figure 6.4.

$$I_{d-ref} = \left(K_{Pdc} + \frac{K_{Idc}}{S}\right)\left(V_{DC-ref} - V_{DC}\right) \tag{6.13}$$

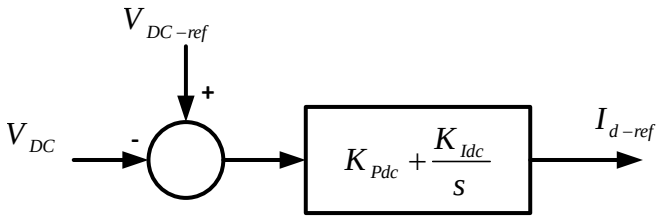

Figure 6.4: The diagram of PI-controller for DC voltage regulator.

6.1.4.4 The PI-Current Controller

As can be seen from the Figure 6.5, The I_d, $I_{d\text{-}ref}$, I_q and $I_{q\text{-}ref}$ are the inputs of the PI-current controller. The outputs of the current controller are the modulation signal *m* and the phase angle $\emptyset$. These outputs control the operation of PWM. Then the *dq*-to-*abc*-transformation is used to transform the modulation signal *m* into the stationary reference (m_a, m_b and m_c) to obtain the switching signals for the VSC.

The control limits of the controller are the current limits in the electronic switches, and the dc voltage. The controllers have a bias, which corresponds to the steady state

value of the modulation index (m_o) for the voltage magnitude controller and to the phase angle (δ) for the dc voltage controller. This value changes as the system variables change during the simulation. m_o can be determined as follows

$$m_0 = \sqrt{\frac{8}{3}}\,\frac{V_{ac-ref}}{V_{DC-ref}} \tag{6.14}$$

In this study, the considered value of m_o is

$$m_0 = \sqrt{\frac{8}{3}}\,\frac{V_{ac-ref}}{V_{DC-ref}} = \sqrt{\frac{8}{3}}\,\frac{380}{650} = 0.95$$

The inputs and outputs of the PI-controller can be determined as follows

$$V_d = \left(K_P + \frac{K_I}{S}\right)\left(I_{d-ref} - I_d\right) \tag{6.15}$$

$$V_q = \left(K_P + \frac{K_I}{S}\right)\left(I_{q-ref} - I_q\right) \tag{6.16}$$

$$m = \sqrt{{V_d}^2 + {V_q}^2} \tag{6.17}$$

$$\emptyset = tan^{-1}\left(V_d + V_q\right)\frac{180}{\pi} \tag{6.18}$$

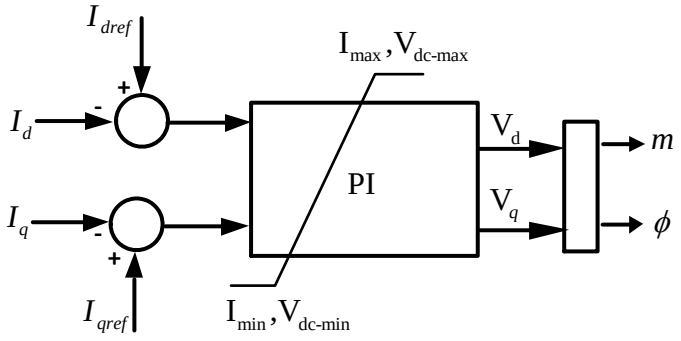

Figure 6.5: The diagram of the main current controller.

6.1.5 Voltage Regulation

If the output voltage of the VSC (V_i) is greater than AC bus terminal voltages (V_{PCC}), DSTATCOM acts like a capacitor generating reactive power to the bus. The current flows from the inverter through the coupling transformer into PCC. So, it will compensate the reactive power through AC system and regulates missing voltages. Whereas when the V_i is lower than V_{PCC}, DSTATCOM acts like an inductance absorbing reactive power from the bus. The current flows from the grid into the DSTATCOM. These voltages are in phase and coupled with the AC system through the reactance of coupling transformers [209]. In steady state, due to inverter losses the bus voltage always leads the inverter voltage by a small angle to supply a small active power [210].

The DSTATCOM mitigates the voltage sag by dynamically injecting a current of desired amplitude and phase angle into the grid line. As can be seen from Figure 6.1, the DSTATCOM injects current (I_D) to correct the voltage at PCC by adjusting the voltage drop on the system impedance (Z_{th}). The amplitude of I_D can be controlled by adjusting the output voltage of DSTATCOM (V_i). Where $I_D = I_L - I_S$.

When the I_D is kept in quadrature with V_{PCC}, the desired voltage regulation can be achieved without injecting any active power into PCC. The *d*-component of the grid voltage (v_d) is zero due to the d-axis aligned with the grid flux vector in the synchronous reference frame. Moreover, the *q*-component of the injecting current (i_q) is set to zero due to the fact that only reactive power injection is considered [147]. The injected reactive power in the *dq*-frame can be calculated as

$$Q(t) = v_q(t)\, i_d(t) \tag{6.19}$$

6.1.6 Simulation Results

The Simulink block diagram of the DSTATCOM utilized to regulate the voltage at PCC is shown in Figure 6.6. The system Parameters and controller parameters used in simulation are given in Tables 6.1 and 6.2.

TABLE 6.1

SYSTEM PARAMETERS

Parameter	Value
V_S	380V
L_S	1mH
R_s	12.4mΩ
V_{dc}	650V
L_f	2mH
R_L	24.8mΩ
f_s	10kHz
C_f	5μF
R_f	5Ω
C_{dc}	10,000 μF

TABLE 6.2

CONTROLLER PARAMETERS

Parameter	Value
K_{Pac}	10
K_{Iac}	1000
K_{Pdc}	8
K_{Idc}	100
K_P	10
K_I	0.3

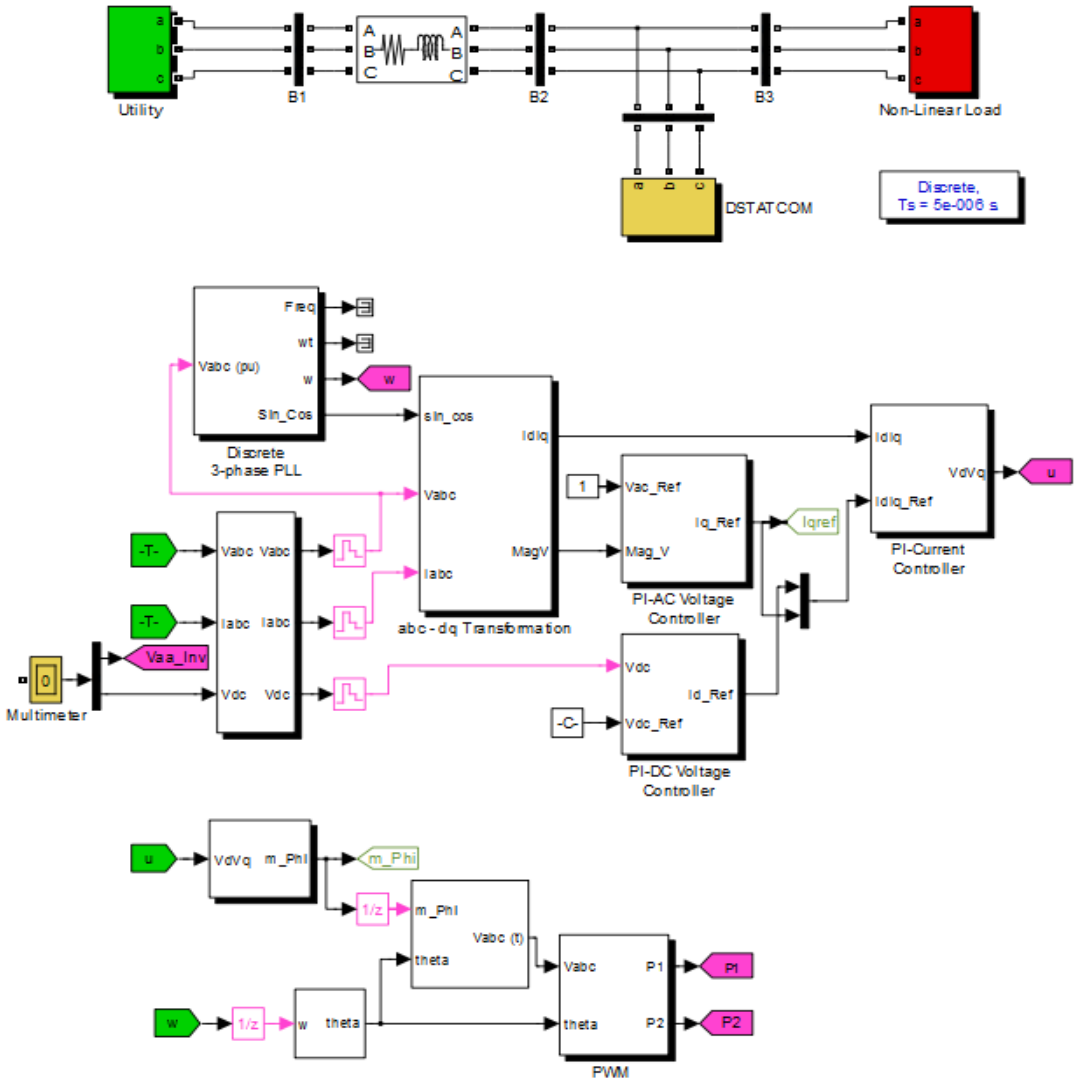

Figure 6.6: Simulink diagram representing the distribution network and control system of the DSTATCOM.

The dynamic response of the DSTATCOM tested on two cases which are voltage sag and voltage swell, the programmable AC voltage source block is used to modulate these cases. The voltage is first programmed to be at PCC 1 p u in order to keep the DSTATCOM initially floating, the event duration is considered to be 6 cycles (100ms) starting at 0.2 s and stopping at 0.3s. The simulated voltage sag and swell magnitudes are 0.9 pu and 1.1 pu, respectively.

6.1.6.1 Simulation Results of Voltage Sag

Figure 6.7 shows the three phase waveform of voltage sag, the voltage magnitude at the PCC drops to 0.9pu during the sag event. The PCC voltage is regulated by the designed controller which produces the q-axis reference current ($I_{q\text{-}ref}$) for current controller. The q-axis reference current for voltage sag mitigation is shown in Figure 6.8.

During the voltage sag, the voltage magnitude at PCC lower than the reference voltage, thus the DSTATCOM acts like capacitor generating reactive power to regulate PCC voltage magnitude to be around the reference magnitude. Figure 6.9 shows the inverter current during voltage sag mitigation, Figure 6.10 shows generating reactive power by DSTATCOM to mitigate the voltage sag at PCC. The voltage magnitudes at PCC with and without DSTATCOM during the voltage sag are shown in Figures 6.11 and 6.12. As can be noted from the results, the voltage magnitude during the sag event enhanced with DSTATCOM and becomes within the acceptable operation range (0.95 pu -1.05 pu).

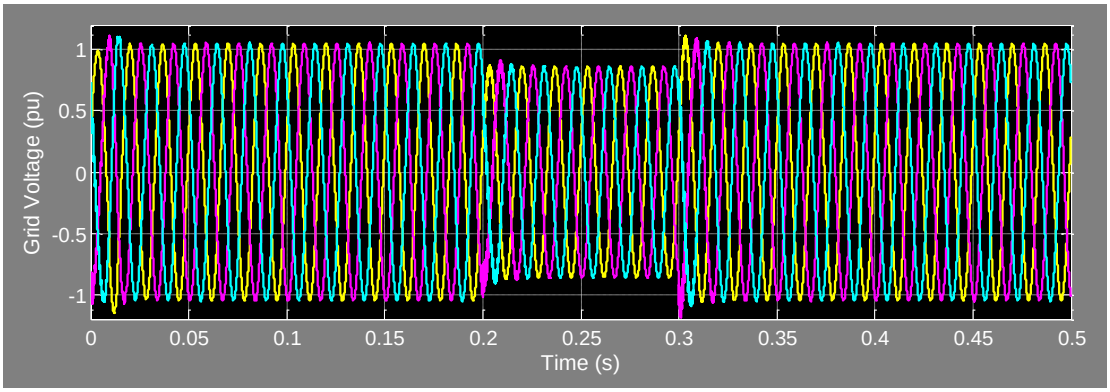

Figure 6.7: Three phase voltage sag.

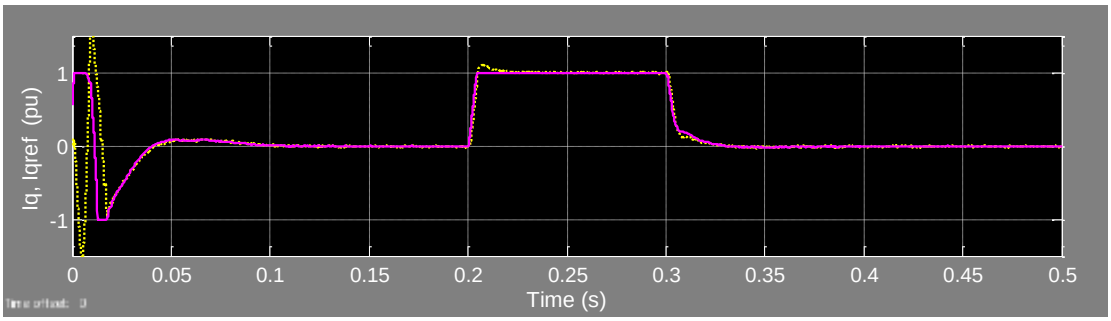

Figure 6.8: The q-axis reference current for voltage sag mitigation.

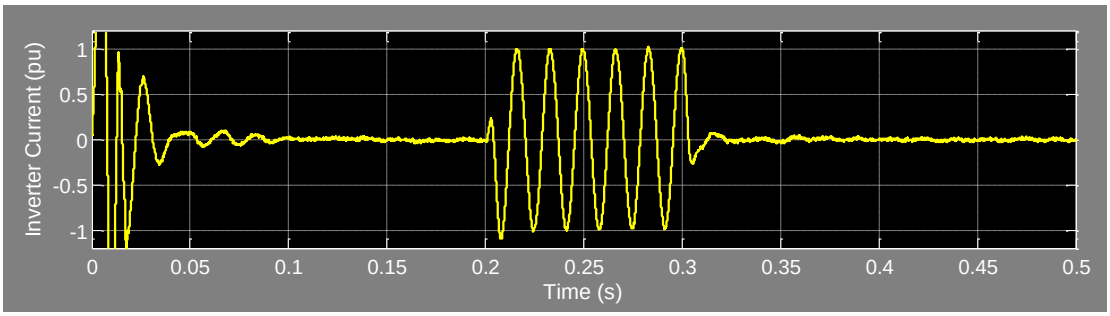

Figure 6.9: Inverter current during voltage sag.

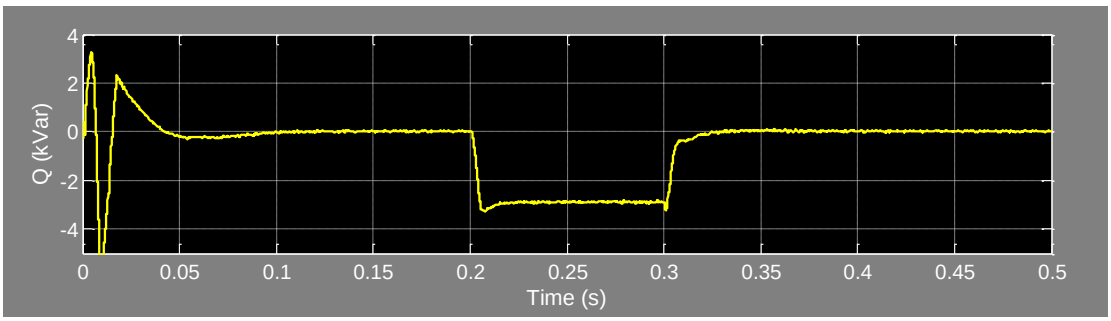

Figure 6.10: Injected reactive power by DSTATCOM during voltage sag.

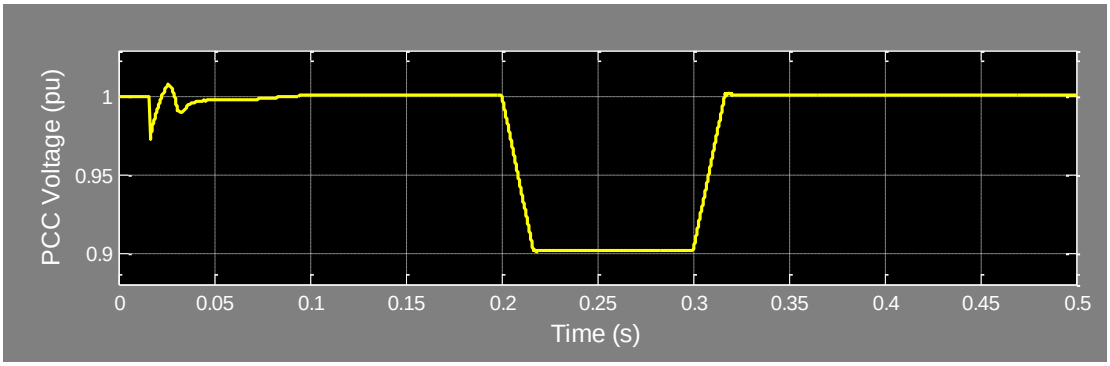

Figure 6.11: Voltage magnitude at the PCC during voltage sag without DSTATCOM.

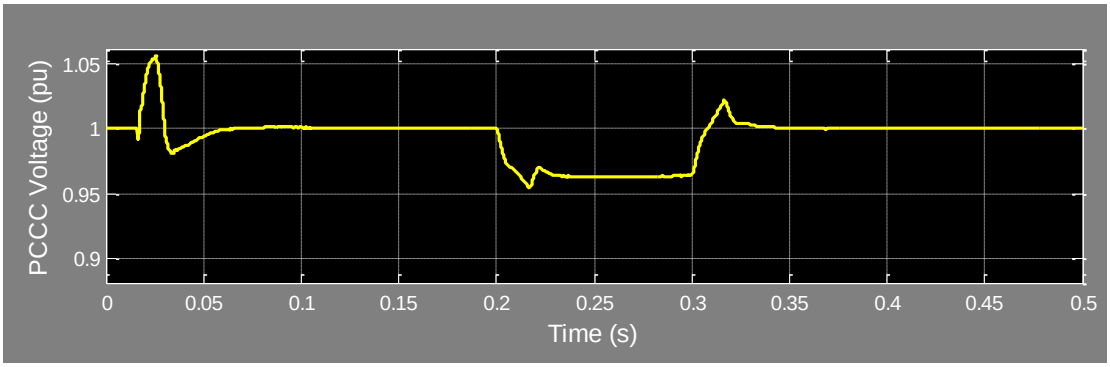

Figure 6.12: Voltage magnitude at the PCC during voltage sag with STATCOM.

6.1.6.2 Simulation Results of Voltage Swell

Figure 6.13 shows the waveform of the simulated three phase voltage swell. During the voltage swell, the voltage magnitude at load bus is 1.1pu, which is higher than the reference voltage. The DSTATCOM acts like inductor absorbing reactive power to maintain load bus voltage within the allowed limit. Figure 6.14 shows the reference q-axis current for the DSTATCOM to mitigate the voltage swell. The response of DSTATCOM to voltage swell is shown in Figures 6.15 and Figure 6.16. The voltage magnitude at the PCC without DSTATCOM during the voltage swell is 1.1pu as shown in Figures 6.17. However, the PCC voltage magnitude with DSTATCOM

during the swell event is regulated to be within the acceptable range as can be seen from Figure 6.18.

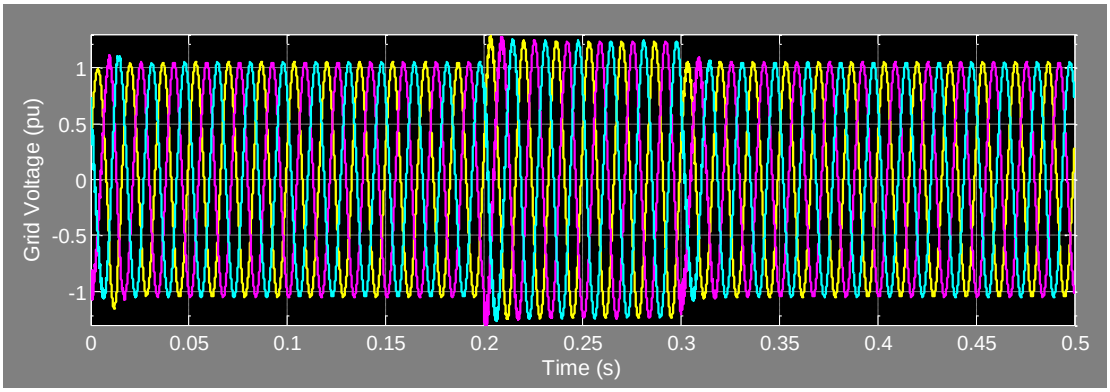

Figure 6.13: Three phase voltage swell.

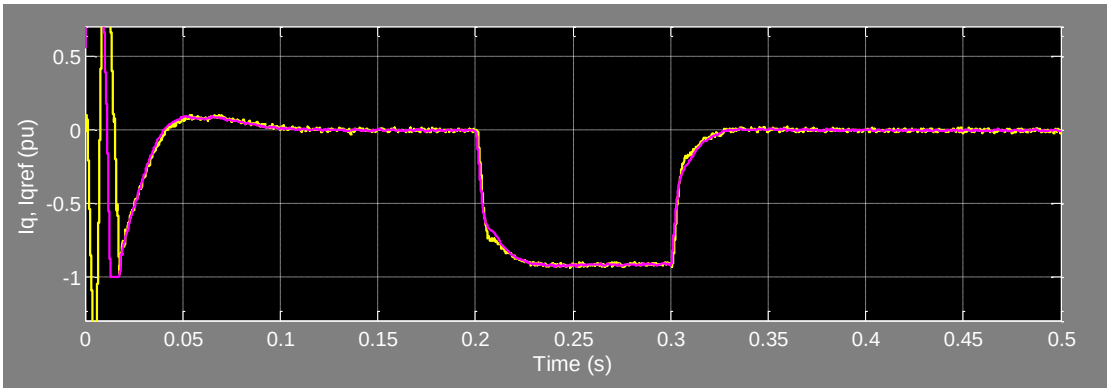

Figure 6.14: Reference q-axis current for voltage swell mitigation.

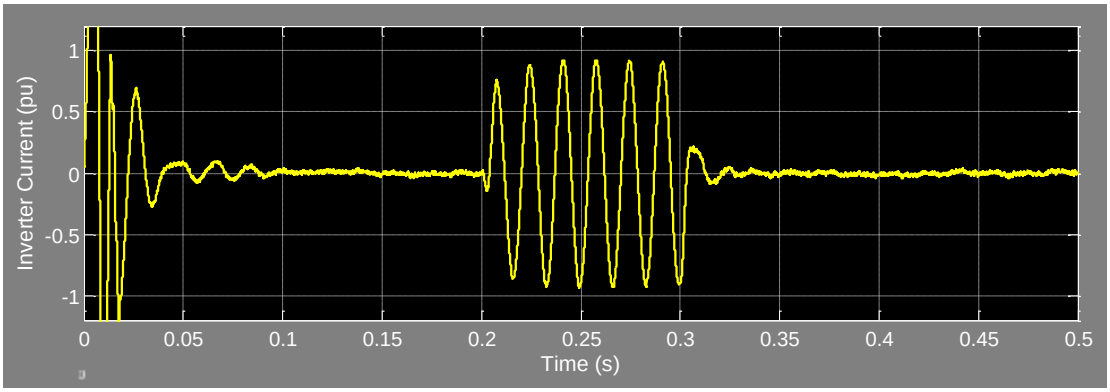

Figure 6.15: Generated inverter current during voltage swell.

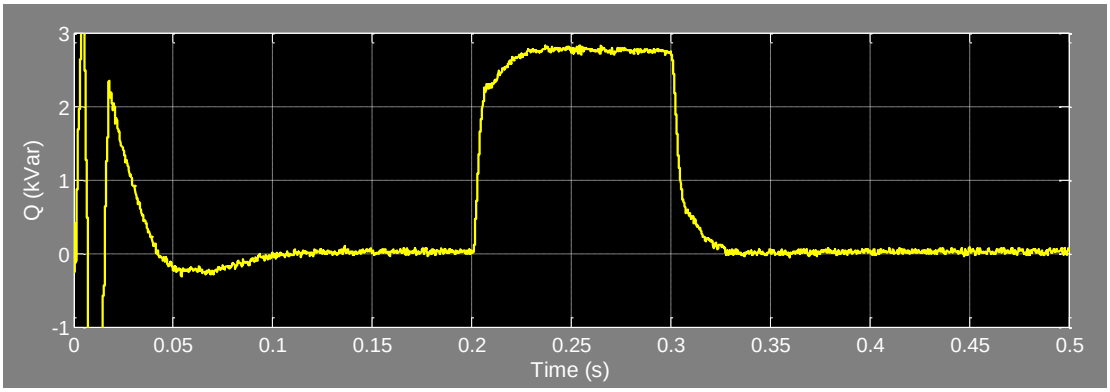

Figure 6.16: Absorbed reactive power by DSTATCOM during voltage swell.

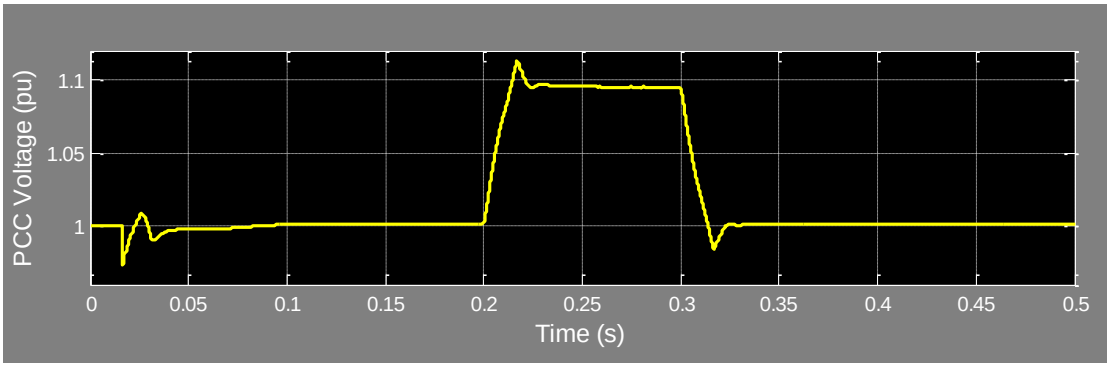

Figure 6.17: Voltage magnitude at the PCC during voltage swell without DSTATCOM.

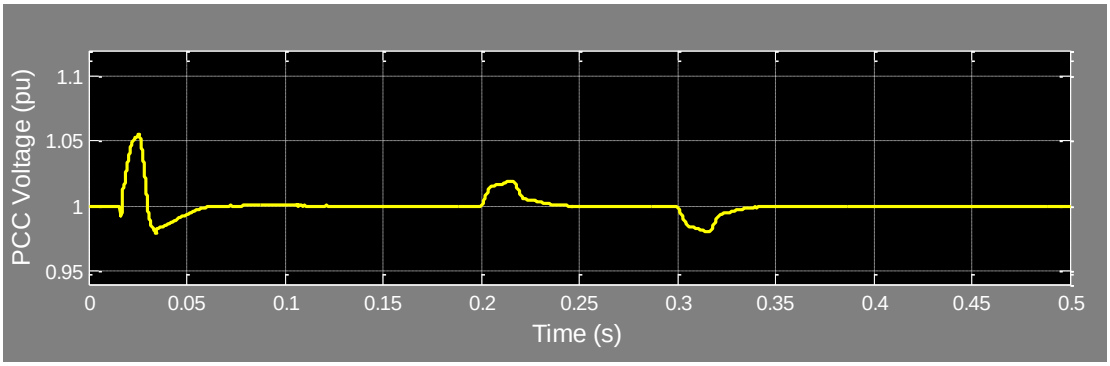

Figure 6.18: Voltage magnitude at the PCC during voltage swell with DSTATCOM.

To check the robustness of the controller, the value of each L_f and C_{dc} with ±10% has been change and then the simulation is run. The results show the efficient of the controller under this parameters uncertainty which confirms the robustness of the proposed controller. It was out aim to implement the controller experimentally on the DSTATCOM; however, due to some unforeseen commissioning problems and limitations this will be shifted to the future work.

6.2 SHUNT ACTIVE POWER FILTER

6.2.1 Shunt Active Power Filter Topology

The topology of the three-phase shunt active power filter presented in this work is shown in Figure 6.19. The adopted SAPF topology is based on voltage source inverter (VSI), since VSI is lighter and cheaper than current source inverter (CSI). The VSI operates as a current-controlled voltage source. The SAPF compensate current harmonics by injecting equal but opposite harmonic compensating current.

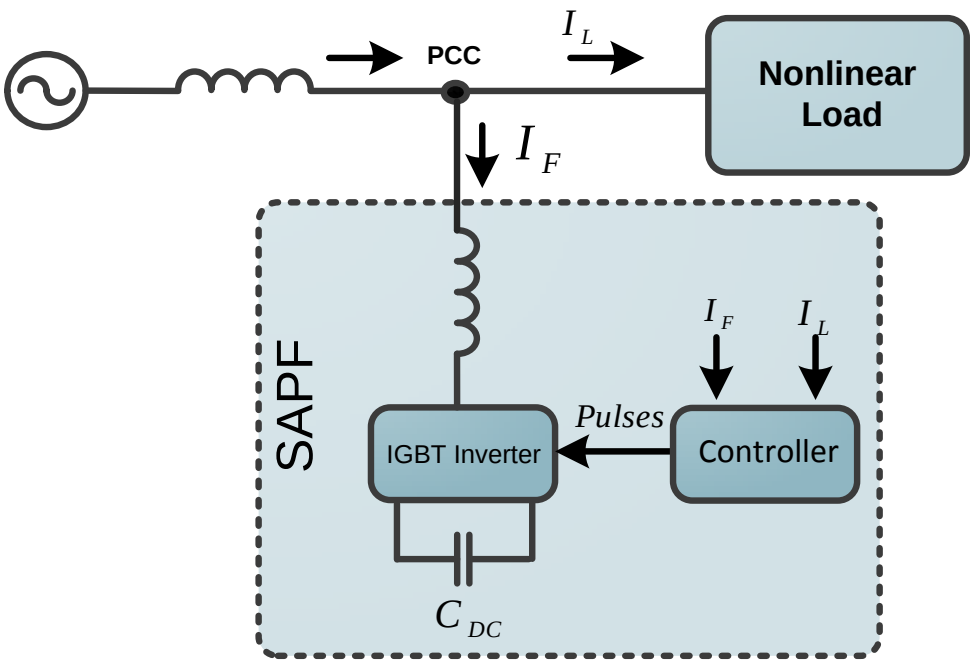

Figure 6.19: Topology circuit of shunt active power filter.

6.2.2 Proposed Control Scheme for SAPF

As well-known the most critical issues associated with the controller of active power filter is that of creating an algorithm which can provide an accurate harmonic reference signal for control purpose.

In this dissertation, the adaptive noise canceling (ANC) theory utilized for designing control strategy of the three-phase SAPF. The ANC theory is effective and simple method for creating control signal for SAPF and used widely in the signal processing [245], [246]. The ANC used to extract the reactive power and harmonics components of the load current as the control signal of the SAPF. The block diagram of the adaptive detecting circuit used in this work is shown in Figure 6.20 [245].

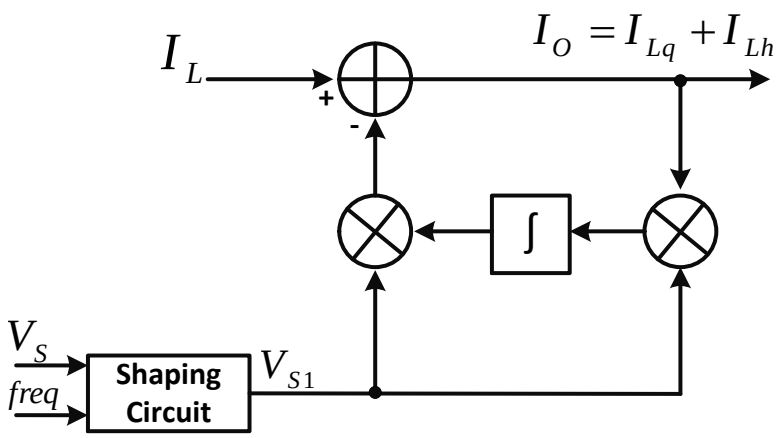

Figure 6.20: Adaptive detecting block diagram for harmonic and reactive power.

As can be seen from Figure 6.20,

$$I_O = I_L - (V_{S1} \int_0^t I_O \; V_{S1} \; dt) \tag{6.20}$$

$$V_{S1} = V_{Sm} \sin \omega t_0 \tag{6.21}$$

Where

- I_o represents the output of the detecting circuit.
- I_L represents the load current.
- V_s represents the source voltage.
- V_{s1} represents the fundamental component of V_s.
- V_{sm} represents the peak value of the V_s.

From the equations (6.20) and (6.21), I_o can be written as

$$I_O = I_L - V_{Sm} \sin \omega t \, (K_0 + \frac{1}{\omega RC} \int_{t_0}^{t} I_O \; V_{Sm} \sin \omega t \;\; d\omega t) \tag{6.22}$$

Where

- K_0 is the dc component of the integrator output.
- RC is the time constant is approximately 20ms [245].

Let

$$K_1 = \frac{1}{\omega RC} \int_{t_0}^{t} I_O \; V_{Sm} \sin \omega t \;\; d\omega t) \tag{6.23}$$

Then

$$I_O = I_L - K_0 V_{Sm} \sin \omega t - K_1 \, V_{Sm} \sin \omega t \tag{6.24}$$

Due to the large time constant of the integrator and the orthogonality, all components in K_1 except the fundamental real component which in phase with reference input, i.e. the system voltage will be approximately zero, and the fundamental real component of I_L is approximately zero in the steady state, then K_1 will be also approximately zero. Consequently, the last term of (6.24) can be omitted [246].

Let assume that the load current can be expressed as

$$I_L = I_{Lp} + I_{Lq} + I_{Lh} \tag{6.25}$$

Where

- I_{Lp} is the fundamental active component of I_L.

- I_{Lq} is the fundamental reactive component of I_L.
- I_{Lh} is the harmonic components of I_L.

Then

$$I_O = I_{Lp} + I_{Lq} + I_{Lh} - K_0 V_{Sm} \sin \omega t \tag{6.26}$$

$$I_O = I_{Lq} + I_{Lh} \tag{6.27}$$

$$I_{Lp} = K_0 V_{Sm} \sin \omega t \tag{6.28}$$

Figure 6.21 shows the block diagram of the SAFP controller that proposed in this study. The controller of SAPF uses adaptive PLL (adaptive detecting circuit) to generate reference sinusoidal source current (I_{ref}) which is in-phase with the load current (I_L) and its rms value same as rms value of the I_L. The current error between I_{ref} and I_L is generated by the inverter via the hysteresis switching technique which used to produce suitable firing pulses for the inverter. The SAPF aims to inject the current error (I_{err}) at the PCC in order to match the source current (I_S) with the I_{ref}.

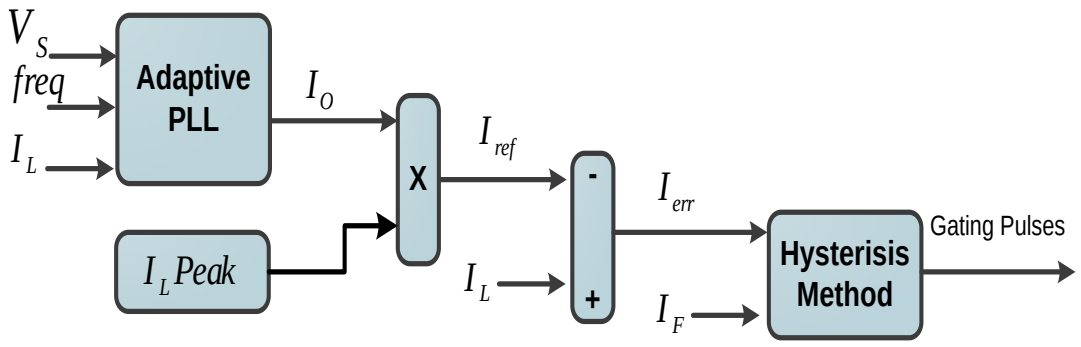

Figure 6.21: The adopted controller scheme of the SAPF.

6.2.3 Parameters Design

The selection of dc-link capacitor and ac-link reactor values affects directly the performance of the SAPF.

6.2.3.1 The DC Link Capacitor

The capacitor and the inverter bridge limit the maximum value of the dc voltage while the inverter gain limits the minimum value of the dc voltage [245].

$$V_C \geq \frac{V_{Sm}}{1 - f_s\,(T_{min} + T_d)} \tag{6.29}$$

Where

- V_C is the capacitor voltage
- V_{sm} is the maximum value of the source voltage.
- f_s is the switching frequency of the switching device.
- T_{min} is the minimum on-time of the switching device.
- T_d is the dead time of the switching device.

The dc-link capacitor designed according to keeping the dc-link voltage fluctuation limited. The storage energy variation of the dc-link capacitor can be

$$\Delta W = \frac{1}{2}\,C\left({V_C}^2 - {V_O}^2\right) = \int_0^t V_S\,I_L\,dt - \frac{1}{2}\,L\,{I_L}^2 \tag{6.30}$$

$$\Delta W = \frac{1}{2}\,C\left({V_C}^2 - {V_O}^2\right) \approx C\;\Delta V_C\,V_O \tag{6.31}$$

$$C \approx \frac{\Delta W}{\Delta V_C \, V_O} = \frac{\Delta W}{\varepsilon \, {V_O}^2} \tag{6.32}$$

Where V_o is the reference capacitor, ε represents the voltage ripple.

Thus, the required dc-link capacitor (C_{dc}) value can be determined using (6.32) with the acceptable voltage ripple (ε). The selected value of dc-link capacitor is

$$C_{dc} = \frac{40}{0.05 * 600^2} = 2200 \, \mu F$$

6.2.3.2 The AC Link Inductor

In this work, the considered criterion to design the ac link reactor is the maximum current (I_{max}) that the filter must supply in order to compensate a totally inductive load. The inductance value can be determined as follows

$$L_{min} = \frac{\Delta V_{min}}{\omega \, I_{max}} \tag{6.33}$$

Where

- ΔV_{min} is the difference between the rms source voltage and the fundamental component rms inverter voltage. The considered value of ΔV_{min} is 20V.
- ω is the supply angular frequency (ω = 377).
- The considered value of I_{max} is 30A.

Thus

$$L_{min} = \frac{20}{377 * 30} = 1.77 \, mH$$

If the inductive voltage drop is made small the inductance will be small and there is better utilization of the dc voltage. However, a very small inductance implies a high voltage gain and introduces a higher complexity in the controller design. In order to keep the inductive voltage drop at a reduced level, the selected value of *L* is 2mH.

6.2.4 Simulation Results

The work presented in this section is based on the simulation of SAPF for compensating the current harmonics created by nonlinear loads. The simulation of the proposed SAPF carried out under the Matlab/Simulink environment. Three different cases studies for nonlinear loads producing harmonics are simulated:

Case I. Three-phase diode rectifier with RL load.

Case II. Three-phase diode rectifier with variable dc load.

Case III. Three-phase thyristor rectifier with dc motor drive.

The case study-I used to test the effectiveness and the performance of the designed control strategy of the SAPF in compensating the harmonic components produced by the nonlinear load. The case study-II besides the aim of case-I proposed to examine the capability of the proposed controller of the SAPF in capturing new reference current when the load current changes during the simulation running. Furthermore, the case study-III used to test the efficiency of the SAPF controller in compensating the current harmonics components when the load current is highly distorted.

The FFT analysis tool used to analyze the THD for the source current without and with SAPF to evaluate the performance of the proposed SAPF analytically for each case study.

For simplicity, the waveforms of the load current, the filter current and the source current are shown for phase A for all cases studies in this section.

6.2.4.1 Case I- Three-Phase Diode Rectifier with RL Load

In this case study, the nonlinear load consists of three-phase diode rectifier with RL load isolated by Δ-Y transformer. The rectifier injects current harmonics in the system; the characteristic harmonics injected by a 6-pulse rectifier are $6n \pm 1\,, n = 1,2,3,\ \ldots$. The Simulink model of the proposed SAPF with the load is depicted in Figure 6.22. The aim of using this type of load is to examine the performance of the proposed control strategy for compensating the current harmonics components.

The Figure 6.23 shows the simulation results of case-I. These results are the current load waveforms, the filter current and the actual source current. As can be seen from the source current waveform, the source current follows the reference current in a suitable manner. The simulation results show the desired design of SAPF control strategy.

The harmonics analysis of the source current without and with the SAPF is depicted in Figure 6.24. The harmonics analysis results presented based on the percentage of the fundamental component of the source current. The harmonics of the source current are substantially reduced with SAPF. For example, the 5^{th} harmonics without

SAPF was 19% whereas the one with SAPF is reduced to 0.7%. Furthermore, The THD of the source current without the filter was 28.14% and is reduced to 5.15% with the filter.

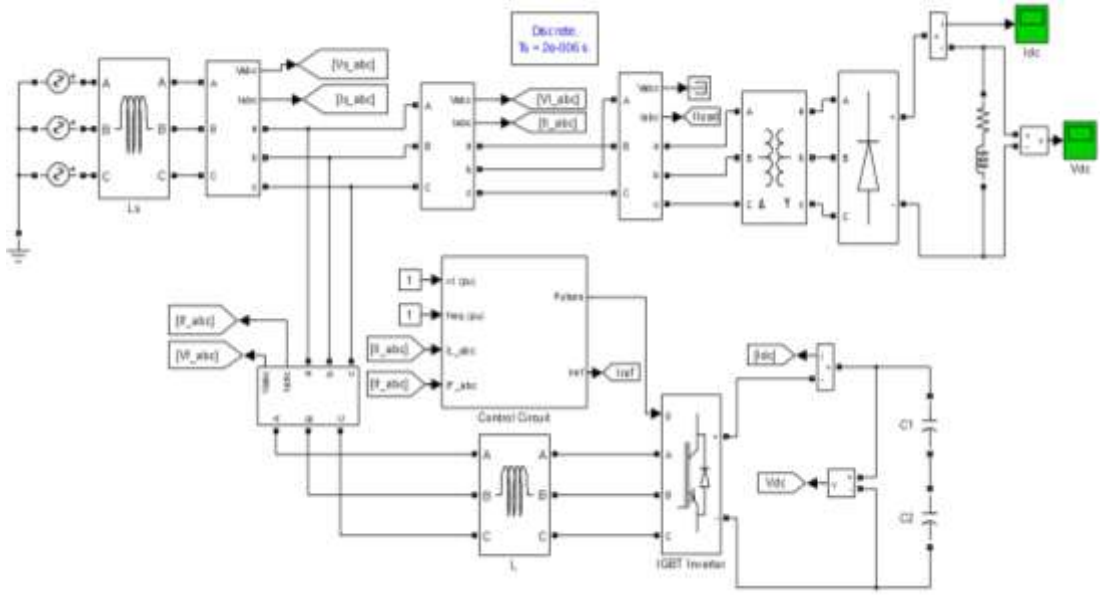

Figure 6.22: The Simulink model of the power system with SAPF of Case-I.

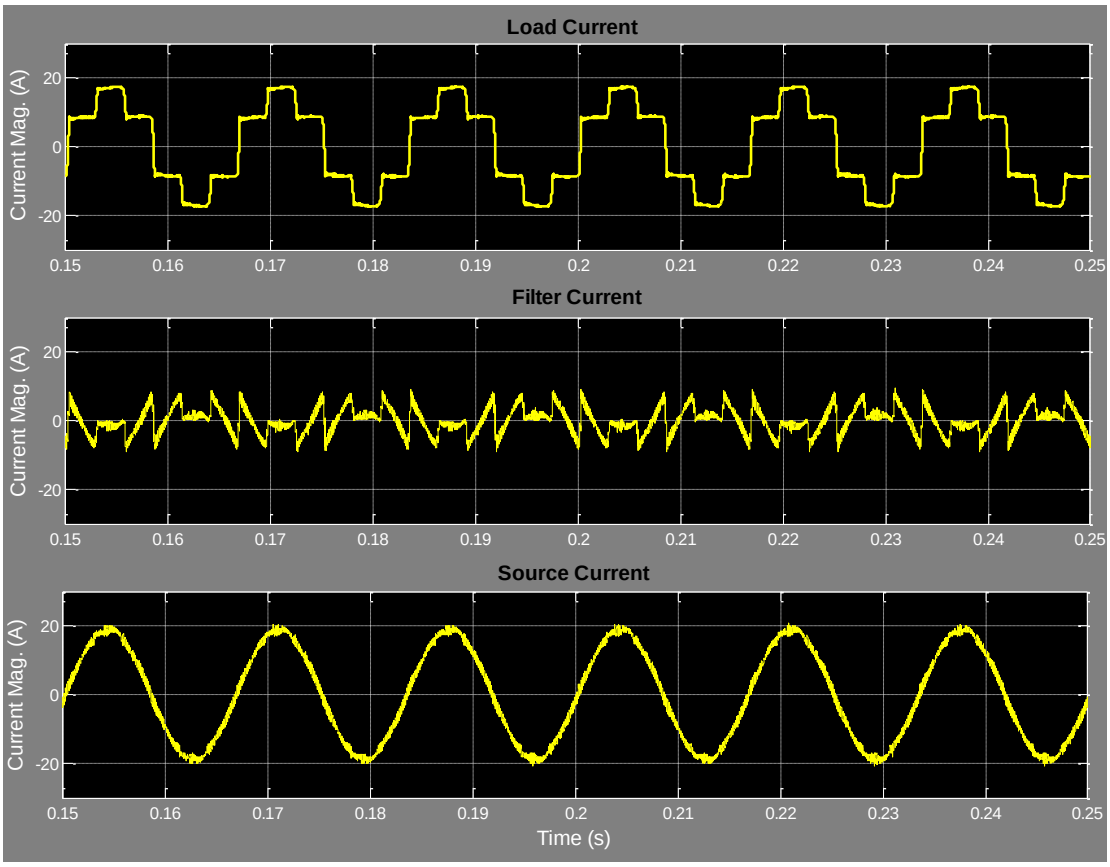

Figure 6.23: The simulation results of case-I.

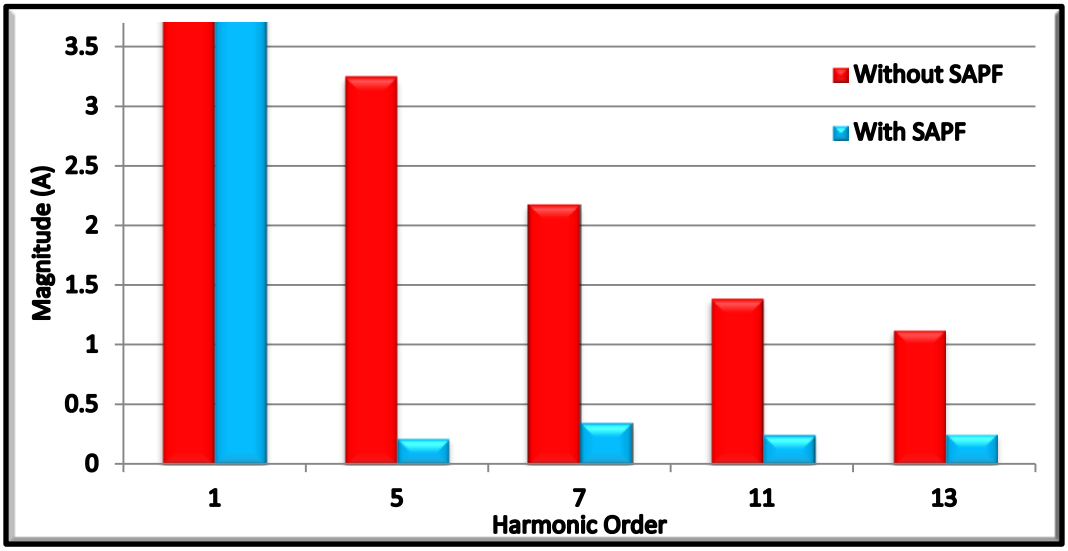

Figure 6.24: The harmonics spectra of the load current without/with SAPF.

6.2.4.2 Case II- Three-Phase Diode Rectifier with Variable Load

The considered nonlinear load in this case study contains three-phase diode rectifier with variable load isolated by Δ-Y transformer. Figure 6.25 shows the Simulink model of the proposed SAPF with the considered load. The variable nonlinear load used in this case for testing the capability of the proposed controller to capture new reference current for the source current when the load current changes during the simulation time.

The simulation results for this case study are shown in Figure 6.26. At *t=0s*, the dc load current is set at 40A. At *t=0.13s* the dc load current increased to 50A. As can be seen from the waveforms in Figure 6.26, the proposed SAPF effectively respond to this change in load and captures the new reference current within one cycle. The THD of the source current was reduced from 27.07% to 2.14% as shown in Figure 6.27.

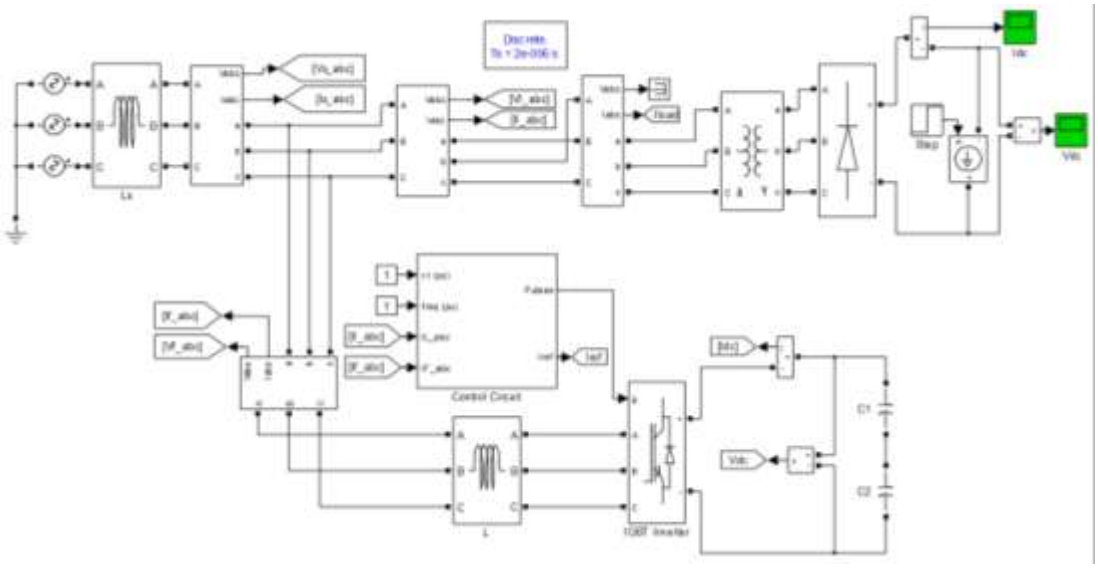

Figure 6.25: The Simulink model of the power system with SAPF of Case-II.

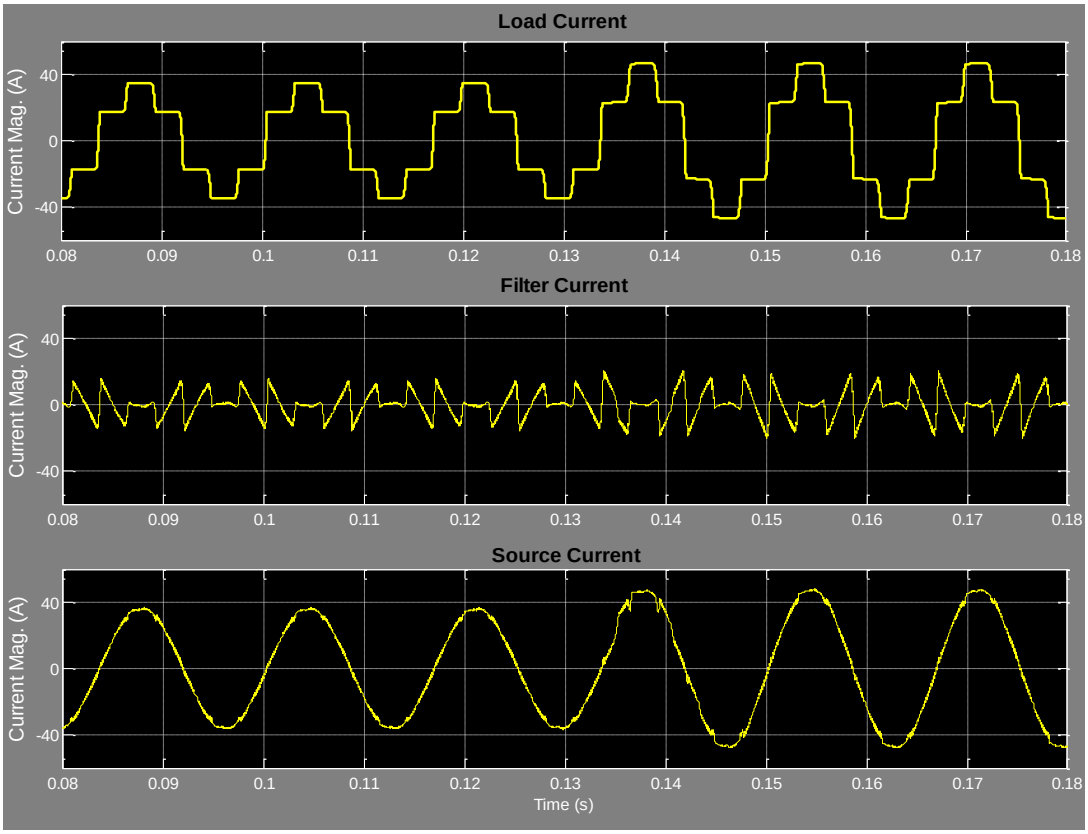

Figure 6.26: The simulation results of case-II.

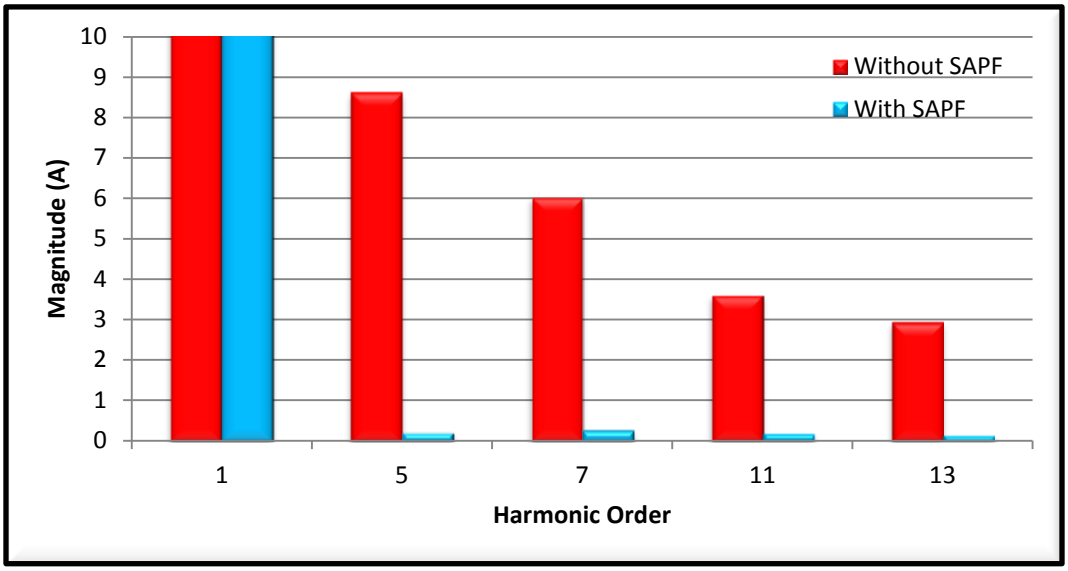

Figure 6.27: The harmonics spectra of the load current without/with SAPF.

6.2.4.3 Case III- Three-Phase Thyristor Rectifier with DC Motor Drive

The load considered in this case study is three-phase thyristor rectifier with dc motor drive isolated by Δ-Y transformer, the Simulink block diagram of this case study is shown in Figure 6.28. This load generates high THD value for the source current. The main target of this case study is test the efficiency and capability of the proposed control strategy for reducing the high THD value of the source current.

The simulation results for this case study are shown Figure 6.29. Despite of the high distortion in the source current waveform because of the load characteristics, the proposed SAPF effectively captures the reference current for the desired source current. Further, the high THD value of the source current is reduced to 9.16% where 100.87% was, as can be seen from Figure 6.30.

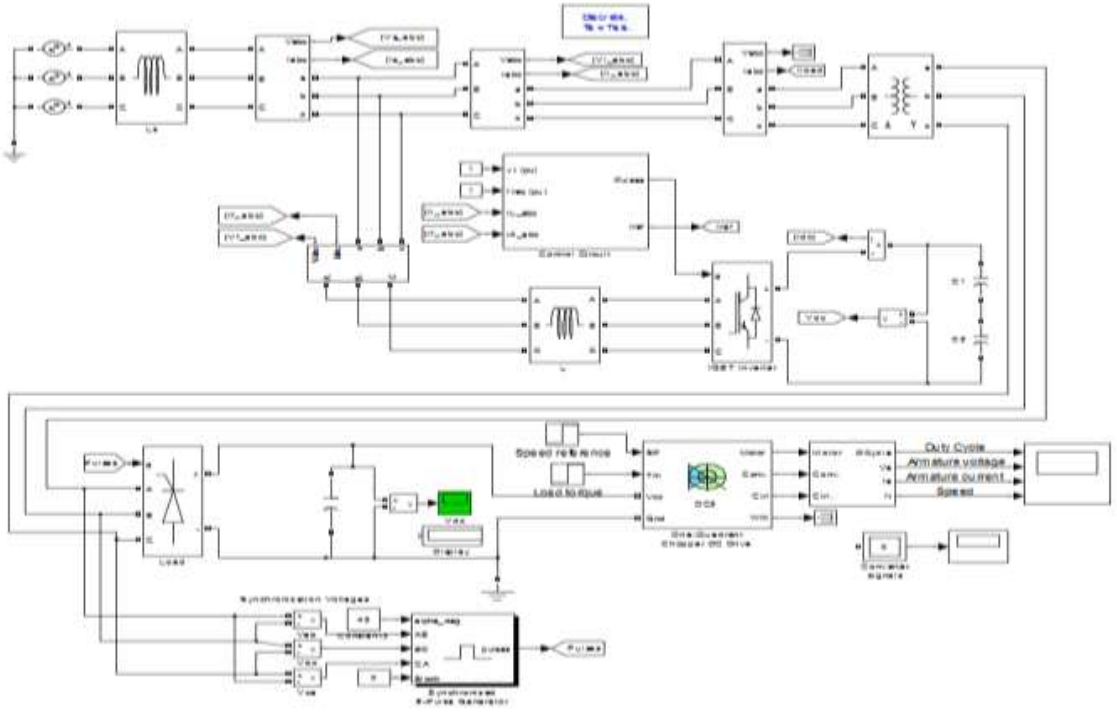

Figure 6.28: The Simulink model of the power system with SAPF of Case-III.

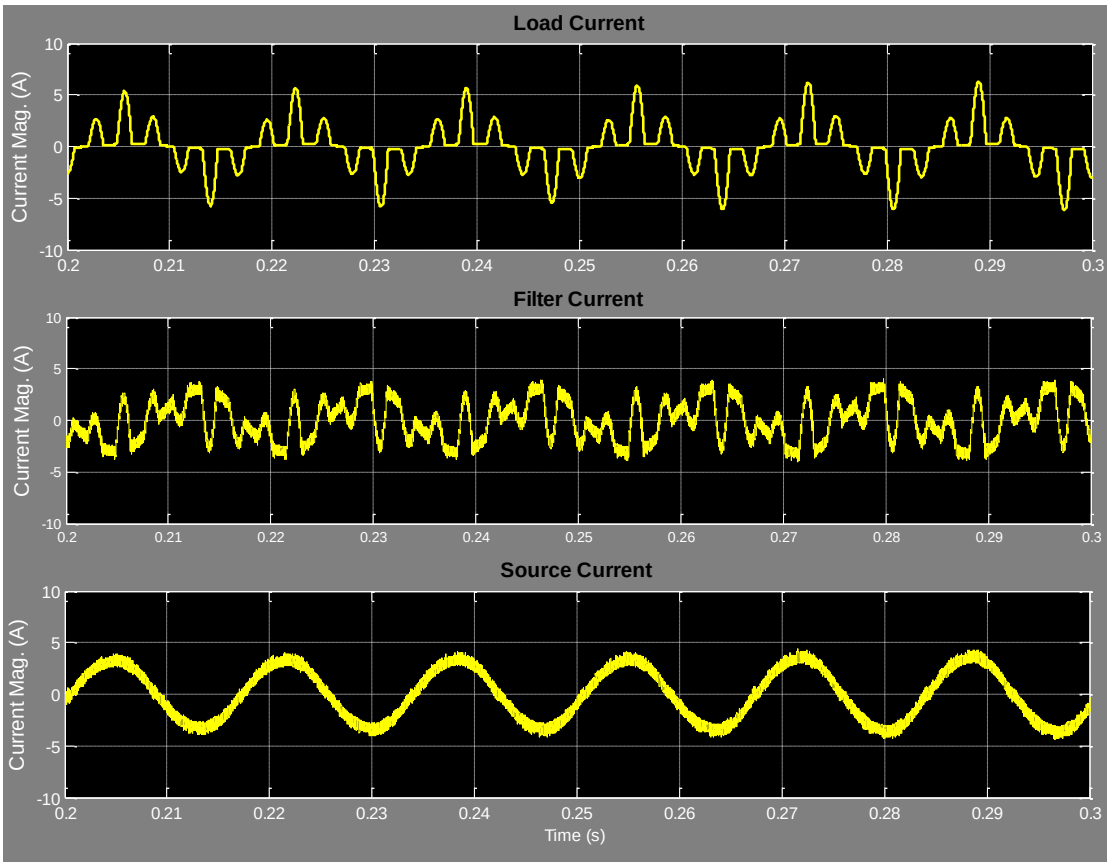

Figure 6.29: The simulation results of case-III.

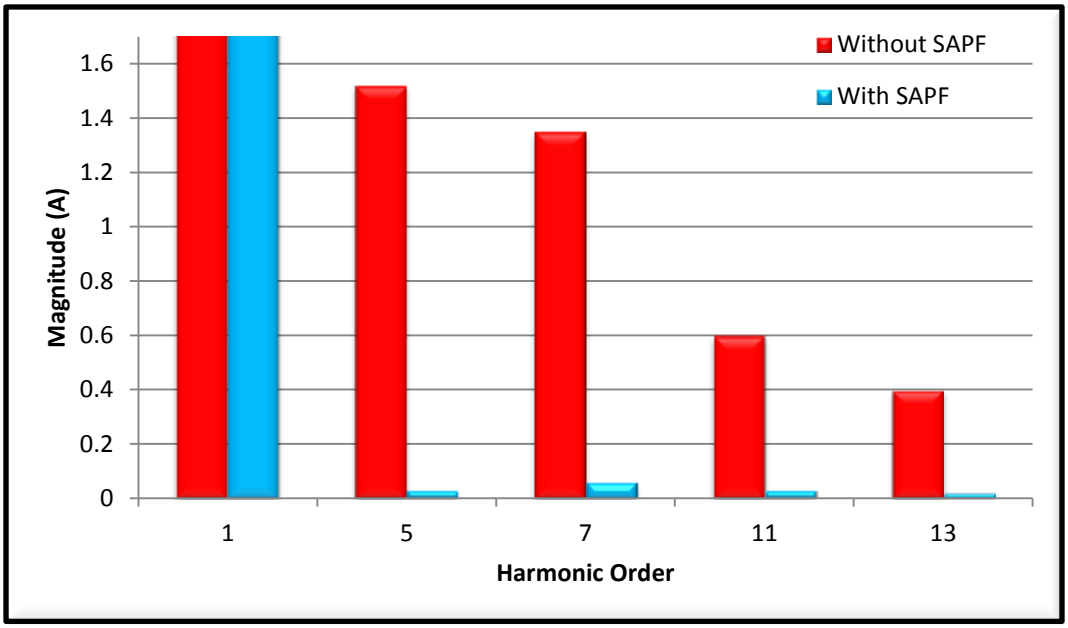

Figure 6.30: The harmonics spectra of the load current without/with SAPF.

CHAPTER SEVEN

CONCLUSIONS AND FUTURE WORK

7.1 CONCLUSIONS

The purpose of this dissertation was to develop a monitoring and mitigation system for power quality problems based on proposing efficient techniques. The system would collect voltage and current waveforms from various locations in power distribution networks. These waveforms were then to be processed in order to find the power quality parameters, which are important for both the utility and customers.

In this dissertation, a comprehensive literature review has been accomplished, and new efficient methods for PQ events monitoring, detection and tracking have been proposed, developed, simulated and implemented. Laboratory scale prototype has been built for power quality. The main conclusions of this dissertation can be summarized as follow:

- A comprehensive literature review has been accomplished for real time monitoring, detection, tracking, classification and mitigation of PQ problems as well as optimal harmonic estimation.

- A novel new method for voltage events monitoring, tracking, and classification based on calculation of rms voltage using 2-sample/half-cycle has been proposed and developed.

- A new efficient technique based on wavelet multiresolution analysis has been proposed and developed for the purpose of voltage events monitoring, tracking, and classification in power distribution networks.

- The simulation results of the proposed methods demonstrate the effectiveness and suitability of these methods for monitoring, tracking and classification voltage events.

- A new intelligent technique for online optimal harmonics estimation based on separable least squares has been proposed.

- The simulation results of the proposed separable least squares show the suitability of the proposed technique for online harmonics estimation.

- The proposed monitoring, detection, tracking, and classification techniques for PQ events have been implemented in laboratory scale prototype using LabVIEW software, cRIO, developed data acquisition cards, real time signal processors and a simplified model for the distribution network with its associated bulk loads.

- The necessary experimental work to validate the proposed techniques has been run. Additionally, the results of the all proposed methods have been compared with the results of the conventional methods. The results demonstrate the

superiority, accuracy, robustness, suitability and capability of the proposed methods for real time applications.

- This dissertation provides hardware system that can be used to monitor and control the quality of power flowed in distribution network. This system discussed has been shown to accurately records and collects data of voltage and current waveforms then pass the collected data through the NI modules to the LabVIEW environment where the data can be processed.

- The developed PQ monitoring system provides accurate measurements for the most important values that quantify the power quality. These measurements include statistical data on the voltage and current waveforms including rms values, angle, frequency, PF, CF, and power values as well as harmonics analysis.

- The developed system has also shown accuracy in detection and classification of voltage events. Furthermore, from the results of testing, the developed system was shown to be a valuable tool for PQ monitoring and controlling as well as the developed system has been proven to accurately assess the PQ in power distribution system.

- Control strategy of DSTATCOM was designed and simulated using the Simulink/Matlab program to mitigate the voltage sag and swell events using reactive power flow in electrical distribution networks.

- Control strategy of SAPF was designed and simulated using the Simulink program to compensate the current harmonics components at the PCC.

- A novel intelligent technique for the optimal harmonics estimation was proposed and developed based on SLS.
- For the laboratory work, the results from this practical implementation showed the same general patterns as those of the monitoring, tracking, and classification simulations.

7.2 FUTURE WORK

For a future work on the system presented in this dissertation, some points could be proposed such as:

- The proposed research work can be extended to design and develop a new technique for online harmonics estimation using wavelet packet transform. Since the discrete wavelet transform produces non-uniform output frequency bands. On the other hand, the wavelet packet transform decomposes a waveform into uniform frequency bands. Additionally, the output frequency bands of the wavelet packet transform can be made compatible with the harmonics groups defined in IEC Std-61000-4-30.
- The rms-based method for PQ monitoring is simple and easy, however, it has shortcoming in detection start time and end time of PQ events. To overcome this shortcoming, a hybrid rms-based method with wavelet multiresolution analysis can be designed for accurate detection and classification PQ events.
- The proposed classification system for PQ events can be developed to classify power quality events according to their underlying causes.

- Implement a full model of the monitoring and mitigation system of the power quality problems in the laboratory.

REFERENCES

[1]. R.C. Dugan, M.F. Megranghan, and H.W. Benty, "*Electrical power system quality*". MC Graw_Hill, New York, 2004.

[2]. W. E Kazibwe & M. H. Sendaula, "*Electric Power Quality Control Techniques*", Van Nostrand Reinhold New York, NY, 1993.

[3]. International Electro-technical Commission, "*IEC 61000-3-2 Harmonics Standards*". Nov 2010.

[4]. Institute of Electrical and Electronics Engineers, "*IEEE 519-1992 IEEE Recommended Practices and Requirements for Harmonic Control in Electrical Power Systems*", USA. 1992.

[5]. *IEEE Recommended Practice for Monitoring Electric Power Quality, IEEE Std 1159,*USA, 1995.

[6]. M. Jan; K. Jako; H. Bill; Z. Francisc; T. Liliana; G. Romero; M. Jovica, "Contemporary and future aspects of cost effective power quality monitoring—Position paper of CIGRE WG C4.112," *Electric Power Quality and Supply Reliability Conference*, pp. 1-6, 2012.

[7]. T. P. Sunil; N. Loganathan, "Power quality improvement of a grid-connected wind energy conversion system with harmonics reduction using FACTS device," *2012 International Conference on Advances in Engineering, Science and Management (ICAESM),* pp. 415–420, 2012.

[8]. M. Music; A. Bosovic; N. Hasanspahic; S. Avdakovic; E. Becirovic, "Integrated Power Quality Monitoring Systems in smart distribution grids," *2012 IEEE International Energy Conference and Exhibition (ENERGYCON),* pp.501–506, 2012.

[9]. J. Sjolte; G. Tjensvoll; M. Molinas, "All-electric Wave Energy Converter array with energy storage and reactive power compensation for improved power quality," *2012 IEEE Energy Conversion Congress and Exposition (ECCE)*, pp. 954 – 961, 2012.

[10]. Jing Chen; Tianhao Tang, "Power quality analysis based on LABVIEW for current power generation system," *2012 International Symposium on Power Electronics, Electrical Drives, Automation and Motion (SPEEDAM)*, pp. 865 – 870, 2012.

[11]. S. Vanga; S. N. V. Ganesh, "Comparison of Fourier Transform and Wavelet Packet Transform for quantification of power quality," *2012 International Conference on Advances in Power Conversion and Energy Technologies (APCET)*, pp. 1 – 6, 2012.

[12]. S. H. Laskar; S. Khan; Mohibullah, " Power quality monitoring in sustainable energy systems," *2012 IEEE International Symposium on Sustainable Systems and Technology (ISSST)*, pp.1 – 6, 2012.

[13]. J. Kilter; J. Meyer; B. Howe; F. Zavoda;L. Tenti; J. V. Milanovic; M. Bollen; F. Ribeiro; P. Doyle; J. Gordon, "Current practice and future challenges for power quality monitoring - CIGRE WG C4.112 perspective," *2012 IEEE 15th International Conference on Harmonics and Quality of Power (ICHQP)*, pp.390 – 397, 2012 .

[14]. W. Zhan; Z. Xiangjun; H. Xiaoxi; H. Jingying. "The multi-disturbance complex power quality signal HHT detection technique," *2012 IEEE Innovative Smart Grid Technologies - Asia (ISGT Asia)*, pp.1– 5, 2012.

[15]. M. Farhoodnea; A. Mohamed; H. Shareef; H. Zayandehroodi, "Power quality improvement using an enhanced premium power park configuration," *2012 IEEE International Power Engineering and Optimization Conference (PEDCO) Melaka, Malaysia*, pp.129-134, 2012.

[16]. A. A. Abdelsalam, A. A. Eldesouky, A. A. Sallam "Characterization of power quality disturbances using hybrid technique of linear Kalman filter and fuzzy-expert system," *Electric Power Systems Research, vol. 83, iss. 1,* pp.41-50, Feb. 2012.

[17]. H. Junfeng, S. Hao, W. Xiaolin, "Design of Power Quality Monitor Based on Embedded Industrial Computer," *Physics Procedia, vol. 24, Part A,* pp. 63-69, 2012.

[18]. R. Bátorfi, A. V. Szarka, "Parameter identification of electrical power quality by a new synchronisation method and an innovative measuring instrument," *Measurement, vol. 46, iss.1,* pp. 697-709, Jan. 2013.

[19]. H. Yang and C. Liao, " A De-Noising Scheme for Enhancing Wavelet-Based Power Quality Monitoring System," *IEEE Trans. on Power Delivery., vol.16, no 3,* pp. 353-360, Jul. 2001.

[20]. H. Zhang, P. Liu, O.P. Malik, "Detection and classification of power quality disturbances in noisy conditions," *IEE Generation Transmission Distribution. Vol. 150,* pp. 567–572, 2003.

[21]. U.D. Dwivedi, S.N. Singh, "A robust energy features estimation for detection and classification of power quality disturbances," *IEEE Power India Conf.,* pp. 1–7, 2006.

[22]. J. Wang, C. Wang, "Power quality disturbance signals de-noising based on improved soft-threshold method," *TENCON 2007-IEEE Region 10 Conf., Tianjin Univ., Tianjin,* pp. 1–4, 2007.

[23]. U. D. Dwivedi, S. N. Singh, "A wavelet-based denoising technique for improved monitoring and characterization of power quality disturbances," *Electric Power Components and Systems, vol. 37,* pp. 753–769, 2009.

[24]. U. D. Dwivedi, S. N. Singh, "Denoising techniques with change-point approach for wavelet-based power-quality monitoring," *IEEE Trans. on Power Delivery*, *vol. 24*, pp. 1719–1727, 2009.

[25]. U. D. Dwivedi, S. N. Singh, "Enhance detection of power-quality events using intra and interscale dependencies of wavelet coefficients," *IEEE Trans. on Power Delivery*, *vol. 25*, pp. 358–366, 2010.

[26]. C.-C. Liao, H.-T. Yang, H.-H. Chang, "Denoising techniques with a spatial noise suppression method for wavelet-based power quality monitoring," *IEEE Trans. on Instrumentation & Measurements*, *vol. 60*, pp. 1986–1996, 2011.

[27]. J. Chung, E.J. Powers, and W.M. Grady, "Power quality assessment via the Teager Energy Operator" *IEEE Summer meeting proceedings*, July 2000.

[28]. Shyh-Jier Huang, Cheng-Tao Hsieh, "Feasibility of fractal-based methods for visualization of power system disturbances", *International Journal of Electrical Power and Energy Systems, Vol. 23, No. 1*, pp. 31-36, January 2001.

[29]. S. Santoso, E.J. Powers, and P. Hofmann, "Power quality assessment via wavelet transform analysis" *IEEE Trans. on Power Delivery, Vol. 11, No. 2*, pp. 924–930, 1996.

[30]. A.M. Gaouda, M. M. Salama, "Application of multiresolution signal decomposition for monitoring short-duration variations in distribution systems", *IEEE Trans. on Power Delivery*, *Vol. 15*, pp. 478-484, 2000.

[31]. S. K. Mitra, *Digital Signal Processing A Computer-Based Approach*, McGraw-Hill, Boston, 2001.

[32]. A. V. Oppenheim and R. W. Schafer, *Discrete-Time Signal Processing*, 2nd ed. Prentice-Hall, Upper Saddle River, NJ, 1999.

[33]. L. R. Rabiner and R. W. Schafer, *Digital Processing of Speech Signals*, Prentice-Hall, Upper Saddle River, NJ. 1978.

[34]. C. N. Bhende, S. Mishra, and B. K. Panigrahi, "Detection and classification of power quality disturbances using S-transform and modular neural network," *Electric Power System Research,vol. 78*, (1), pp. 122–128, 2008.

[35]. L. Eren and M. J. Devaney, "Calculation of power system harmonics via wavelet packet decomposition in real time metering," *in Proc. IEEE IMTC, Anchorage, AK*, May 21–23, pp. 1643–1647, 2002.

[36]. Girgis, W. B. Chang, and E. B. Makram, "A digital recursive measurement scheme for online tracking of power system harmonics," *IEEE Trans. on Power Delivery, vol. 6*, pp. 1153-1160, July 1991.

[37]. P. K. Dash, D. P. Swain, A. C. Liew, and S. Rahman, "An adaptive linear combiner for on-line tracking of power system harmonics," *IEEE Trans. on Power Delivery, vol. 11*, pp. 1730 -1735, Nov. 1996.

[38]. T. K. Abdel-Galil, E. F. El-Saadany, M. M. A. Salama, "Online tracking of voltage flicker utilizing energy operator and Hilbert transform," *IEEE Trans. on Power Delivery, vol 19, iss.* 2, pp 861-867, Apr. 2004.

[39]. G. T. Heydt, P. S. Fjeld, C. C. Liu, D. Pierce, L. Tu, and G. Hensley, "Applications of windowed FFT to electric power quality assessment," *IEEE Trans. on Power Delivery, vol. 14*, pp 1411-1416, Oct. 1999.

[40]. D. C. Robertson, O. I. Camps, J. S. Mayer, and W. B. Gish, "Wavelets and electromagnetic power system transient," *IEEE Trans. on Power Delivery, vol. 11*, pp. 1050-1058, Apr. 1996.

[41]. S. Santoso, W. M. Grady, E. J. Powers, J. Lamoree, and S. C. Bhatt, "Characterization of distribution power quality events with fourier and wavelet transforms," *IEEE Trans. on Power Delivery, vol. 15*, pp. 247-254, Jan. 2000.

[42]. M. B. I. Reaz, F. Choong , M. S. Sulaiman, and F. Mohd-Yasin, "Prototyping of wavelet transform, artificial neural network and fuzzylogic for power quality disturbance classifier," *Electric Power Components & Systems,vol. 35, (1),* pp. 1–17, 2007.

[43]. M. B. I. Reaz, F. Choong, M. S. Sulaiman, F. Mohd-Yasin, M. Kamada, "Expert system for power quality disturbance classifier," *IEEE Trans. on Power Delivery, vol. 22, no. 3*, pp. 1979–1988, 2007.

[44]. F. Choong, M. B. I. Reaz, F. Mohd, "Advances in signal processing and artificial intelligence technologies in the classification of power quality events: a survey," *Electric Power Components & Systems, 33, (12),* pp. 1333–1349, 2005.

[45]. Milchevski, and D. Taskovski, "Improvement of wavelet based methods for classification of power quality disturbances", *14th ICHQP*, pp.1-4, 2010.

[46]. P. Janik, "Automated classification of power-quality disturbances using SVM and RBF networks," *IEEE Trans. on Power Delivery., vol. 21, iss. 3*, pp. 1663- 1669, Jul. 2006.

[47]. A. Teke, K. Bayindir, M. Tumay, "Fast sag/swell detection method for fuzzy logic controlled dynamic voltage restorer," *IET Generation Transmission Distribution, 4, (1),* pp. 1–12, 2010

[48]. P. K. Dash, R. K. Jena, M. M. A.Salama, "Power quality monitoring using an integrated Fourier linear combiner and fuzzy expert system," *International Journal of Power & Energy Systems, 21, (7),* pp. 497–506, 1999.

[49]. B. K. Panigrahi, V. R. Pandi, "Optimal feature selection for classification of power quality disturbances using wavelet packetbased fuzzy K-nearest neighbour algorithm," *IET Generation Transmission Distribution, 3, (3),* pp. 296–306, 2009.

[50]. K. S. Manish, R. Kapoor, "Classification of power quality events – A review Original Research Article," *International Journal of Electrical Power & Energy Systems, vol.43, iss.1*, pp.11-19, Dec. 2012.

[51]. O. Ozgonenel, T. Yalcin, I. Guney, U. Kurt, "A new classification for power quality events in distribution systems Original Research Article," *Electric Power Systems Research, vol. 95*, pp.192-199, Feb. 2013.

[52]. P.Kailasapathi, D. Sivakumar, "Methods to Analyze Power Quality Disturbances*," European Journal of Scientific Research*, pp.6-16, 2010.

[53]. S. Chen, and H. Y. Zhu, "Wavelet transform for processing power quality disturbances," *EURASIP Journal on advances in signal processing*, vol. 2007, Article ID 47695, 20 pages, 2007.

[54]. The Mathworks, "*Wavelet tool box- user's guide*", 2012.

[55]. G. Strang and T. Nguyen, *Wavelet and Filter Banks*, Wellesley-Cambridge Press, 1996.

[56]. C. K. Chui, *An Introduction to Wavelets*, Academic, Boston, 1992.

[57]. C. K. Chui, *Wavelets: A Tutorial in Theory and Applications*, Academic, Boston, 1992.

[58]. E. Fuchs; B. Trajanoska; S. Orhouzee; H. Renner, "Comparison of wavelet and Fourier analysis inpower quality," *Electric Power Quality and Supply Reliability Conference (PQ),* pp. 1-7, 2012.

[59]. H. Erişti; Y. Demir, "Automatic classification of power quality events and disturbances using wavelet transform and support vector machines," *Generation, Transmission & Distribution, IET, vol. 6, iss.10*, pp. 968-976, 2012.

[60]. Y. Hai; J. Chen, “Power quality evaluation based on wavelet packet decomposition and fuzzy logic,” *2012 IEEE International Conference on Computer Science and Automation Engineering (CSAE), vol.3* pp. 504 – 507, 2012.

[61]. I. D. Nicolae; P. M. Nicolae; M. S. Nicolae, “Improved wavelet-based techniques for power quality evaluation in three-phase systems,” *2012 IEEE International Symposium on Electromagnetic Compatibility (EMC)*, pp. 766 – 771, 2012.

[62]. N. C. F. Tse; J. Y. C. Chan; W. H. Lau; J. T. Y. Poon; L.L. Lai, “Real-Time Power Quality Monitoring with Hybrid Sinusoidal and Lifting Wavelet Compression Algorithm,” *IEEE Trans. on Power Delivery, vol. 27*,pp.1718 – 1726, 2012.

[63]. J. Barros, R. I. Diego, M. de Apráiz, “Applications of wavelets in electric power quality: Voltage events Review,” *Electric Power Systems Research, vol.88*, pp.130-136, Jul. 2012.

[64]. H. Dehghani, B. Vahidi, R.A. Naghizadeh, S.H. Hosseinian “Power quality disturbance classification using a statistical and wavelet-based Hidden Markov Model with Dempster–Shafer algorithm,” *International Journal of Electrical Power & Energy Systems, vol. 47*, pp.368-377, May 2013.

[65]. M.B.I. Reaz, F. Choong, M.S. Sulaiman, F.M. -Yasin, M. Kamada, “Expert system for power quality disturbance classifier,” *IEEE Trans. on Power Delivery, vol. 22*, pp. 1979–1988, 2007.

[66]. O. Gencer, S. Ozturk, T. Erfidan, “A new approach to voltage sag detection based on wavelet transform,” *Electric Power & Energy Systems, vol. 32*, pp. 133–140, 2010.

[67]. N.S. Tunaboylu, E.R. Collins, “The wavelet transform approach to detect and quantify voltage sags,” *IEEE ICHQP*, pp. 619–624, 1996.

[68]. S. Pastore, S. Quaia, L. Torelli, "Voltage sag analysis through wavelet transform," *9th IEEE MELECON, vol. 2*, pp. 959–963, 1998.

[69]. L. Angrisani, P. Daponte, M. D'Apuzzo, A. Testa, "A measurement method based on the wavelet transform for power quality analysis," *IEEE Trans. on Power Delivery, vol. 13*, pp. 990–998,1998.

[70]. O. Poisson, P. Rioual, M. Meunier, "New signal processing tools applied to power quality analysis," *IEEE Trans. on Power Delivery, vol. 14*, pp. 561–566, 1999.

[71]. J. Chung, E.J. Powers, W.M. Grady, S.C. Bhatt, "An automatic voltage sag detector using a discrete wavelet transform and a CFAR detector," *IEEE PES Summer Meet. 2*, pp. 689–693 2001.

[72]. S.-J. Huang, C.-T. Hsieh, C.-L. Huang, "Application of wavelets to classify power system disturbances," *Electric Power Systems Research,vol. 47*, pp. 87–93, 1998.

[73]. S.J. Huang, C.T. Hsieh, C.L. Huang, "Application of Morlet wavelets to supervise power system disturbances," *IEEE Trans. on Power Delivery, vol. 14*, pp. 235–243, 1999.

[74]. O. Poisson, P. Rioual, M. Meunier, "Detection and measurement of power quality disturbances using wavelet transform," *IEEE Trans. on Power Delivery, vol. 15*, pp. 1039–1044, 2000.

[75]. H. He, X. Shen, J.A. Staryk, "Power quality disturbances analysis based on EDMRA method," *Electric Power & Energy Systems, vol.* 31, pp. 258–268, 2009.

[76]. P. Gao, W. Wu, "Power quality disturbances classification using wavelet and support vector machines," *6th IEEE Int. Conf. on Intelligent Systems Design and Applications*, pp. 1–6, 2006.

[77]. S. Avdakovic, A. Nuhanovic, M. Kusljugic, M. Musi, "Wavelet transform applications in power system dynamics," *Electric Power Systems Research, vol. 83, iss. 1*, pp. 237-245, Feb. 2012.

[78]. W.G. Morsi, "A wavelet-based approach for reactive power metering in modern three phase grids considering time-varying power quality disturbances," *Electric Power Systems Research, vol. 87*, pp. 31-38, Jun 2012.

[79]. T. Zafar, W.G. Morsi "Power quality and the un-decimated wavelet transform: An analytic approach for time-varying disturbances," *Electric Power Systems Research, vol. 96*, pp. 201-210, 2013.

[80]. H. Shareef, A. Mohamed, A. A. Ibrahim, "An image processing based method for power quality event identification," *International Journal of Electrical Power & Energy Systems, vol.46*, pp.184-197, 2013.

[81]. M. A. A. Lima, A. S. Cerqueira, D.V. Coury, C. A. Duque, "A novel method for power quality multiple disturbance decomposition based on Independent Component Analysis," *International Journal of Electrical Power & Energy Systems, vol.42, iss. 1*, pp. 593-604, Nov 2012.

[82]. L. Angrisani, P. Daponte, M. D'Apuzzo, A. Testa, "A measurement method basedon the wavelet transform for power quality analysis," *IEEE Trans. on Power Delivery, vol. 13*, pp. 990–998, 1998.

[83]. M. Misiti, Y. Misiti, G. Oppenheim, and J.-M. Poggi, *Matlab wavelet toolbox user's guide*, MathWorks, Natick, MA, 1996.

[84]. T. K. Moon and W. C. Stirling, *Mathematical Methods and Algorithms for Signal Processing*, Prentice-Hall, Upper Saddle River, NJ, 2000.

[85]. O. Poisson, P. Rioual, and M. Meunier, "New signal processing tools applied to power quality analysis," *IEEE Transactions on Power Delivery, vol. 14, no. 2, pp.* 561–566, Apr. 1999.

[86]. J. Barros, R. I. Diego, and M. de Apráiz, "Applications of wavelets in electric power quality: Voltage events," *Electric Power Systems Research*, vol, 88, pp. 130-136, 2012.

[87]. S. Santoso, E. Powers, and P.Hofmann, "Power Quality Assesment Via Wavelet transform Analysis," *IEEE Trans. on Power Delivery, vol.11, no. 2*, pp. 924-930, Apr.1996.

[88]. O. Poisson, P. Rioual, and M. Meunier, " Detection and Measurement of Power Quality Disturbances Using Wavelet Transform," *IEEE Trans. on Power Delivery, vol. 15, no. 3*, pp. 1039-1044, Jul. 2000.

[89]. M. Manjula, A.V.R.S. Sarma, "Comparison of Empirical Mode Decomposition and Wavelet Based Classification of Power Quality Events," *Energy Procedia, vol. 14*, pp.1156-1162, 2012.

[90]. S. Nath, P. Sinha, S. K. Goswami, "A wavelet based novel method for the detection of harmonic sources in power systems," *International Journal of Electrical Power & Energy Systems, vol.40, iss. 1*, pp.54-61, Sep 2012.

[91]. D. Kostadinov; D. Taskovski, "Automatic voltage disturbance detection and classification using wavelets and multiclass logistic regression," *2012 IEEE International Instrumentation and Measurement Technology Conference (I2MTC)*, pp. 103–106, 2012.

[92]. F. B. Costa; J. Driesen, "Assessment of Voltage Sag Indices Based on Scaling and Wavelet Coefficient Energy Analysis," *IEEE Trans. on Power Delivery, vol. 28, iss. 1*, pp. 336 – 346, 2013.

[93]. Y. Zhang; H. Zhang, "Short Duration Voltage Variation Characterization through Wavelet Analysis," *Power and Energy Engineering Conference (APPEEC), 2011* Asia-Pacific. pp. 1–5, 2011.

[94]. M. Gaouda, M. M. A. Salam, M. R. Sultan, and A. Y. Chikhani, "Power quality detection and classification using wavelet-multiresolution signal

decomposition," *IEEE Trans. on Power Delivery, vol. 14, no. 10*, pp.1469–1476, Oct. 1999.

[95]. S.Santoso, W. Grady, and E. Powers, " Characterization of Distribution power Quality Events with Fourier and Wavelet Transforms*," IEEE Trans. on Power Delivery, vol. 15, no.1*, pp. 247-254, Jan. 2000.

[96]. X. X. Chen, "A wavelet-based method to detect, locate, quantify and identify slight deviations of amplitude and phase in power systems," *Paper presented at the IEEE Power Engineering Society General Meeting*, Toronto, July 2003.

[97]. Z.-L. Gaing, Implementation of power disturbance classifier using wavelet-based neural networks," *Paper presented at the IEEE Bologna Power Tech Conference*, Bologna, Italy, June 2003.

[98]. S.-J. Huang, C.-T. Hsieh, and C.-L. Huang, "Application of Morlet wavelets to supervise power system disturbances," *IEEE Trans. on Power Delivery, vol.14, no. 1*, pp. 235–243, January 1999.

[99]. O. Poisson, P. Rioual, and M. Meunier, "Detection and measurement of power quality disturbances using wavelet transform," *IEEE Trans. on Power Delivery, vol. 15, no. 3*, pp. 1039–1044, July 2000.

[100]. S. Santoso, W. M. Grady, E. J. Powers, J. Lamoree, and S. C. Bhatt, "Characteristics of distribution power quality events with Fourier and wavelet transforms," *IEEE Trans. on Power Delivery, vol. 15, no. 1*, pp. 247–254, Jan. 2000.

[101]. S. Santoso, E. J. Powers, and W. M. Grady, "Power quality disturbance data compression using wavelet transforms methods," *IEEE Trans. on Power Delivery, vol. 12, no. 3*, pp.1250–1257, Jul. 1997.

[102]. S. Santoso, E. J. Powers, W. M. Grady, and A. C. Parsons, "Power quality disturbance waveform recognition using wavelet-based neural classifier—part

1: Theoretical foundation," *IEEE Trans. on Power Delivery, vol. 15, no. 1*, pp. 222–228, Jan. 2000.

[103]. S. Santoso, E. J. Powers, W. M. Grady, and A. C. Parsons, "Power quality disturbance waveform recognition using wavelet-based neural classifier—Part 2: Application," *IEEE Trans. on Power Delivery, vol. 15, no. 1*, pp. 229–235, Jan. 2000.

[104]. N. S. Tunaboylu and E. R. Collins, "The wavelet transform approach to detect and quantify voltage sags," *Paper presented at the International Conference on Harmonics and Quality of Power*, Las Vegas, NV, Oct. 1996.

[105]. W. A. Wilkinson and M. D. Cox, "Discrete wavelet analysis of power system transients," *IEEE Trans. on Power Systems, vol. 11, on. 4,* pp. 2038–2044, Nov. 1996.

[106]. W. Kanitpanyacharoean, "Power Quality Problem Classification Using Wavelet Transformation and Artificial Neural Networks", *Power Systems Conference and Exposition, 2004. IEEE PES. vol.3*, pp 1496-1501, Oct. 2004.

[107]. T. K. Abdel-Galil, M. Kamel, A. M. Youssef, E. F. El-Saadany, and M. M. A. Salama, "Power quality Disturbance Classification Using the Inductive Inference Approach," *IEEE Trans. on power Delivery, vol. 19, no. 4*, pp. 1812-1818, Oct. 2004.

[108]. H. He, and J. Starzyk, "A Self-Organizing Learning Array System for power Quality Classification based on Wavelet transform", *IEEE Trans. on Power Delivery. Vol. 21, no. 1*, Jan. 2006.

[109]. M. A. S. Masoum, S. Jamali, and N. Ghaffarzadeh, "Detection and classification of power quality disturbances using discrete wavelet transform and wavelet networks," *IET Science, Measurement & Technology, vol.4, iss. 4*, pp. 193-205, 2010.

[110]. *IEEE recommended practice for monitoring electric power quality*, IEEE Std. 1159-2009, New York: IEEE, 2009.

[111]. S. Cho; C. Park; J. Han; G. Jang, "A Waveform Distortion Evaluation Method Based on a Simple Half-Cycle RMS Calculation," *IEEE Trans. on Power Del., vol. 27, iss. 3,* pp. 1461 – 1467, 2012.

[112]. J. R. Macedo Jr., I. N. Gondim, J. A. F. Barbosa Jr., C. E. Tavares, A. J. P. Rosentino Jr, "Practical Aspects of Performance Tests on Power Quality Analyzers", *International Conference on Renewable Energies and Power Quality ,(ICREPQ'12),* Santiago de Compostela, Spain, 28-30 March, 2012.

[113]. M. Albu and G.T. Heydt, "On the Use of RMS Values in Power Quality Assessment*," IEEE Trans. on Power Delivery, vol. 18, no. 4,* Oct. 2003, pp. 1586-1587.

[114]. M. McGranaghan, "Trends in power quality monitoring," *IEEE Power Engineering Review, vol. 12, no. 10*, pp. 3–9, Oct. 2001.

[115]. H. Ribeiro, H. Marques, B.V. Borges, "Characterizing and monitoring voltage transients as problem to sensitive loads," *International Journal of Electrical Power & Energy Systems, vol.43, iss.1*, pp. 1305-1317, Dec. 2012.

[116]. A. Honrubia-Escribano, E. Gómez-Lázaro, A. Molina-García, J.A. Fuentes, "Influence of voltage dips on industrial equipment: Analysis and assessment," *International Journal of Electrical Power & Energy Systems, vol. 41, iss. 1*, pp. 87-95, Oct. 2012.

[117]. H. Akagi, "New trends in active filters for power conditioning," *IEEE Trans. on Industrial Applications, vol. 32, no. 6,* pp. 1312–1322, Nov. 1996.

[118]. S. Srivastava, S. Suryanarayanan, P. Ribeiro, D. Cartes and M. Stcurer," A Conceptual Power Quality Monitoring Technique Based on Multi-Agent Systems," *Power Symposium, 2005. Proceedings of the 37th Annual North American* , pp 358-363, 2005.

[119]. C.F.M. Almeida, N. Kangan, "Allocation of Power Quality Monitors by Genetic Algorithms and Fuzzy Sets Theory," *15th International Conference on Intelligent System Applications to Power Systems, 2009. ISAP '09*, pp 1-6, 2009.

[120]. T.Lobos, T.Kozina and H.J.Koglin, "Power system harmonics estimation using linear least squares method and SVD," *IEE Generation, Transmission and Distribution, vol. 148, no. 6*, pp.567-572, 2001.

[121]. T. X. Zhu, "Exact harmonics/interharmonics calculation using adaptive window width," *IEEE Trans. on Power Delivery, vol. 22, no. 4*, pp. 2279–2288, Oct. 2007.

[122]. P.K. Dash, A.M. Sharaf, "A Kalman filtering approach for estimation of power system harmonics," *Proc. 3rd Int. Conf. on Harmonics in Power Systems, 1988*, Nashville, TN, pp. 34–40..

[123]. H. Ma and A.A. Girgis, "Identification and tracking of harmonic sources in a power system using Kalman filter," *IEEE Trans. on Power Delivery,vol. 11,* , no. 4, pp. 1659–1665, 1996.

[124]. K. K. C Yu, "An adaptive Kalman filter for dynamic harmonic state estimation and harmonic injection tracking," *IEEE Trans. on Power Delivery,vol. 20,* , no. 2, pp. 1577–1584, Apr. 2005.

[125]. F. F. Costa, A. J. M. Cardoso, and D. A. Fernandes, "Harmonic analysis based on kalman filtering and prony's method," *Int. Conf. Power Engineering, Energy Electrical Drives*, Setúbal, Portugal, Apr. 12-14, 2007, pp. 696–701.

[126]. E. Y. Hamid and Z. Kawasaki, "Wavelet packet transform for rms values and power measurements," *IEEE Power Engineering Review, vol. 21, no. 9*, pp. 49–51, Sep. 2001.

[127]. E. Y. Hamid and Z. Kawasaki, “Instrument for the quality analysis of power systems based on the wavelet packet transform,” *IEEE Power Engineering Review*, vol. 22, no. 3, pp. 52–54, Mar. 2002.

[128]. L. Eren and M. J. Devaney, “Calculation of power system harmonics via wavelet packet decomposition in real time metering,” *IEEE IMTC, Anchorage*, AK, May 21–23, pp. 1643–1647, 2002.

[129]. M. Bettayeb; Q. Uvais, “A hybrid least squares-GA-based algorithm for harmonic estimation,” *IEEE Trans. on Power Delivery, vol. 18, no. 2,* pp.377-382, 2003.

[130]. V.Suresh Kumar, P.S.Kannan, K.Kalaiselvi, and D.Kavitha, "Optimal Estimation of Harmonics in Power System using Intelligent Computing Techniques," *International Joint Conference on Neural Networks, IJCNN 2007*, pp. 142-147, 2007.

[131]. Z. Lu, T. Y. Ji, W. H. Tang, and Q. H. Wu, “Optimal Harmonic Estimation Using A Particle Swarm Optimizer,” *IEEE Trans. on Power Delivery, vol.23, no. 2*, pp. 1166-1174, Apr. 2008.

[132]. T.Y. Ji, M.S. Li, Q.H. Wu, and L. Jian, “Optimal estimation of harmonics in a dynamic environment using an adaptive bacterial swarming algorithm,” *IET Generation, Transmission & Distribution, vol. 5, iss. 6*, pp. 609– 620, 2011.

[133]. P. K. Ray and B. Subudhi, “BFO optimized RLS algorithm for power system harmonics estimation,” *Applied Soft Computing 12*, pp.1965–1977, 2012

[134]. J. Bruls, C.T. Chou, B.R.J. Haverkamp and M. Verhaegen, “Linear and non-linear system identification using separable least-squares,” *Delft University of Technology*, 15 Dec. 1997.

[135]. M. S. Ballal, H.M. Suryawanshi, and T. Venkateswara Reddy, “Mitigation of Voltage Dip and Voltage Flickering by Multilevel D-STATCOM,” *Advances in Power Electronics, vol. 2012, Article ID 871652*, pp.1-11, 2012.

[136]. K. W. Lao; N. Dai; W. G. Liu; M. C. Wong, "Hybrid Power Quality Compensator With Minimum DC Operation Voltage Design for High-Speed Traction Power Systems," *IEEE Trans. on Power Electronic., vol. 28, iss. 4*, pp. 2024 – 2036, 2013.

[137]. J. M. Guerrero; Poh Chiang Loh; Tzung-Lin Lee; M. Chandorkar, "Advanced Control Architectures for Intelligent Microgrids—Part II: Power Quality, Energy Storage, and AC/DC Microgrids," *IEEE Trans. on Industrial Electronics, vol. 60, iss. 4*, pp.1263–1270, 2013.

[138]. Qing-Chang Zhong; T. Hornik, "Cascaded Current–Voltage Control to Improve the Power Quality for a Grid-Connected Inverter with a Local Load," *IEEE Trans. on Industrial Electronics, vol. 60, iss. 4*, pp. 1344-1355, 2013.

[139]. K. R. Suja; I. J. Raglend, "Power quality improvement in grid connected wind energy system using STATCOM," *2012 International Conference on Computing, Electronics and Electrical Technologies (ICCEET),* pp. 259 – 266, 2012.

[140]. X. Yang; T. Q. Zheng; Z. Lin; T. Xiong; X. You, "Power quality controller based on hybrid modular multilevel converter," *2012 IEEE International Symposium on Industrial Electronics (ISIE),* pp.1997 – 2002, 2012

[141]. T. Zaveri, B. Bhalja, N. Zaveri, "Comparison of control strategies for DSTATCOM in three-phase, four-wire distribution system for power quality improvement under various source voltage and load conditions," *International Journal of Electrical Power & Energy Systems, vol. 43, iss.1*, pp. 582-594, Dec. 2012.

[142]. B. B. Bukata; Y. Li, "A novel model-free prediction of power quality problems via DSTATCOM," *2012 18th International Conference on Automation and Computing (ICAC),* pp. 1 – 6, 2012.

[143]. H. Ghosh; P. K. Saha; G. K. Panda, "Performance comparison between DVR and DSTATCOM used for load voltage control in distribution side," *2012 International Conference on Advances in Power Conversion and Energy Technologies (APCET),* pp. 1 – 6, 2012.

[144]. C. Bhattacharjee; A. K. Roy; B. K. Roy, "Improvement of available load voltage for a constant speed WECS coupled with fuzzy-controlled DSTATCOM," *2012 IEEE 15th International Conference on Harmonics and Quality of Power (ICHQP),* pp. 637 – 641, 2012.

[145]. J. G. P. Reddy; K. R. Reddy, "Power quality improvement using Neural Network controller based cascaded H-Bridge multilevel inverter type D-STATCOM," *2012 International Conference on Computer Communication and Informatics (ICCCI),* pp.1-6, 2012.

[146]. C. J. Hatziadoniu, F. E. Chalkiadakis, "A 12-pulse static synchronous compensator for the distribution system employing the 3-level GTO-inverter," *IEEE Trans. Power Delivery., vol.12, iss.4*, pp.1830–1835, 1997.

[147]. C. Sharmeela, G. Uma, M. R. Mohan, "Multi-level distribution STATCOM for voltage sag and swell reduction," *IEEE PES GM, vol. 2*, pp. 1303–1307, 2005.

[148]. H. Masdi, N. Mariun, S. M. Bashi, A. Mohamed, S. Yusuf, "Design of a prototype D-Statcom using DSP controller for voltage sag mitigation," *IEEE Int. Conf. Power Electronics and Drives Systems, PEDS, vol. 1*, 2006, pp. 569–574.

[149]. H. Akagi, S. Inoue, T. Yoshii, "Control and performance of a transformerless cascade PWM STATCOM with Star configuration," *IEEE Trans. on Industrial Applications, vol. 43, iss. 4*, pp. 1041–1049, 2007.

[150]. K. V. Patil, R. M. Mathur, J. Jiang, S. H. Hosseini, "Distribution system compensation using a new binary multilevel voltage source inverter," *IEEE Trans. Power Delivery., vol. 14, iss. 2*, pp. 459–464, 1999.

[151]. G. F. Reed, M. Takeda, I. Iyoda, "Improved power quality solutions using advanced solid-state switching and static compensation technologies," *IEEE Power Engineering Society WM, vol. 2*, pp. 1132–1137, 1999.

[152]. "Application of a 5 MVA, 4.16 kV D-STATCOM system for voltage flicker compensation at Seattle iron & metals," *IEEE PES SM*, pp. 1605–1611, 2000.

[153]. J. Sun, D. Czarkowski, Z. Zabar, "Voltage flicker mitigation using PWM-based distribution STATCOM," *IEEE PES*, Chicago SM, 21–25 July 2002.

[154]. K. Sano and M. Takasaki, "A transformer less D-STATCOM based on a multi voltage cascade converter requiring no DC sources," *IEEE Trans. on Power Electronics, vol. 27, no. 6*, pp. 2783–2795, 2012.

[155]. A. K. Jain, K. Joshi, A. Behal, and N. Mohan, "Voltage regulation with STATCOMs: modeling, control and results," *IEEE Trans. on Power Delivery, vol. 21, no. 2*, pp. 726–735, 2006.

[156]. B. Singh, R. Saha, A. Chandra, K. Al-Haddad, "Static synchronous compensators (STATCOM): a review," *IET Power Electronics, Vol. 2, Iss. 4*, pp. 297–324, 2009.

[157]. B. Singh, J. Solanki, "A Comparison of Control Algorithms for DSTATCOM," *IEEE Trans. on Industrial Electronics, vol. 56, no. 7*, Jul. 2009.

[158]. R. Singh; D. K. Singh, "Simulation of D-STATCOM for Voltage Fluctuation," *2012 Second International Conference on Advanced Computing & Communication Technologies (ACCT)*, pp. 225–230, 2012.

[159]. N. K. Kummari; A. K. Singh; P. Kumar, "Comparative evaluation of DSTATCOM control algorithms for load compensation," *2012 IEEE 15th International Conference on Harmonics and Quality of Power (ICHQP),* p. 299 – 306, 2012.

[160]. B. Singh; S. Arya, "Adaptive Theory Based Improved Linear Sinusoidal Tracer Control Algorithm for DSTATCOM," *IEEE Trans. on Power Electronics, vol. PP, iss. 99,* pp.1-11, 2012.

[161]. T. Zaveri, B. R. Bhalja, N. Zaveri, "Load compensation using DSTATCOM in three phase, three-wire distribution system under various source voltage and delta connected load conditions," *International Journal of Electrical Power & Energy Systems, vol. 41, iss. 1,* pp. 34-43, Oct 2012.

[162]. G. Karmiris, G. Tsengenes, G. Adamidis, "A multifunction control scheme for current harmonic elimination and voltage sag mitigation using a three phase three level flying capacitor inverter," *Simulation Modelling Practice and Theory, vol. 2*4, pp.15-34, May 2012.

[163]. D. Sreenivasarao, P. Agarwal, B. Das, "A T-connected transformer based hybrid D-STATCOM for three-phase, four-wire systems," *International Journal of Electrical Power & Energy Systems, vol. 44, iss. 1,* pp. 964-970, Jan 2013.

[164]. S. Li, L. Xu, T. A. Haskew, "Control of VSC-based STATCOM using conventional and direct-current vector control strategies," *International Journal of Electrical Power & Energy Systems, vol. 45, iss. 1,* pp. 175-186, Feb 2013.

[165]. X. Tan, Q. Li, H. Wang, "Advances and trends of energy storage technology in Microgrid*," International Journal of Electrical Power & Energy Systems, vol. 44, iss. 1,* pp.179-191, Jan 2013.

[166]. N. Chellammal, S. Sekar Dash, S. Premalatha, N. K. Rajaguru, “Three Phase Multicarrier PWM Switched Cascaded Multilevel Inverter as Voltage Sag Compensator,” *AASRI Procedia, vol. 2*, pp. 282-287, 2012.

[167]. R. M Gnativ; J. V. Milanovic, “Identification of voltage sag characteristics from the measured responses," *10th International Conference on Harmonics and Quality of Power, 2002, vol. 2*, pp. 535- 540, 2002.

[168]. V. B. B. a. P. N. Enjeti, "An active line conditioner to balance voltage in a three-phase system," *IEEE Trans. on Industry Applications, vol. 32*, pp. 287-292, 1996.

[169]. V. Kaura and V. Blasko, "Operation of a phase locked loop system under distorted utility conditions," *IEEE Trans. on Industry Applications, vol. 33*, pp. 58-63, 1997.

[170]. P. Rodríguez, J. Pou, J. Bergas, J. Ignacio, R. P. Burgos and D. Boroyevich, “Decoupled Double Synchrounous Reference Frame PLL for Power Converters Control,” *IEEE Trans on Power Electronics, vol. 22, no. 2*, pp. 584-592, Mar 2007.

[171]. S. K. Chung, “Phase-Locked Loop for Grid-Connected Three-Phase Power Conversion Systems,” *IEE Proc. of Electrical Power Application, vol. 147, no. 3*, pp. 213-219, May 2000.

[172]. M. Nakamura, A. Yamagishi, M. Harada and K. Kishine, “Fast acquisition PLL using fully digital natural-frequency-switching technique,” *Electronics Letters, vol. 44*, pp. 267-268, 2008.

[173]. P.Wang, N. Jenkins, and M. H. J. Bollen, “Experimental investigation of voltage sag mitigation by an advanced static VAR compensator,” *IEEE Trans. on Power Delivery, vol. 13, no. 4*, pp. 1461–1467, Oct. 1998.

[174]. M. Takeda, K. Ikeda, A. Teramoto, and T. Aritsuka, "Harmonic current and reactive power compensation with an active filter," *Power Electronic Specialist Conference,* 1988, pp. 1174–1179.

[175]. H. Fujita and H. Akagi, "The unified power quality conditioner: The integration of series active filter and shunt active filters*," IEEE Trans. on Power Electroics, vol. 13, no. 2*, pp. 315–322, Mar. 1998.

[176]. T. Manmek and C. P. Mudannayake, "Real-Time Implementation of Voltage Dip Mitigation using D-STATCOM with Fast Extraction of Instantaneous Symmetrical Components," *Power Electronics and Drive Systems, PEDS '07*, pp.568-575, 2007

[177]. M. Aredes, K. Heumann, and E. H. Watanable, "An universal active power line conditioner," *IEEE Trans. on Power Delivery, vol. 13, no. 2*, pp. 545–551, Apr. 1998.

[178]. S. Bhattacharya, D. M. Divan, and B. Banerjee, "Synchronous frame harmonic isolator using active series filter," *Europian Power Electronics and Applications Conf.*, 1993, pp. 30–35.

[179]. H. Ma and A. A. Girgis, "Identification and tracking of harmonic sources in a power system using a kalman filter," *IEEE Trans. on Power Delivery., vol. 11, no. 3*, pp. 1659–1665, Jul. 1996.

[180]. A. A. Girgis and E. B. Makram, "Measurement of voltage flicker magnitudeand frequency using a kalman filtering based approach," *in Proc.Canad. Conf. Electrical and Computer Engineering*, 1996, pp. 659–662.

[181]. H. M. Beides and G. T. Heydt, "Dynamic state estimation of power system harmonics using kalman filter methodology," *IEEE Trans. on Power Delivery, vol. 6, no. 4*, pp. 1663–1670, Oct. 1991.

[182]. M. Kubis, and C. S. Choo, “Real-Time Monitoring and Analysis System for power Quality,” *A white paper published by National instrument*s, Texas, 2005.

[183]. L. Sevgi, “ A LabVIEW-Based Analog Modulation Tool for Virtual and real Experimentation,” *IEEE Antennas and Propoagation magazine, vol. 54, no. 6*, pp.246-254, Dec, 2012.

[184]. Y. Yang, X. Wang, C. Chen, “Real-time Power Quality Monitoring and analysis Platform of Rural power Networks Based on Virtual Instruments,” *The 9th Int. Conf. on Electronic Measurement & Instruments*, pp.630-635, 2009.

[185]. S. Laskar, M. Muhammad, “power Quality Monitoring by Virtual Instrumentation using LabVIEW,” *46th Unversities’ Power Engineering Conf., 5-8 Sep 2011*, Soest, Germany, 2011.

[186]. R. Pecen, M. D. Salim, and Zora, Ayhan., "A LabVIEW Based Instrumentation system for a Wind- Solar Hybrid Power Station," *Journal of National Association of Industrial Technology, vol. 20, no. 3*, pp. 1-8, Aug 2004.

[187]. C. Zang, and Y. Wen, “The Application of Virtual Instrument Technology in High voltage Measuring system,” *Transmission and Distribution Conference and Exhibition 2002: Asia Pacific. IEEE/PES, vol 3*, pp. 2300-2304, 2002.

[188]. J. Chen, T. Tang, “ Power Quality analysis based on labVIEW for Current Power Generation System,” *Internationl Symposium on Power Electronics*, pp. 865- 870, 2012.

[189]. Z. Li, “ Voltage Fluctuation and Flicker Monitoring System Using LabVIEW and Wavelet Transform,” *Journal of Computer, vol.5, no.3*, pp.417-424, Mar 2010.

[190]. P. Yin, m. Chilukuri, “Remote Power Quality Monitoring and Analysis System Using LabVIEW Software,” *12MTC 2009-International Instrumentation and Measurement Technology Conference*, pp. 279-283, Singapore,5-7 May 2009.

[191]. G. Gasparesc, “ Remote Monitoring System for Power Quality Analysis Based on Virtual Instrumentation,” *35th International Conference on Telecommunications and Signal Processing (TSP),* pp. 302- 306, 2012.

[192]. M. Misiti, Y. Misiti, G. Oppenheim, and J.-M. Poggi, *Matlab wavelet toolbox user’s guide*, MathWorks, Natick, MA, 1996.

[193]. D. C. Robertson, O. I. Camps, J. S. Mayer, and W. B. Gish Sr.,“Wavelets and electromagnetic power system transients,” *IEEE Trans. on Power Delivery, vol. 11, no. 2,* pp. 1050–1056, 1996.

[194]. A.C. Parsons, W.M. Grady, E.J.Powers, “ A wavelet-based procedure for automatically determining the beginning and end of transmission system voltage sags,” *IEEE PES Winter Meeting 1999*, pp.1310–1315.

[195]. J. Barros, E. Pérez, “A combined wavelet - Kalman filtering scheme for automatic detection and analysis of voltage dips in power systems,” *PowerTech. Conf*., 2005, pp.1–5.

[196]. M. H. J. Bollen, *Understanding Power Quality Problems: Voltage Sags and Interruptions*. Piscataway, NJ: IEEE Press, 2000.

[197]. J. Barros and E. Pérez, “Limitations in the Use of rms Value in Power Quality Analysis,” *IEEE Instrumentation and Measurement Technology Conference, IMTC2006*, Sorrento, Italy, pp. 2261 – 2264.

[198]. J. Howard and H. Landgraf, “Quadrature sampling phase detection,” *American Institute of physics, Review of scientific instruments , vol. 65, no.6*, pp. 2130-2133,1994.

[199]. S. Wetterlin, (2007), A *Method of Using Quadrature Sampling to Measure Phase and Magnitude,* www.wetterlin.org/sam/QuadratureSampling.pdf.

[200]. F. Herrera, M. Lozano and J.L. Verdegay," Tackling Real Coded Genetic Algorithms_ Operators and Tools for Behavioural Analysis," *Kluwer Academic Publishers*, pp. 265-319, 1998.

[201]. J. Kennedy and R. Eberhart, "Particle swarm optimization," *in Proc. IEEE Int. Conf. Neural Networks, Perth, Australia, vol. 4*, pp.1942–1948, 1995.

[202]. H.Mori, "An artificial neural network based method for power system voltage harmonics," *IEEE Trans. on Power delivery, vo1.7, no.1*, pp.402-409, 1992.

[203]. S.Osowski, "Neural network for estimation of harmonic components in a power system," *IEE Proceeding-C Generation, Transmission and Distribution, vol 139, no.2*, pp.129-135, 1992.

[204]. http://www.mathworks.com/moler/leastsquares.pdf

[205]. J. Faires and R. Burden, *Numerical Methods,* Books/Cole, Cengage Learning, 4th Ed, 2013.

[206]. J. Devore, *Probability and Statistics for Engineering and Sciences*, Books/Cole, Cengage Learning, 8th Ed, 2012.

[207]. M. Bettayeb and U. Qidwai, "Recursive estimation of power system harmonics," *Electric Power Systems Research, vol. 47*, pp. 143–152, 1998.

[208]. Hingorani NG, Gyugyi L, *Understanding FACTS. Concepts and Technology of Flexible AC Transmision Systems*, New York: IEEE Press, 1999.

[209]. Ghosh A, Ledwich G, *Power Quality Enhancement Using Custom Power Devices*, Bostom, Dordrecht, London: Kluwier Academic Publishers, 2002.

[210]. Antonio Moreno-Muñoz (Ed.), *Power Quality Mitigation Technologies in a Distributed Environment*, Springer-Verlag London Limited, 2007.

[211]. R. Bitter, T. Mohiuddin, and M. Nawrocki, *LabVIEW Advanced Techniques*, second edition, 2007.

[212]. National Instruments, *LabVIEW Graphical Programming Course*, 2007.

[213]. National Instruments, *CompactRIO Developers Guide*, Dec. 2009.

[214]. D. Alexa, A. Sarbu, I. V. Pletea, C. Filote, R. Chiper, "Variants of Rectifiers with Near Sinusoidal Input Currents – a Comparative Analysis with the Conventional Diode Rectifier," *IET Power Electronics, vol. 4, no. 6*, pp. 632–641, 2011.

[215]. A. I. Maswood, E. Firmansyah, "Current Injection in a Controlled Rectifier under Unbalanced Supply and Variable Line and Load Inductances," *IET Power Electronics, vol. 2, no. 4*, pp. 387–397, 2009.

[216]. M. E. Villablanca, J. I. Nadal, F. A. Cruzat, W. C. Rojas, "Harmonic Improvement in 12-Pulse Series-Connected Line-Commutated Rectifiers," *IET Power Electronics, vol. 2, no. 4*, pp. 466–473, 2009.

[217]. J. C. Das, "Passive filters – potentialities and limitations," *IEEE Trans. on Industry Applications, vol. 40, no. 1*, pp. 232–241, 2004.

[218]. A. B. Nassif, W. Xu, W. Freitas, "An Investigation on the Selection of Filter Topologies for Passive Filter Applications," *IEEE Trans. on Power Delivery, vol. 24, no. 3*, pp. 1710-1718, 2009.

[219]. Z. Shu, S. Xie, Q. Li, "Single-Phase Back-To-Back Converter for Active Power Balancing, Reactive Power Compensation, and Harmonic Filtering in Traction Power System," *IEEE Trans. on Power Electronics, vol. 26, no. 2*, PP. 334-343, 2011.

[220]. M. Gol, O. Salor, B. Alboyac, B. Mutluer, I. Cadırc, M. Ermis, "A New Field-Data-Based EAF Model for Power Quality Studies," *IEEE Trans. on Industry Applications*, vol. 46, no. 3, pp. 1230-1242, 2010.

[221]. T. L. Lee, S. H. Hu, "Discrete Frequency-Tuning Active Filter to Suppress Harmonic Resonances of Closed-Loop Distribution Power Systems," *IEEE Trans.on Power Electronics, vol. 26, no. 1,* pp. 137-148, 2011.

[222]. C. Cecati, A. D. Aquila, V. G. Monopoli, "Design of H-Bridge Multilevel Active Rectifier for Traction Systems," *IEEE Trans. on Industry Applications, vol. 39, no. 5,* pp. 1541–1550, 2003.

[223]. H. Fujita, "A Single-Phase Active Filter Using an H-Bridge PWM Converter with a Sampling Frequency Quadruple of the Switching Frequency," *IEEE Trans. on Power Electronics, vol. 24, no. 4,* pp. 934–941, 2008.

[224]. G. W. Chang, Y. J. Liu, V. Dinavahi, H. J. Su, "On Real-Time Simulation for Harmonic and Flicker Assessment of an Industrial System With Bulk Nonlinear Loads," *IEEE Trans. on Industrial Electronics, vol. 57, no. 9,* pp. 2998-3009, 2010.

[225]. Z. Shuai, A. Luo, W. Zhu, R. Fan, K. Zhou, "Study on a Novel Hybrid Active Power Filter Applied to a High-Voltage Grid," *IEEE Trans. on Power Delivery, vol. 24, no. 4,* pp. 2344-2352, 2009.

[226]. H. Akagi, R. Kondo, "A Transformerless Hybrid Active Filter Using a Three-Level Pulsewidth Modulation (PWM) Converter for a Medium-Voltage Motor Drive," *IEEE Trans. on Power Electronics, vol. 25, no. 6,* pp. 1365-1374, 2010.

[227]. K. Lee, V. Blasko, T. M. Jahns, T. A. Lipo, "Input Harmonic Estimation and Control Methods in Active Rectifiers," *IEEE Trans. on Power Delivery, vol. 25, no. 2,* pp. 953-960, 2010.

[228]. R. Pragale, T. J. Dionise, D. D. Shipp, "Harmonic Analysis and Multistage Filter Design for a Large Bleach Production Facility," *IEEE Trans. on Industry Applications, vol. 47, no. 3,* pp. 1201-1209, 2011.

[229]. B. Singh, S. Singh, S. P. H. Chender, "Harmonics Mitigation in LCI-Fed Synchronous Motor Drives," *IEEE Transactions on Energy Conversion, vol. 25, no. 2,* pp. 369-380, 2010.

[230]. J. Yong, L. Chen, S. Chen, "Modeling of Home Appliances for Power Distribution System Harmonic Analysis," *IEEE Transactions on Power Delivery, vol. 25, no. 4,* pp. 3147-3155, 2010.

[231]. P. Xiao, G. K. Venayagamoorthy, K. A. Corzine, "Seven-Level Shunt Active Power Filter for High-Power Drive Systems," *IEEE Trans. on Power Electronics, vol. 24, no. 1,* pp. 6-13, 2009.

[232]. P. Kumar, A. Mahajan, "Soft Computing Techniques for the Control of an Active Power Filter," *IEEE Trans. on Power Delivery, vol. 24, no. 1,* pp. 452-461, 2009.

[233]. W. Zhao, A. Luo, Z. J. Shen, C. Wu, "Injection-Type Hybrid Active Power Filter in High-Power Grid with Background Harmonic Voltage," *IET Power Electronics, vol. 4, no. 1,* pp. 63–71, 2011.

[234]. H. Akagi, K. Isozaki, "A Hybrid Active Filter for a Three-Phase 12-Pulse Diode Rectifier Used as the Front End of a Medium-Voltage Motor Drive," *IEEE Trans. on Power Electronics, vol. 24, no. 1,* pp. 69-77, 2012.

[235]. A. Teke, L. Saribulut, M. Tumay, "A Novel Reference Signal Generation Method for Power-Quality Improvement of Unified Power-Quality Conditioner," *IEEE Trans. on Power Delivery, vol. 26, no. 4,* pp. 2205-2214, 2011.

[236]. M. A. M. Radzi, N. A. Rahim, "Three-Phase Switched Capacitor Active Power Filter with Modified Artificial Neural Network and Flexible-Band Hysteresis," *International Review of Electrical Engineering (IREE), vol. 6, no. 5,* pp. 2114-2121, 2010.

[237]. H. Akagi, "Active Harmonic Filters," *Proceedings of IEEE, vol. 93, no. 12*, pp. 2128– 2141, 2005.

[238]. M. El-Habrouk, M. K. Darwish, P. Mehta, "Active Power Filters: A Review," *Electric Power Applications, IEE Proceedings, vol. 147, no. 5,* pp. 403–413, 2000.

[239]. B. Singh, K. Al-Haddad, A. Chandra, "A Review of Active Filters for Power Quality Improvement," *IEEE Trans. on Industrial Electronics, vol. 46, no. 5*, pp. 960–971, 1999.

[240]. T. C. Green, J. H. Marks, "Control Techniques for Active Power Filters," *Electric Power Applications, IEE Proceedings, vol. 152, no. 2,* pp. 369–381, 2005.

[241]. P. Mehta, M. Darwish, T. Thomson, "Switched-Capacitor Filters," *IEEE Trans. on Power Electronics, vol. 5, no. 3,* pp. 331–336,1990.

[242]. P. Mehta, M. Darwish, "Active Reactive-Power Controller," *Electric Power Applications, IEE Proceedings, vol. 142, no. 6,* pp. 405–409, 1995.

[243]. M. El-Habrouk, M. K. Darwish, "A New Control Technique for Active Power Filters Using a Combined Genetic Algorithm/Conventional Analysis," *IEEE Trans. on Industrial Electronics, vol. 49, no.1*, pp. 58–66, 2002.

[244]. T. Kandil, L. Lopes, W. Xu, "Analysis and Design of a New Current Controlled Switched Capacitor Filter for Harmonic Mitigation," *Electric Power Components & Systems vol. 33, no. 1*, pp. 1–20, 2005.

[245]. C.Weiji, C. Wenhong, M. Xiaojun, C. Jianye, W. Zhonghong, and H. Yingdua, " An Adaptive Noise Canceling Theory Based Single-Phase Shunt Active power Filter," *PCC-Nagaoka 97*, pp.191-196, 1997.

[246]. S. Luo, Z. Hou, "An adaptive Detecting Method for Harmonic and reactive Currents," *IEEE Trans. on Industrial Electronics, vol.42, no.1*, pp.85-89, 1995.

[247]. B. Singh, S. Arya, "Design and control of a DSTATCOM for power quality improvement using cross correlation function approach," *International Journal of Engineering, Science and Technology, vol. 4, no.1*, pp. 74-86, 2012.

[248]. C. Canizares, M. Pozzib, S. Corsib, E. Uzunovic "STATCOM Modeling for Voltage and Angle Stability Studies," *International Journal of Electrical power & Energy Systems, vol. 25, iss. 6*, pp. 431–441, July 2003.

[249]. K. Somsai, T. Kulworawanichpong, N. Voraphonpiput, "Design of DC Voltage Control for D-STATCOM," *World Academy of Science, Engineering and Technology, vol. 71*, pp.420-426, 2012.

[250]. B. Singh, P. Jayaprakash, D. Kothari, "A three Phase four-wire DSTATCOM for power quality improvement," *Journal of power Electronics, vol.8, no.3*, pp.259-265, 2008.

[251]. S. Du, J. Liu, J. Lin, Y. He, "A Novel DC Voltage Control Method for STATCOM Based on Hybrid Multilevel H-Bridge Converter," *IEEE Trans. on Power Electronics, vol.28, no.1*, pp. 101-111, Jan. 2013.

[252]. C. Schauder, H. Mehta, "Vector Analysis and control of advanced static VAR Compensators," *IEE Proceedings-C, vol.140, no.4*, pp. 299-306, Jul. 1993.

[253]. S. Woo, D. Kang, W. Lee, D. Hyum, "The distribution STATCOM for Reducing the effect of Voltage Sag and Swell," *The 27th Annual Conference of the IEEE Industrial Electronics Society*, pp. 1132-1137, 2001.

PUBLICATIONS

PATENTS:

1. **F. R. Zaro**, M. A. Abido, M. A. Elgibiely, "A New Method for Real-Time Voltage Events Detection and Classification Based on Wavelet Transform,". (Filed)

2. **F. R. Zaro**, M. A. Abido, "Efficient On-Line Detection Scheme of Voltage Events Using Quadrature Method,". (Filed)

PAPERS:

1. **F. R. Zaro**, M. A. Abido, M. A. Elgibiely, "Real-Time Voltage Events Detection and Classification Based on Wavelet Transform," *IEEE Transaction on Power Delivery*. (Submitted)

2. **F. R. Zaro**, M. A. Abido, "Efficient On-Line Detection Scheme of Voltage Events Using Quadrature Method," *Electrical Engineering Journal*. (Submitted)

3. **F. R. Zaro** and M. A. Abido , "Real Time Detection and Classification Wavelet Transform-Based for Voltage Events," *Towards carbon free society through smarter grids, Grenoble France,* 16-20 June 2013. (Accepted)

4. S. Ameenuddin, **F. R. Zaro** and M. A. Abido, "Implementation of quadrature based RMS calculation on real-time systems," *Power and Energy Conference at Illinois*, February 22-23, 2013, USA.

5. **F. R. Zaro**, S. Elferik and M. A. Abido, "Optimal Estimation of Harmonics in Power System Using Intelligent Techniques," *The 32nd IASTED International Conference on Modelling, Identification and Control ~MIC 2013*~February 11 – 13, 2013,Innsbruck, Austria.

6. **F. R. Zaro**, M. A. Abido, S. Ameenuddin and I. M. El-Amin, " Characterization of Short-duration Voltage Events," *IEEE International Conf. on Power and Energy (PECon),* 2-5 December 2012, Kota Kinabalu Sabah, Malaysia, pp.650-654.

7. **F. R. Zaro**, M. A. Abido, "Real-Time Detection and Classification Scheme for Voltage Events Based on Wavelet Transform," 4th Scientific Conference, 29-4 to 2-5, 2013, Makkah, KSA.(submitted)

VITA

- Fouad Rashed Fouad Zaro.
- Born in Hebron City of Palestine in 1981.
- Received Bachelor's degree in Science of Electrical Engineering from Palestine Polytechnic University, Hebron-Palestine in June 2004.
- Received M.Sc degree in Science of Electrical Engineering from King Fahd University of Petroleum and Minerals in January of 2010.
- I am Lecturer_B in Electrical Engineering Department of King Fahd University of Petroleum and Minerals, since February of 2010 tell now.
- I was Research Assistant in Electrical Engineering Department of King Fahd University of Petroleum and Minerals, for August of 2007 to January of 2010.
- I was lecturer in Palestine Polytechnic University from September of 2005 up to June of 2007.
- E-mails: zarofuad@yahoo.com, zarofuad@gmail.com, zaro@kfupm.edu.sa
- Skype Name "zarofuad"
- Mobile # +966 597 620 452

APPENDIX A

DETAILED EXPERIMENTAL SETUP FOR PQ MONITORING AND MITIGATION

This appendix describes the components of the experimental setup for the proposed real-time power quality monitoring, analysis, and controlling system as well as the mitigation system of the power quality problems. This appendix contains the software components, hardware components, the graphical user interface panel components, and the whole structure of the prototype system.

A.1 INTRODUCTION

The power quality problems decrease the efficiency of both the power supplies and equipment. Direct measurement in the point of common coupling (PCC) is required in order to get valid information the PQ indices. The monitoring is essential for both power utilities and their customers to ensure optimal power system performance, efficient energy management, and easy identification of the disturbance causes in the power system.

The monitoring equipment must have functions which include the detection, localization, and classification of transient events. If the event is classified accurately, the PQ engineers can specify the major effects of the disturbance at the load and analyze the source of the disturbances. Therefore a solution can be investigated.

Any successful PQ monitoring system should have:

- Capability of providing reliable information about the problem under examination.
- Measuring the relevant parameters with sufficient accuracy.
- Implementing the relevant measurement methods in an economical and efficient way.

PQ monitoring has two targets: the characterization of the quality status or the localization of the source of disturbances.

A.2 COMPONENTS OF THE IMPLEMENTED SYSTEM.

The prototype system has both software and hardware components for real-time detection and tracking voltage and current signals. These components include CompactRIO hardware, LabVIEW software, and main components of power distribution system such as programmable ac power source, programmable electronic loads, dc motor drive, and several types of static and dynamic loads. In this appendix, all the components that have been used to build the prototype system are described.

A.2.1 SOFTWARE COMPONENTS

The PQ monitoring system is realized based on the program system LabVIEW (Laboratory Virtual Instrument Engineering Workbench). LabVIEW is a graphically-based programming language developed by National Instruments (NI). The programs implemented in LabVIEW are called virtual instruments (VI) [211]-[212].

In this dissertation, The LabVIEW software has been used to develop the real-time monitoring, analysis, and controlling system for power quality problems. The developed system is continuously monitoring the voltage and current signals of the three-phase and saves the signals for further analysis included the distorted signal.

The structure of the main VI of the developed system is shown in Figure A.1. Each of the VI in the system consists of a block diagram which represents the structure of the program and contains the code for the VI which performs the work. The front panel represents the user interface and it is utilized to show controls and indicators for the user. VI handles the function inputs and outputs. One of the front panels interface and one of the block diagrams of the developed system are shown in Figures A.2 & A.3, respectively.

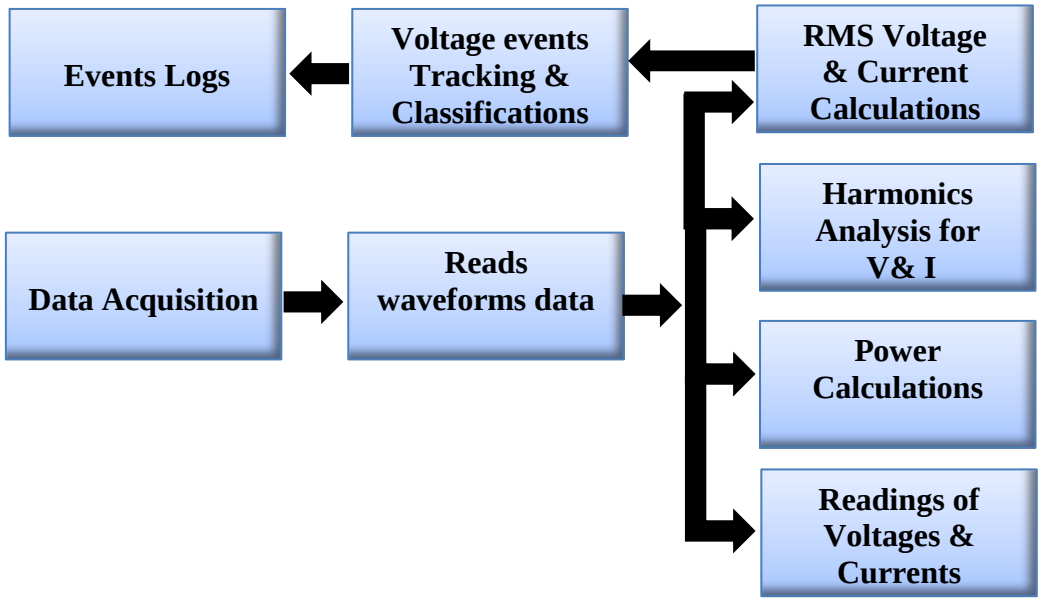

Figure A.1: The structure of the main VI of the developed package.

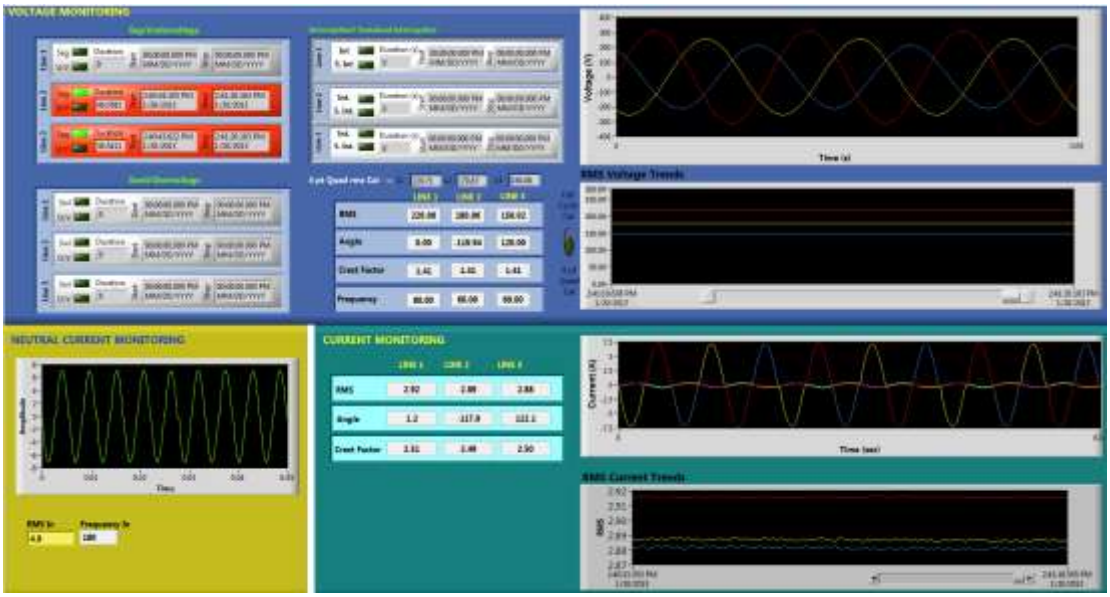

Figure A.2: The front panel interface of the developed system.

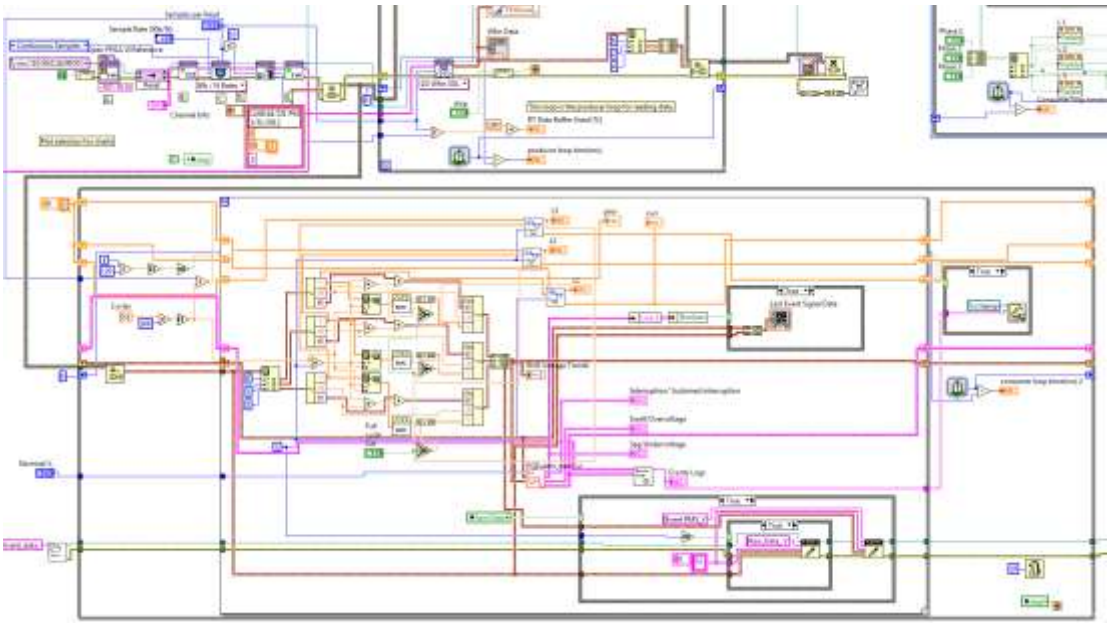

Figure A.3: The block diagram of the developed system.

LabVIEW has been communicated with Real-time controller and multifunction data acquisition (DAQ). LabVIEW also has been used to connect the developed application to the Web using the LabVIEW Web server and software standards TCP/IP networking for remote control purposes.

For developing real-time PQ monitoring and controlling system using CompactRIO, the following software has been used:

- LabVIEW development system: to create the users interfaces on the workstation PC (host PC).
- LabVIEW Real-Time Module: to program the data analysis functions.
- LabVIEW FPGA Module: to accomplish the data acquisition process and sampling frequency adaptation.
- NI-RIO driver: for cRIO modules.

- Measurement and Automation Explorer (MAX): to configure the cRIO settings.

There is no need to run the host application all the time when the cRIO runs, since when cRIO runs completely independently.

During this work, the completed LabVIEW package for power quality monitoring and controlling has been created with sampling rate is 10kS/s (kilo Sample/Second) as 166 samples/cycle and a 2,000 sample time window; furthermore, these settings are changeable as per the requirements for application.

A.2.2 HARDWARE COMPONENTS

A.2.2.1 NI CompactRIO Platform

The reconfigurable embedded system used in this application is NI cRIO (Compact Reconfigurable Input/Output). It is composed of a real-time controller, reconfigurable field programmable gate array (FPGA) chassis, and various swappable input output (I/O) modules. Each I/O module is connected directly to the FPGA, providing low-level customization of timing and I/O signal processing. The FPGA is connected to the real-time processor using high-speed PCI bus.

The cRIO allows the user to redesign and upgrade the embedded systems as per the requirements of the application. Because of its low cost, reliability, and suitability for high-volume embedded measurement and control applications, cRIO is utilized in this

prototype system to be the core of the system. The NI cRIO utilized in this application and its architecture are shown in Figures A.4 and A.5, respectively.

Figure A.4: The NI CompactRIO used in the application.

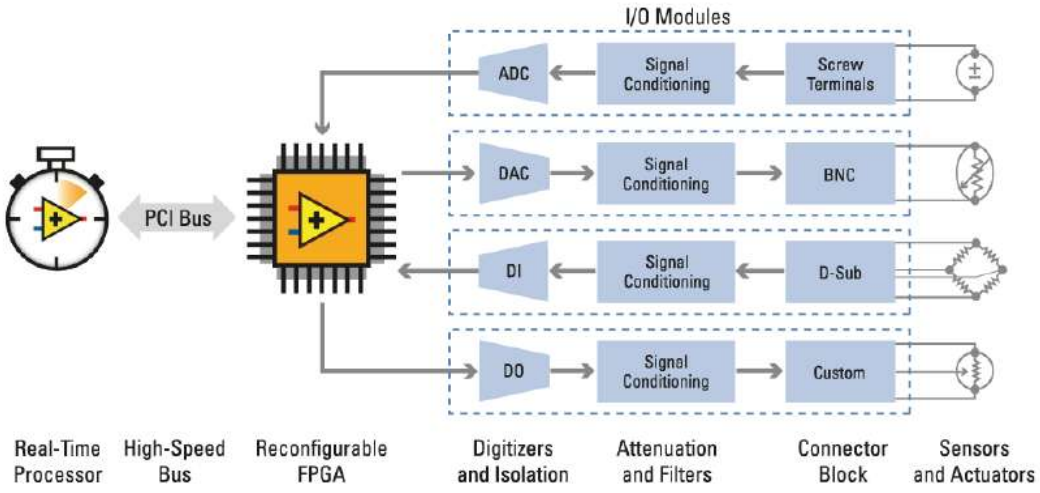

Figure A.5: Reconfigurable Embedded System Architecture [213].

The main components of cRIO that has been used to build the proposed PQ monitoring and controlling system are:

A.2.2.1.1 Input and output modules

The implemented setup of real-time PQ monitoring and controlling system contains various I/O modules. I/O modules contain isolation, conversion circuitry, signal conditioning and built-in connectivity for direct connection to industrial sensors/actuators [213]. Each used module is capable of sampling at the rate of 50kS/s. However, the sampling rate has been considered in this application is10kS/s. The NI I/O modules that have been used for the experimental setup of the PQ monitoring and controlling system are listed below:

a) Voltage input module

The NI-9225 module has been selected to measure rms voltage directly from the line. It is analog input module consists of 3-Channel, it can directly measure rms phase voltage up to 300V. Figure A.6 shows the voltage analog input module NI-9225 model. The module connected to the main power feeders directly to measure the instantaneous phase voltages for the three phases as shown in Figure A.7.

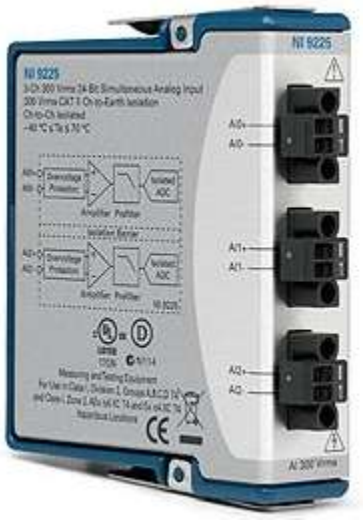

Figure A.6: The voltage analog input module NI-9225model.

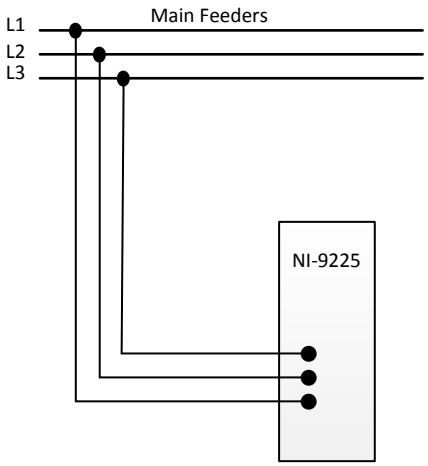

Figure A.7: The general connection diagram of the NI-9225 module with power feeders.

b) Current input module

The NI-9227 module has been selected to measure the current. It has 4 channels, and can measure rms current directly up to 5 A. On the other hand, almost the rms current values in the system are larger than 5A. For this reason, current transformer (CT 200/5 A) has been used to measure the currents through the module in each

phase as well as the neutral line. Figure A.8 shows the current analog input module NI-9227 model. The module connected to the main power feeders and the neutral line through 4 CTs to measure the instantaneous current for each line as well as for the neutral line as shown in Figure A.9.

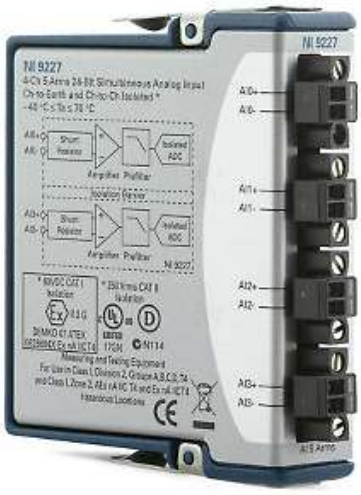

Figure A.8: The current analog input module NI-9227 model.

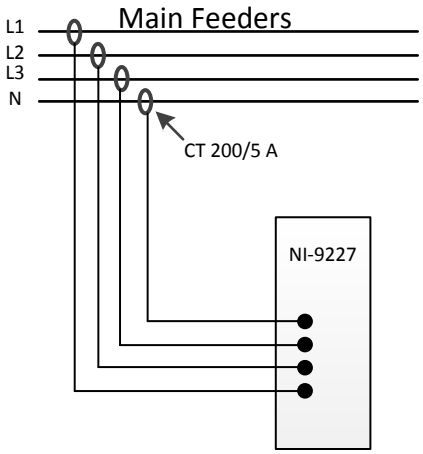

Figure A.9: The general connection diagram of the NI-9227 module with power feeders.

c) Sourcing digital output module

The NI-9476 is a 32-channel, 500 µs sourcing digital output module. Figure A.10 shows the selected NI-9476 module. It has been selected to perform software-timed and static operations in the controlling system. It's directly connected to the relays of the switching control panel of the devices and loads. Each channel can drive up to 250 mA continuous current on all channels simultaneously with 24V signals. However, each relay in the switching control panel is fed by two channels to make sure the continuous output current of each channel doesn't exceed the limits (250mA). Figure A.11 shows the connection philosophy of the digital output module with the relays in the developed system.

Figure A.10: The digital output module NI-9476 model.

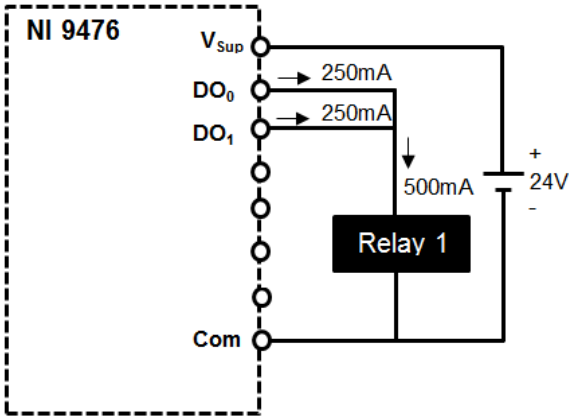

Figure A.11: The connection diagram of the NI-9476 with control relay.

d) Analog output module

The NI-9264 is a 16-channel analog output module with voltage range -10V to +10V. It has been selected to control the mitigation device operation. The actual voltage signal of the controller of the mitigation device is provided by a channel of NI-9264. Figures A.12 & A.13 show the selected analog output module and connection diagram of the module with a controller, respectively.

Figure A.12: The analog output module NI-9264 model.

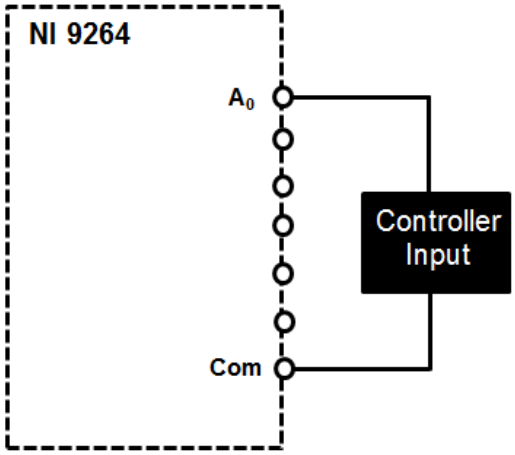

Figure A.13: Connecting a controller to NI-9264.

A.2.2.1.2 Real-time controller

The intelligent real-time embedded controller NI cRIO-9024 model is selected for cRIO as shown in Figure A.14. It is 800 MHz processor, 4 GB nonvolatile storage, 512 MB DDR2 memory. The controller runs LabVIEW Real-Ttime for deterministic control, data logging, and analysis.

The controller has been installed on the cRIO chassis. The static IP address has been assigned to communicate the host computer with the controller over a standard Ethernet connection for remote monitoring and accessing. The MAX software is used for configuring IP settings for the controller and installing LabVIEW Real-Time software and device drivers on the controller. The system clock of the cRIO-9024 is synchronized with the internal high-precision real-time clock to provide timestamp data to the controller.

Figure A.14: Real-Time Controller_ NI cRIO-9024.

A.2.2.1.3 Reconfigurable FPGA chassis

The selected model of reconfigurable FPGA chassis in this application is NI cRIO-9118 that is shown in Figure A.15. The selected chassis is 8-slot and accepts any cRIO I/O module. It has ability to automatically synthesize custom control and signal processing circuitry using LabVIEW. It is directly connected to the I/O module for high-performance access to the I/O circuitry of each module. A local PCI bus connection provides a high-performance interface between the RIO FPGA and the real-time processor

Figure A.15: Reconfigurable FPGA Chassis_ NI cRIO-9118.

The system functionality can be changed and upgraded by changing the LabVIEW FPGA module code and rebuilding and compiling a new bit stream configuration to the FPGA hardware.

A.2.2.2 Components of the power distribution network

A.2.2.2.1 Programmable AC power source

To simulate power quality disturbance conditions, the programmable three-phase ac source Chroma-61511model has been selected. It is utilized for synthesizing distorted voltage waveforms to represent the voltage sag, swell, and interruption events as well as the harmonics and interharmonics components from 0.01 Hz to 2.4 kHz. The specifications of the selected programmable ac source are 12kVA, variable rms phase voltage from 0 ~ 300V, and variable frequency range from 15 ~ 1500Hz. The Figures

A.16 and A.17 show the selected programmable power source and its graphical user interface, respectively.

Figure A.16: Programmable AC source Chroma 61511model.

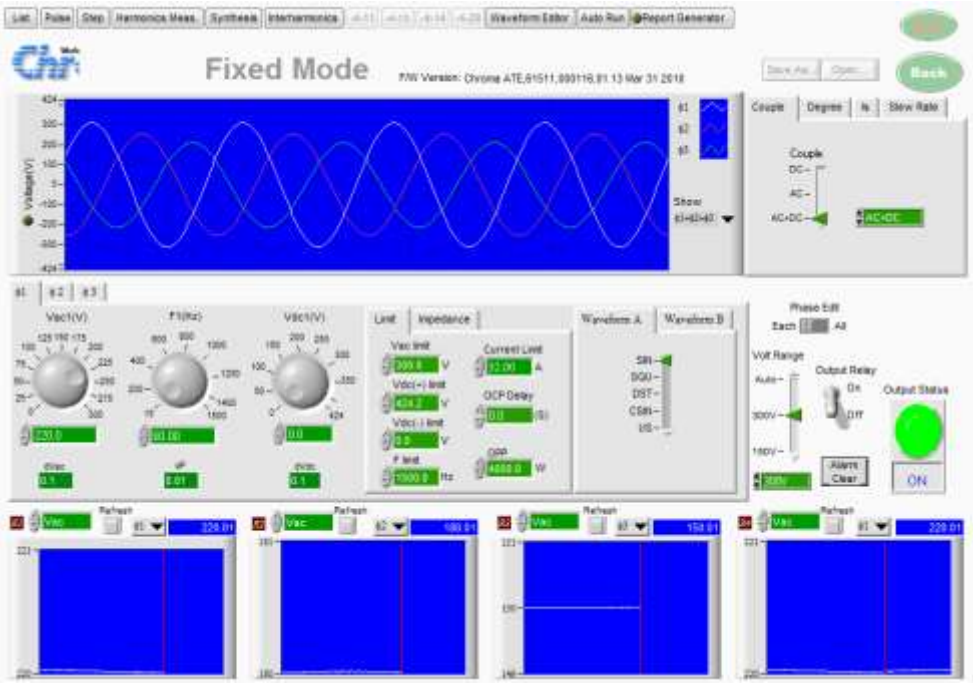

Figure A.17: The main graphical user interface of the programmable AC source.

A.2.2.2.2 Programmable electronic load

The programmable electronic load Chroma-63800 model is selected to simulate load conditions under different scenarios even when the voltage waveform is distorted. In this application three identical units of Chroma-63800 have been utilized to represent three phase load and these units are connected as wye connection where the load unit of the phase A is configured as master unit and the other as slave units.

The main features of the each selected programmable ac load unit are 1.8kW, variable rms phase current 0 ~ 18A, variable rms phase voltage 50 ~ 350V, and variable frequency 45 ~ 440Hz. The Figure A.18 shows the utilized programmable electronic load units that have been used in the experimental setup as variable three-phase load wye connected.

Figure A.18: Programmable Electronic Load Chroma-63802.

A.2.2.2.3 DC Motor Drive

DC motor drive ABB-DCS800 model is utilized in the experimental setup of the proposed application to emulate the harmonics injected from the nonlinear load into the source current. Figure A.19 shows the selected dc motor drive ABB-DCS800 model.

The dc motor drive is controlled rectifier drive, in particular a three-phase bridge thyristor rectifier, converts incoming three-phase ac power into dc power, and its being used where variable speed is required. The dc output voltage of this drive is controlled by the firing angle that is applied to the thyristor-bridge. This will inherently produce harmonics on both ac side (input) and dc side (output) of the rectifier.

The motivation of using the dc motor drive in this study is that, the dc motor drives are used through many industries. It is imperative, especially for utility companies, to realize the PQ impact of having such drives on their system. Through this understanding, both utilities and their customers may use the information to minimize the PQ disturbances which in turn maximizes profit.

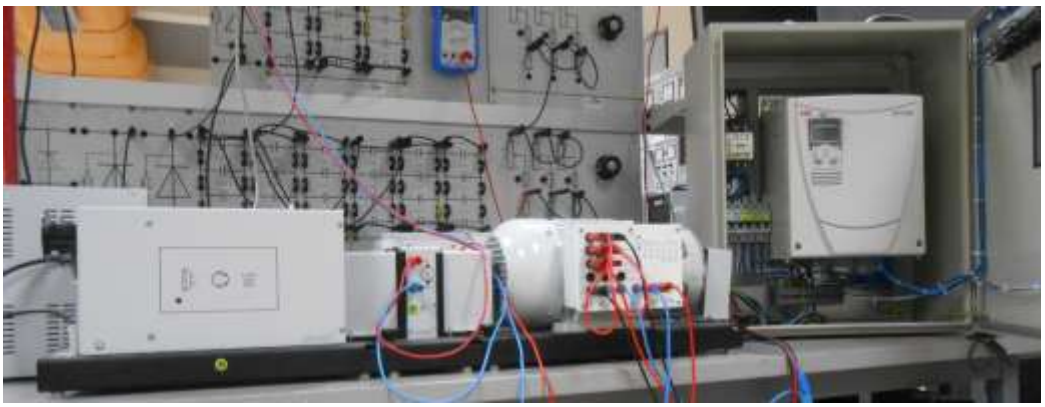

Figure A.19: DC motor drive model of ABB-DCS800.

A.3 DESCRIPTION OF THE DEVELOPED GRAPHICAL USER INTERFACE

The developed front panel interface of the created LabVIEW package for PQ monitoring, analysis and controlling is graphical user interface (GUI) where the user interacts, monitors and controls the program while it's running. The developed GUI contains measurements, readings and elements that need to be communicated to the user running the experiment as shown in Figure A.2.

The configuration settings of the developed GUI are simple, easy, and flexible. The user can specify the power frequency 60Hz or 50Hz, the samples number per read (window size), the nominal voltage (phase voltage). The user selectable the sampling rate determines the resolution of analysis results as well as the user can select a specific phase to be monitored or the three phases together. Figure A.20 shows the main setup of the developed system.

Figure A.20: Setup of the developed system.

Specifically the developed GUI of the created LabVIEW package for PQ monitoring and controlling contains:

1. **Voltage monitoring consists of**

   - The instantaneous waveforms display.
   - The rms voltage values tracking display.
   - The voltage readings for each phase, such as rms values, angle, crest factor, and frequency.

These displays and readings of the voltage monitoring are shown in Figures A.21 and A.22, respectively. During the monitoring process, the status of recorded voltage events is shown on the GUI.

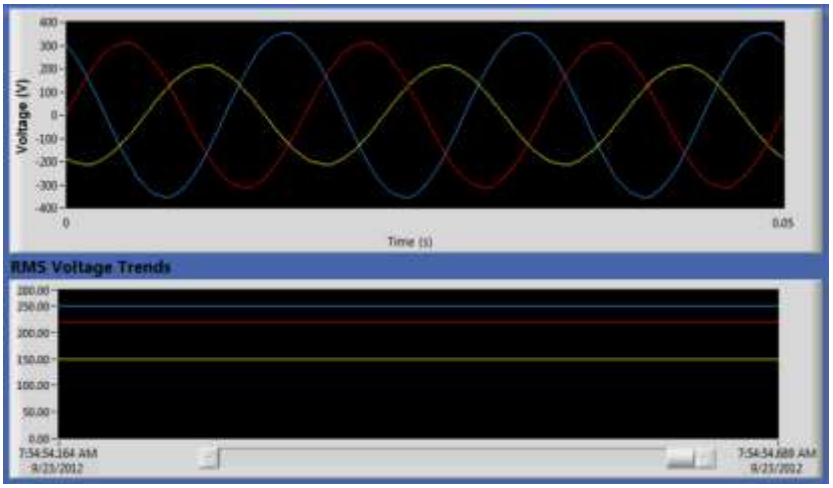

Figure A.21: Three phase instantaneous voltage waveforms and rms voltage trends.

Figure A.22: Voltage values and crest factor of the three phases.

2. Current monitoring consists of

- The instantaneous waveforms display.
- The rms current values tracking display.
- The current readings for each phase, such as rms values, angle, and crest factor.

During the current waveforms monitoring process, the status of the recorded events is shown on the GUI. The displays and readings of the current monitoring are shown in Figures A.23 and A.24, respectively.

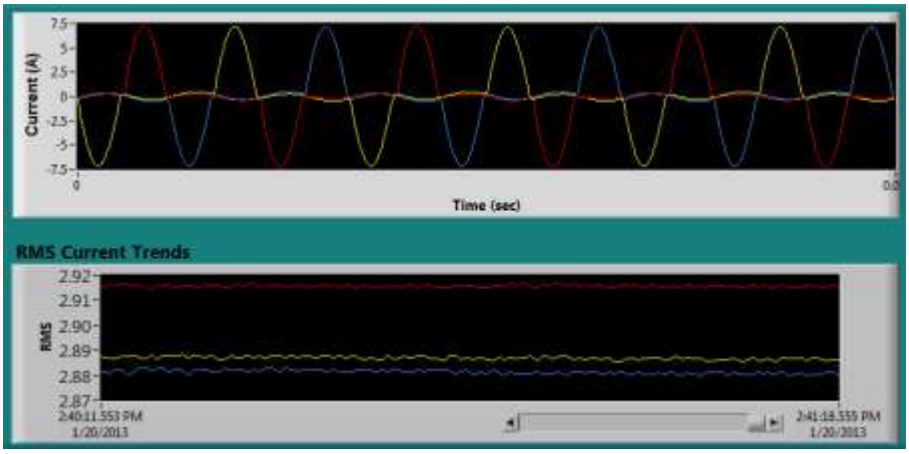

Figure A.23: Three phase instantaneous current waveforms and rms current trends.

Figure A.24: Current readings for the three phases.

3. Neutral current monitoring

The user using the developed GUI can monitors instantaneous waveform, rms current values and frequency of the neutral current in the system. The Figure A.25 shows the neutral current monitoring display in the developed GUI.

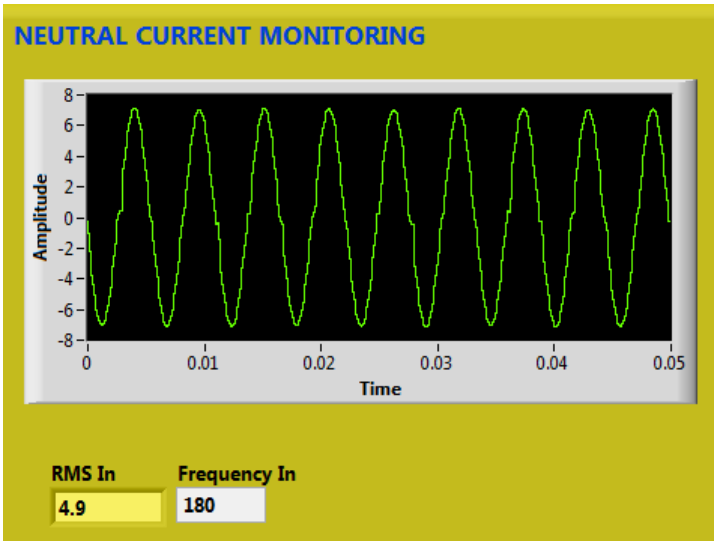

Figure A.25: Neutral current monitoring.

4. The harmonics analysis

Figure A.26 shows the developed LabVIEW-based harmonics analysis tool for the voltage and current signals. In the analysis panel, the user can perform harmonics analysis for the voltage and current waveforms. Further on, the user can select up to 20 harmonics for viewing the trend. The analysis panel displayed the spectrum harmonics and total harmonics distortion (THD) for each phase of voltage and current signals. The user selectable shows the fundamental harmonic or not.

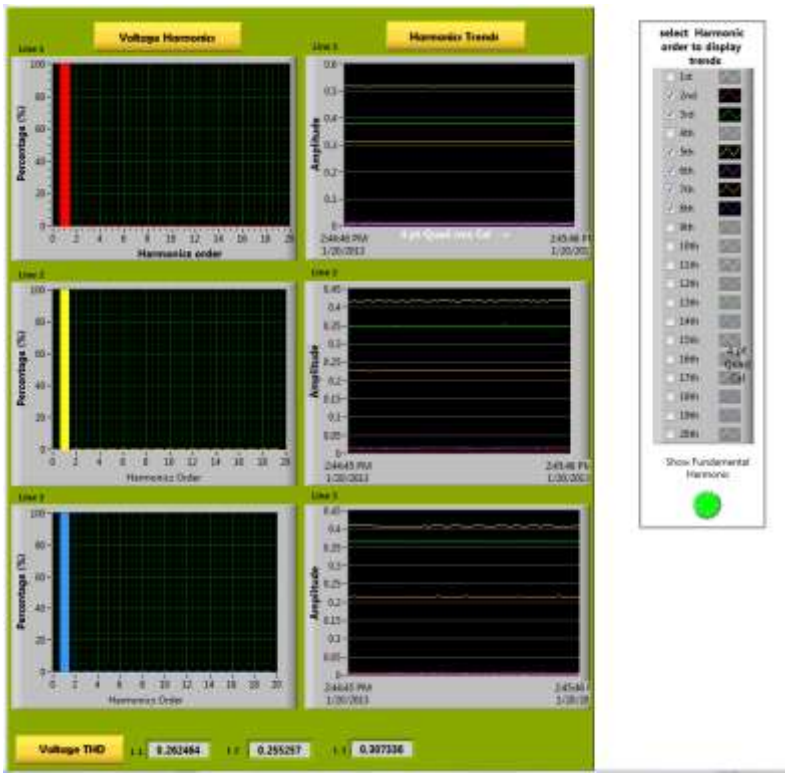

(a)

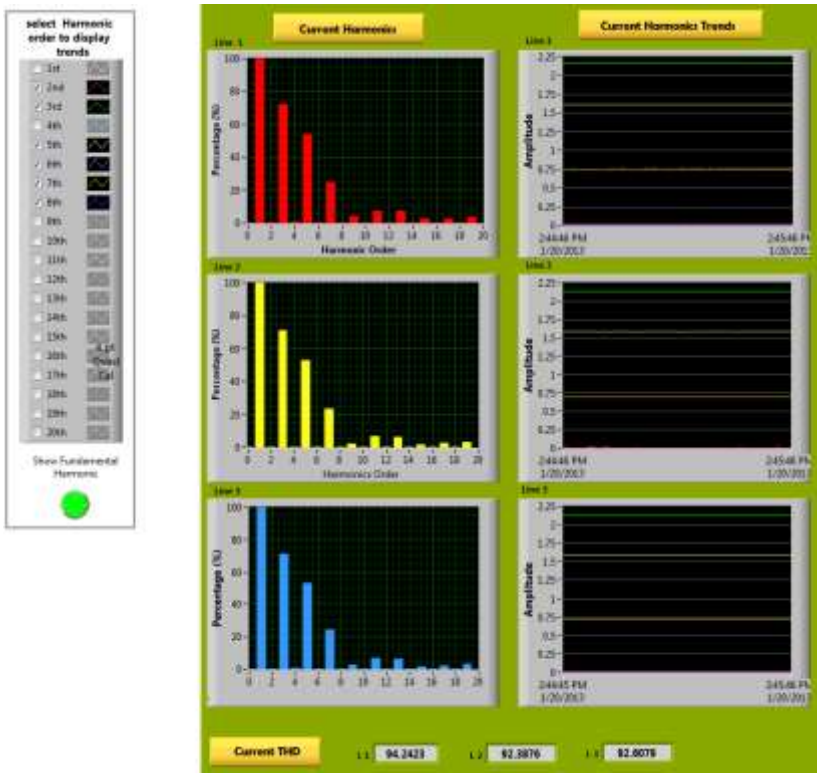

(b)

Figure A.26: Harmonics analysis tool. (a) Voltage waveforms. (b) Current waveforms.

5. Voltage events classification

The developed front panel of the voltage events characterization tool provides the user by detailed information about each event occurred, such as in which phase the event is occurred, event type, starting time, stop time, event duration, and the voltage magnitude.

Figure A.27 shows the developed GUI of the detection and classification system of the voltage events. That can classify the short and long duration voltage events. The short duration voltage events the can be characterized by the developed package are voltage sag, swell, and interruption, whereas the long duration voltage events are undervoltage, overvoltage, and sustained interruption. At the moment of occurring the event, the GUI changes the color of the phase bar to the red color and turns on indicator beside the type of event.

6. Power analysis

The system provides the readings of the real power (W), apparent power (VA), reactive power (VAR), power factor and the total consumed power. In addition, the power analysis panel shows chart for each phase of the power distribution networks. Figures A.28 and A.29 show the developed power chart and power readings, respectively.

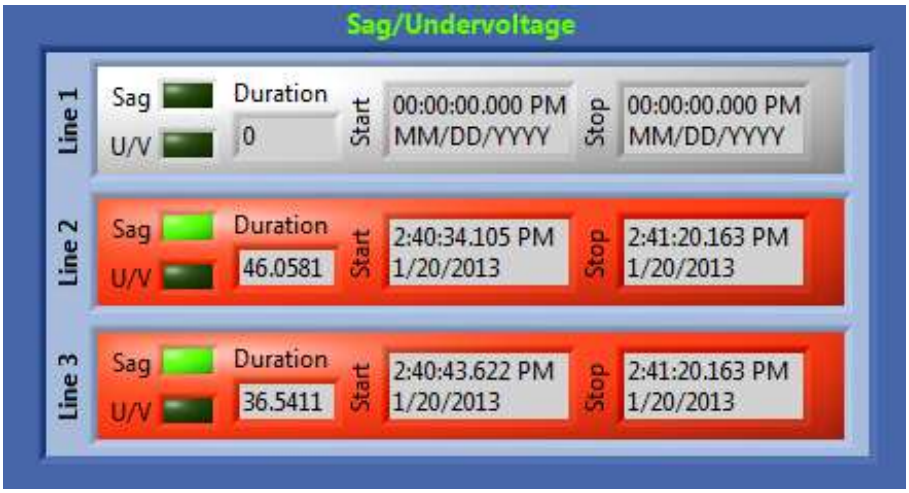

(a)

(b)

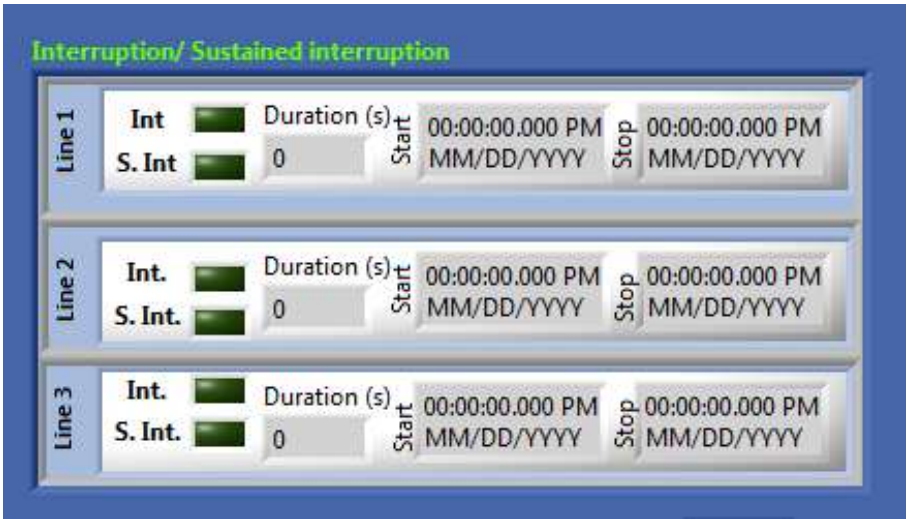

(c)

Figure A.27: Voltage events monitoring. (a) Sag / Undervoltage event.
(b) Swell / Overvoltage event. (c) Interruption / Sustained interruption.

Figure A.28: Real power chart.

	L1	L2	L3	Total
Real Power (Watt)	466.64	379.58	316.54	1.16E+3
Apparent Power (VA)	642.13	519.85	432.32	1.59E+3
Reactive Power (VAR)	441.11	355.19	294.46	1.09E+3
Power Factor	0.73	0.73	0.73	0.73

Figure A.29: Consumed power and power factor for each phase.

7. Data logging and events logs

The developed LabVIEW-based package for PQ monitoring contains a tool for data logging, data storage in the excel files. Further on, the GUI contains events logs, which allow the user to see all the events have been occurred. Events logs contain the complete information for each event occurred, such as event type, start time, end time, duration time, and the event place. Figure A.30 shows the events logs provided by the developed GUI.

8. Instrument control

The GUI of the PQ monitoring system allows the user to control the operation of all loads and devices connected on the system. The GUI also allows the user to do the

default settings for each device and load in the system either normally on or normally off as shown in Figure A.31.

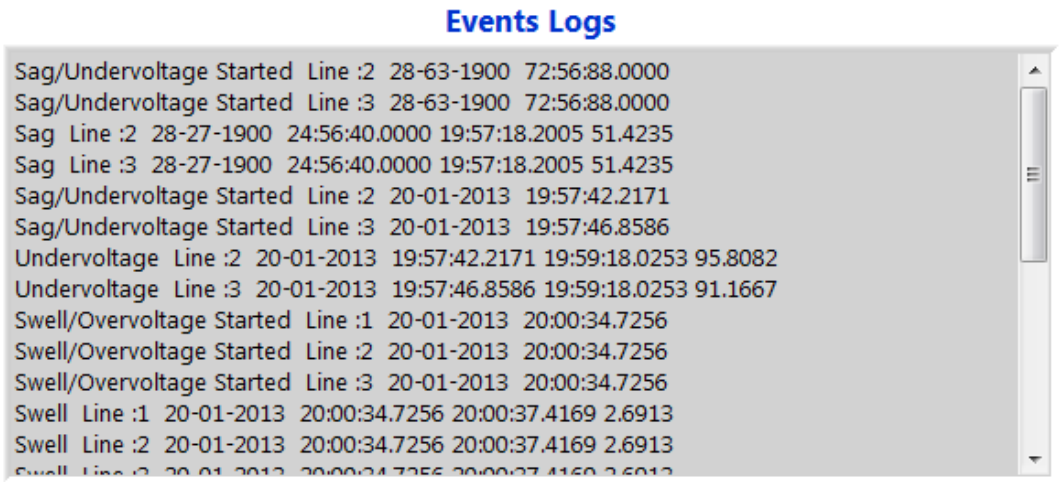

Figure A.30: Events logs.

Figure A.31: The control panel of instrumentation and loads.

Additionally, the developed package allows the user remotely access to cRIO by using TCP protocol over Ethernet. The user can change the setting and configuration of the cRIO as well as remote files browser, as can be seen from the Figures A.32

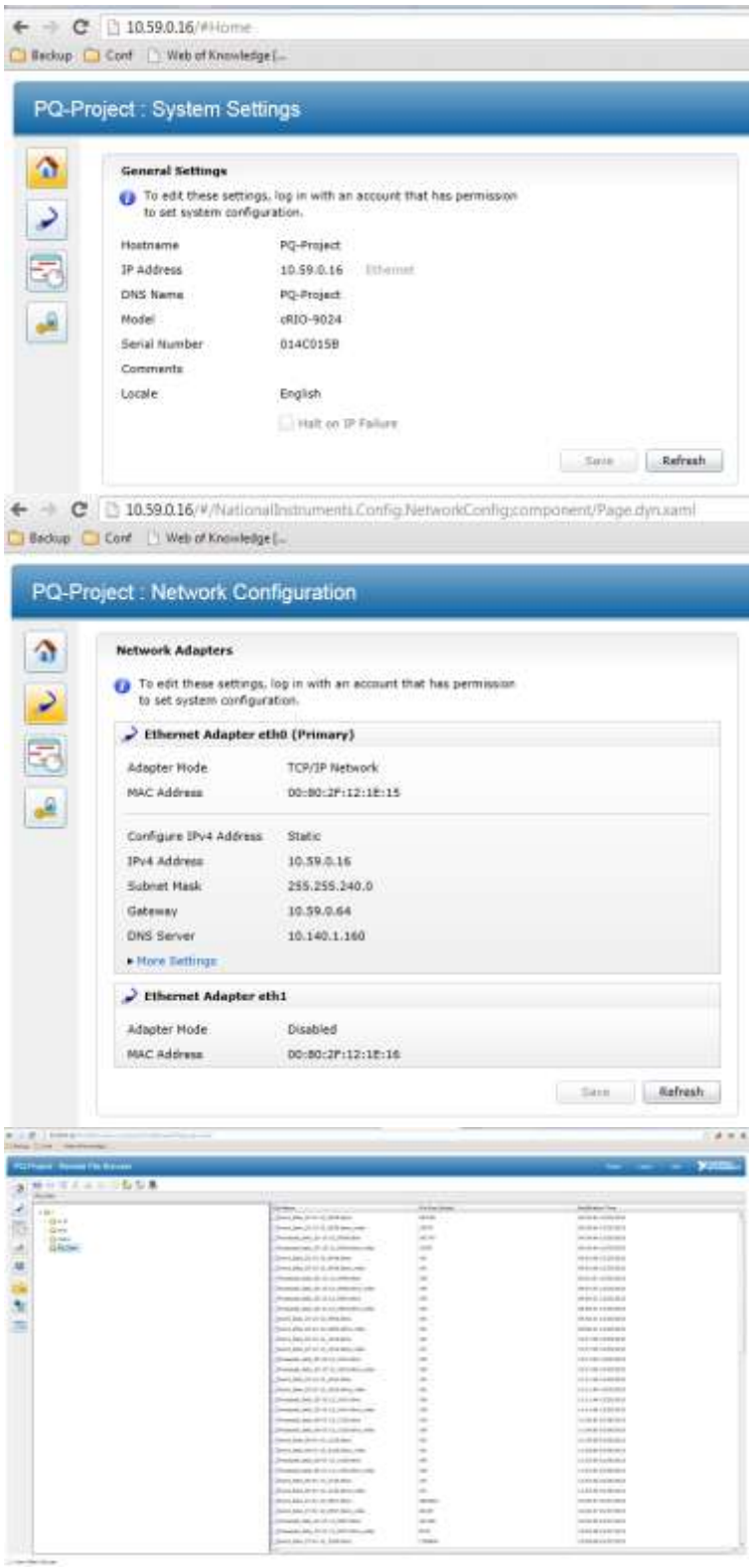

Figure A.32: Remote access to cRIO.